Development of a Velocity Prediction Program for Sailing Yachts

Pedro Francisco Gouveia Teixeira

Thesis to obtain the Master of Science Degree in

Naval Architecture and Ocean Engineering

Supervisor: Prof. Manuel Filipe Simões Franco Ventura

Examination Committee

Chairperson: Prof. Tiago Santos

Supervisors: Prof. Manuel Filipe Simões Franco Ventura

Members of the Committee: Dr. Leigh Sutherland

October 2024

TÉCNICO LISBOA

Development of a Velocity Prediction Program for Sailing Yachts

Pedro Francisco Gouveia Teixeira

DECLARATION

I declare that this document is an original work of my own authorship and that it fulfils all the requirements of the Code of Conduct and Good Practices of the Universidade de Lisboa.

Signature

ACKNOWLEDGEMENTS

To my family for their support,

to my sailor friends for all the precious inputs and especially

Prof. Manuel Ventura for all the guidance, patience and insight provided.

ABSTRACT

In the late 20th century, the global shipbuilding industry transitioned from European to Asian dominance. This shift prompted European shipyards to adapt from steel-intensive ships to recreational crafts like power boats and sailing yachts. At the same time, sailing regattas grew into a highly competitive sport, pushing advancements in yacht design. Given the recreational craft industry growth and the rise in sailing regattas, there has been a corresponding increase in the performance expectations, which influenced the development of this project.

Evaluating the performance of a sailing vessel can be a challenging task. Velocity Prediction Programs are numerical tools designed to simulate the physics of yachts. Their behaviour can be isolated into two main components the aero-hydrodynamic forces and moments. The main algorithm is responsible for balancing the forces and moments of these components for each degree of freedom. Once equilibrium is established, the forces can be used to calculate a variety of outputs, with the vessel's sailing speed being the most important variable.

The developed tool encompasses two empirical models, Hazen's Aerodynamic model paired with the work developed by Delft University, regarding hydrodynamics. The results obtained will be compared with those derived through the International Measurement System (IMS) methodology, using the Maxsurf software, and further evaluated by comparing results with certificates from the Offshore Racing Congress (ORC).

Keywords: sailing yachts performance, VPP, velocity prediction, sailing aero-hydrodynamic

RESUMO

No final do século XX, o mercado da construção naval passou do domínio europeu para o domínio asiático. Esta transformação levou os estaleiros europeus a adaptarem-se, passando da construção de navios em aço para a produção de embarcações de recreio, como barcos a motor e à vela. Com esta transição, a indústria das embarcações de recreio assumiu um papel fundamental, tanto pelo seu impacto ambiental como pela sua importância económica na União Europeia. Ao mesmo tempo, a vela tornou-se um desporto competitivo com projeção mundial, impulsionando vários desenvolvimentos na componente do design de embarcações. Dado o crescimento da indústria das embarcações de recreio e ao aumento da projeção mundial da vela, houve um crescimento correspondente nas previsões de desempenho, o que influenciou o desenvolvimento deste projeto.

A avaliação do desempenho de uma embarcação à vela é por noma uma tarefa difícil. Os programas de previsão da velocidade contêm modelos numéricos concebidos para simular os processos físicos persentes em embarcações à vela. O seu comportamento pode ser isolado em dois componentes principais: forças e momentos aero-hidrodinâmicos. O algoritmo principal é responsável por estabelecer o equilíbrio das forças e dos momentos destas componentes para cada grau de liberdade. Uma vez estabelecido o equilíbrio, as forças podem ser usadas para calcular uma variedade de resultados, sendo a velocidade a variável mais importante.

A ferramenta desenvolvida engloba dois modelos empíricos, o modelo aerodinâmico de Hazen emparelhado com o trabalho desenvolvido pela Universidade de Delft, relativamente à hidrodinâmica. Os resultados obtidos serão comparados com os obtidos através da metodologia do Sistema Internacional de Medição (IMS), utilizando o software Maxsurf, e ainda avaliados através da comparação dos resultados com os certificados do Offshore Racing Congress (ORC).

Palavras-chave: VPP, previsão de velocidade, aerodinâmica e hidrodinâmica de um veleiro

Table Of Contents

LIST OF FIGURES

LIST OF TABLES

LIST OF ACRONYMS

AWA	-	Apparent Wind Angle
AWS	-	Apparent Speed
CAGR	-	Compound Annual Growth Rate
CFD	-	Computational Fluid Dynamics
COE	.	Aerodynamic Centre of Effort
CLR	-	Centre of Lateral Resistance
DOF	-	Degrees Of Freedom
DSYHS	-	Delft Systematic Yacht Hull Series
DSKS	-	Delft Systematic Keel Series
EU	-	European Union
ISO	-	International Standards Organization
ITTC		International Towing Tank Conference
LPP	-	Lines Processing Program
MARIN	-	Maritime Research Institute Netherlands
MHS	-	Measurement Handicap System
NACA	-	National Advisory Committee for Aeronautics
ORC	-	Offshore Racing Council
SQP	-	Sequential Quadratic Programming
TWA	-	True Wind Angle
TWS	-	True Wind Speed
VMG	-	Velocity Made Good
VPP	-	Velocity Program Prediction

SYMBOLOGY

A_F	-	Foretriangle Area
A_J	-	Jib Sail Area
A_{lat}	-	Lateral Surface of Hull with Keel
A_R	-	Sail Aspect Ratio
AR_E	-	Effective Aspect Ratio
A_M	-	Main Sail Area
AMS_{CB}	-	Maximum Section Area of Canoe Body
A_N	-	Nominal Sail Area
A_s	-	Spinnaker Sail Area
A_W	-	Waterplane Area
B	-	Buoyance
B_{cb}	-	Canoe Body Beam
B_{MAX}	-	Maximum Beam
B_{WL}	-	Theoretical Waterline Beam
C_{ARM}	-	Crew Am
C_D	-	Drag Coefficient
C_{DPJ}	-	Jib Viscous Drag Coefficient
C_{DPM}	-	Main Viscous Drag Coefficient
C_{DPS}	-	Spinnaker Viscous Drag Coefficient
C_{D_P}	-	Viscous/Parasitic Drag Coefficient
C_{D0}	-	Mast And Topsides Drag Coefficient
CE_M	-	Main Sail Centre of Effort
CE_J	-	Jib Sail Centre of Effort
CE_S	-	Spinnaker Sail Centre of Effort
C_f	-	Skin Friction Coefficient
C_H	-	Heeled Coefficient
C_{id}	-	Induced Resistance Coefficient
C_L	-	Lift Coefficient
C_{LJ}	-	Jib Sail Lift Coefficient
C_{LM}	-	Main Sail Lift Coefficient
C_{LS}	-	Spinnaker Sail Lift Coefficient
C_m	-	Midship Section Coefficient
C_P	-	Prismatic Coefficient
CW_{rail}		Crew Weight on The Rail
ck	-	Mean Keel Chord
D	-	Aerodynamic Drag Force

d	-	Longitudinal Distance Between the CLR And COE
D_{cb}	-	Canoe Body Depth
F_A	-	Resultant Aerodynamic Force
F_H	-	Heeling Force
F_I	-	Resultant Hydrodynamic Force
F_{LAT}	-	Aerodynamic Side Force
F_M	-	Driving Force
F_y	-	Lateral Force Resultant
F_x	-	Longitudinal Force Resultant
F_Z	-	Vertical Force Resultant
g	-	Acceleration Of Gravity
GZ	-	Righting Arm
h	-	Vertical Distance Between the CLR And COE
L	-	Aerodynamic Lift Force
L_{CB}	-	Longitudinal Centre of Buoyancy Position from The Forward Perpendicular
L_{CF}	-	Longitudinal Centre of Flotation Position from The Forward Perpendicular
L_{OA}	-	Length Overall
L_{WL}	-	Waterline Length
M_{CREW}	-	Crew Righting Moment
$M_{CREWeff}$	-	Effective Crew Righting Moment
M_{heel}	-	Heeling Moment
M_{right}	-	Righting Moment
M_x	-	Resultant Moment in The X-Axis
M_y	-	Resultant Moment in The Y-Axis
M_z	-	Resultant Moment in The Z-Axis
P_{LAT}	-	Hydrodynamic Side Force
R_{Aheel}	-	Appendages Delta Resistance Increase Due to Heel
R_{CBheel}	-	Canoe Body Delta Resistance Increase Due to Heel
R_f	-	Canoe Body Frictional Resistance
$R_{f\,app}$	-	Appendages Frictional Resistance
R_{id}	-	Canoe Body Induced Resistance
RMV	-	Dynamic Righting Moment
Rn	-	Reynolds Number
R_r	-	Canoe Body Residuary Resistance
R_{rk}	-	Keel Residuary Resistance
R_{ru}	-	Rail Under Drag
R_{Rheel}	-	Canoe Body Residuary Resistance Increase Due to Heel
R_{Rheel_k}	-	Keel Residuary Resistance Increase Due to Heel

R_{tot}	-	Total Resistance
R_{upr}	-	Upright Resistance
R_v	-	Viscous Resistance
$R_{v_{app}}$	-	Appendages Viscous Resistance
S_C	-	Wetted Area of The Hull at Zero Speed
SLR	-	Speed Length Ratio
S_{wc}	-	Wetted Area of The Hull in Heel
T	-	Total Draft (With Keel)
T_C	-	Canoe Body Draught
T_{eff}	-	Effective Draft of The Hull and Keel Combination
V	-	Yacht Velocity
Z_{Cbk}	-	Keel's Centre of Buoyancy Vertical Position
Z_{COE}	-	Centre Of Effort Vertical Position
Z_{CLR}	-	Centre Of Lateral Resistance Vertical Position

Sails nomenclature

P	-	Mainsail host
E	-	Foot of mainsail
I	-	Height of foretriangle
J	-	Base of foretriangle
LPG	-	Perpendicular of longest jib
SL	-	Spinnaker leech length
PY	-	Mizzen Hoist
EY	-	Foot of mizzen
YSD	-	Mizzen staysail depth
$YSMG$	-	Mizzen staysail mid-girth
YSF	-	Mizzen staysail foot
BAD	-	Height of main boom above sheer
HBI	-	Height of sheerline at the base of the mast

Greek symbols

$\triangle$	-	Boat displacement
$\triangle_{cb}$	-	Canoe body displacement
∇_C	-	Canoe body volume of displacement
∇_k	-	Keel volume of displacement
λ	-	Leeway angle
ν	-	Kinematic viscosity
ρ	-	Fluid density
φ	-	Heel Angle
Λ	-	Sweep Angle

1. INTRODUCTION

1.1 Motivation

In the late 20th century, the global shipbuilding industry underwent a significant shift, moving from European to Asian dominance. This transition was largely driven by China’s ability to produce ships at a lower cost, backed by strong government support and a focus on high-demand vessels like bulk carriers. (Kamola-Cieślik, 2021). By the early 2000s, Asian shipyards had become global leaders in the industry, which led European shipyards to adapt from steel-intensive ships to recreational crafts like power boats and sailboats.

The recreational craft manufacturing industry is composed predominantly of small and medium-sized enterprises, along with a few large companies employing over 1,000 people. This manufacturing sector encompasses approximately 32,000 businesses employing at least 280,000 people. The European Commission estimates that this segment generates €20 billion annually (European Commission, 2023), with the sailboat industry valued at €3.47 billion in 2023 and projected to grow with a compound annual growth rate (CAGR) at 4.9% from 2024 to 2030 (Grand View Research, 2024).

Prominent sailing events have emerged as competitive and high-stakes sports. The Louis Vuitton 37th America’s Cup attracted 2.56 million attendees over its 59-day duration, reflecting a 50% increase in total broadcast and media audience compared to the previous edition (Emirates Team New Zealand, 2024). Other competitions, such as The Ocean Race, have also demonstrated significant growth over the years (Turner, 2015), with the most recent edition achieving a cumulative media audience of 8.1 billion and a social media listening reach of 2.6 billion (The Ocean Race, 2023). Notable events like the Vendée Globe, SailGP, and Copa del Rey further exemplify this trend. These competitions continually push the boundaries of yacht design, where even minor performance gains can be critical. The significance of VPPs is underscored by their role in the competitive landscape, where performance is paramount.

Velocity prediction programs are vital for naval architects to make informed adjustments (including hull shapes, sail configurations, and weight distributions) in the preliminary design stages of both commercial and custom sailboats. The results obtained at this stage can reveal fewer desirable characteristics of the boat, which would otherwise only be identified when in use. Therefore, the definition of performance measures and the development of methods and tools that allow them to be predicted are fundamental needs of the community dedicated to the various aspects of the design, development and production of sailing vessels

Given the recreational craft industry growth and the rise in sailing competitions, there has been a corresponding increase in the performance expectations, which dictated the development direction of this project.

1.2 Problem

A sailing yacht is a complex system, as it relies on both aerodynamic and hydrodynamic forces to maintain equilibrium and generate propulsion under various sailing conditions. Predicting sailing yacht performance has been a longstanding focus, with several approaches developed over the years.

The basic problem relies on solving a system of nonlinear equations that define the equilibrium conditions among the several yacht's components. A sailing yacht, as a solid object, experiences forces and moments from both the air and water acting on its surfaces (hull, sails, and appendages). These forces are calculated using separate aerodynamic and hydrodynamic models.

By adjusting parameters such as sail trim and hydrodynamic parameters, equilibrium points can be achieved. Some parameters, like the heel angle and velocity, are dependent, while others, like wind angle and speed, are independent. The VPP primary function is to identify the optimal combination of parameters to maximize velocity for varying True Wind Speeds (TWS) and True Wind Angles (TWA). The velocity is the key performance indicator, while Velocity Made Good (VMG) measures the yacht's optimal progression upwind or downwind, especially when speed alone does not fully capture performance.

The developed software, OceanVPP, was created using MATLAB with an object-oriented programming approach. It is designed to predict the performance of sailing yachts in calm waters, considering two degrees of freedom (DOF). The VPP encompasses two empirical models, Hazen's Aerodynamic model paired with the work developed by Delft University, regarding hydrodynamics. The results obtained will be compared with those derived through the International Measurement System (IMS) methodology, using the Maxsurf software, and further evaluated by comparing results with certificates from the Offshore Racing Congress (ORC).

1.3 Work Structure

This project is organized into nine comprehensive chapters, each serving a critical role in developing a robust understanding of the VPP for sailing yachts. The goal is to analyse the hydrodynamic and aerodynamic characteristics of a sailing yacht and explore the associated forces and performance metrics.

Chapter 2 provides a thorough review of existing research, comparing traditional and dynamic VPPs and examining the theoretical foundations, including hydrodynamic and aerodynamic principles relevant to assess the different methods to estimate the forces.

Chapter 3 outlines the VPP architecture, describing the core framework and equilibrium calculations necessary for predicting sailing conditions such as velocity, leeway angle, and heel angle. It also details the solution algorithm, which includes initial estimates, boundary conditions, and a step-by-step approach for solving the equilibrium equations.

In Chapter 4, the focus shifts to the hydrodynamic model, where resistance forces impacting the hull and appendages are analysed in depth. This chapter categorizes resistance into viscous, residuary, and induced types and explores how each force interacts under different conditions, to impact yacht performance. Chapter 5 then develops the aerodynamic model, examining the forces acting on the yacht's sail system, including lift and drag coefficients and the resulting aerodynamic forces. The chapter includes a comparative analysis of methodologies, such as Hazen and Offshore Racing Congress (ORC) standards.

Chapter 6 addresses hydrostatics and stability, focusing on key aspects like righting moment and stability curves, essential for ensuring safety and optimizing performance. This chapter also considers the crew's impact on stability. Chapter 7 introduces the Forsatio YD-41 sailing yacht as the benchmark model for the present case study, describing its specifications and design variables. Chapter 8 consolidates and interprets the results from the hydrodynamic and aerodynamic models, presenting the final VPP outputs and validating them against benchmark software such as Maxsurf and ORC data.

Finally, Chapter 9 summarizes the main findings, discusses the results, and proposes recommendations for future research, including enhancements in VPP methodologies.

2. STATE OF THE ART

2.1 General

The sailing yacht is in its essence a remarkable, complex, and sophisticated physical system that interacts with two different fluid mediums, one 1000 times denser that the other, with an interface between them at the same time, with the hull being the element that shares both interfaces. The equilibrium state achieved by the two-way connection is what generates the propulsion of these vessels in different sailing conditions. To understand its motions, it is necessary to examine its underlying mechanisms and principles to identify the roles of different geometric and dynamic parameters in its overall behaviour. The sailing yacht, like any other system, is composed of interrelated components, such as hull, appendages, sails and rigging.

Figure 1 - A yacht under way.

A sailing yacht under way is susceptible to a broad range of movements, due to the interplay of the multiple forces of various natures. Figure 1 displays a yacht sailing at constant speed. In these conditions, the surface of the boat above the waterline is the one affected by aerodynamic forces, while the submerged surface interacts with water generating hydrodynamic forces. There are two types of forces acting on the boat: static forces (weight and buoyancy), that are influenced by the hull's geometrical parameters, and the dynamic forces that arise from the relative motion between the boat and its surroundings (Fossati, 2013).

When examining the movements of a sailing boat, it can be seen as a rigid body in space and its motion can be described by six different degrees of freedom (DOF), each corresponding to a different fundamental motion, either rotational or linear (Figure 2). A 3D coordinate reference system (xyz) can be established with the origin at the centre of gravity of the boat, the x-axis running along the centreline and pointing forward, the y-axis running athwart the ship and lying on the waterline, and the z-axis pointing upwards.

These six basic motions are surge (along the x-axis), sway (along the y-axis), heave (along the z-axis), roll (rotation around the x-axis), pitch (rotation around the y-axis) and yaw (rotation around the vertical z-axis). (Larsson & Eliasson 2001)

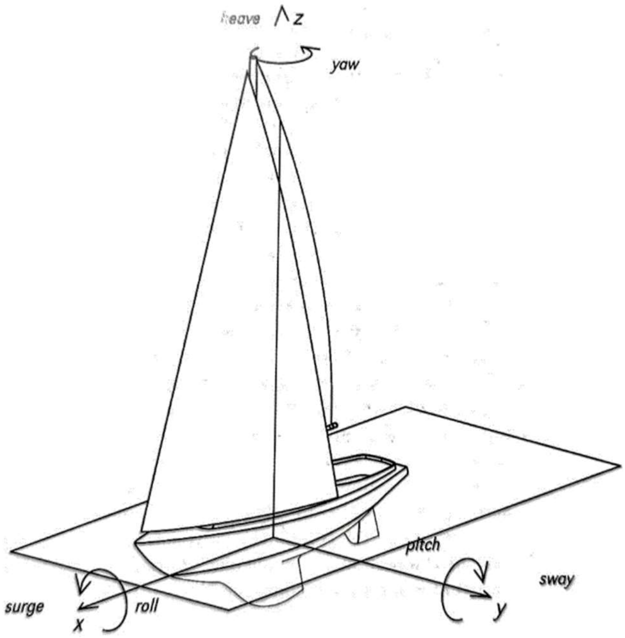

Figure 2 - Reference system (xyz) (Fossati, 2013)

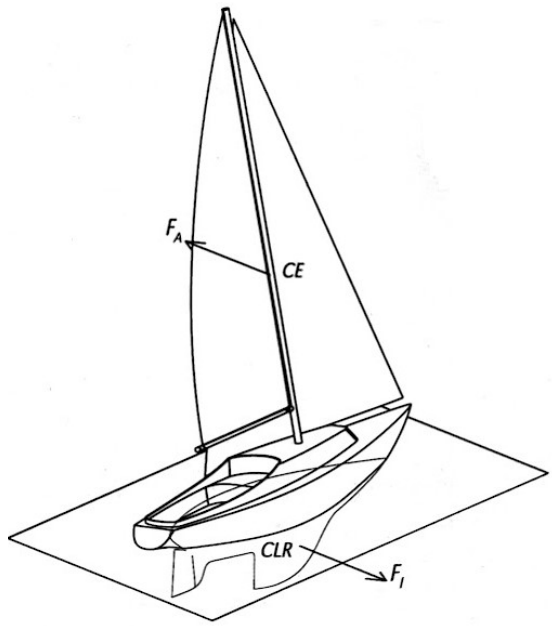

Figure 3 - Balance between the forces developed in the air and in the water. (Fossati, 2013)

The effect of the apparent wind on all the boat's components above the waterline (hull, rigging, and sails) through the fundamental mechanisms that control the interaction between a solid object and a fluid, generates an aerodynamic force (FA). This force is applied to a single point on the boat, referred to as the centre of the sail plan or aerodynamic centre of effort (COE), depicted in Figure 3. Commonly, the assumption that the centre of effort is the geometric centre of the sail area is made.

The aerodynamic forces, due to the sails shape, have a large component perpendicular to the direction of the apparent wind and only a minimal component in the direction of the wind. These components are referred to as aerodynamic lift and aerodynamic drag respectively.

The submerged parts of the hull interacts with the water to produce the hydrodynamic force (FI), which must balance the aerodynamic force. This force is also applied to a single point on the boat, referred to as the centre of lateral resistance (CLR).

The equilibrium within the aero-hydro dynamics forms the cornerstone of every VPP (further developed in Chapter 3.1). The forces and moments from each interface interaction counteract one another along the three reference axes of the boat. The solution algorithm must establish a balanced state for every sailing point. The propulsion generated by the sails must match the resistance produced by hull and rig drag, while the heeling moment from the rig is offset by the righting moment from the hull and crew. The VPP then determines the velocity, heel angle, leeway angle, and possibly other parameters pertaining to the ship's movement, based on the wind conditions.

Due to the complexity of sailing yacht propulsion, research in this area has traditionally focused on examining the aerodynamic and hydrodynamic forces separately, see Figure 4. The goal is to determine the forces from each model and then find the balance where the two reach a steady state.

A sailing yacht VPP, and as demonstrated in ORC (2024) can be then segmented into three main models/components:

1. Aerodynamic model describing the characteristics of the rig, caused by the forces originated from the wind acting on the rig (sails). This model is responsible for determining, for any given wind and boat model, the aerodynamic lift and drag they produce. The output is the heeling force and thrust.
2. Hydrodynamic model, associated with the hull shape and appendages, reflecting on the yachts drag, resistance forces and side force. Its aim is to predicts the resistance and righting moment the hull generates for the assumed speed and heel angle.
3. Formulations to balance these characteristics with respect to optimum speed.

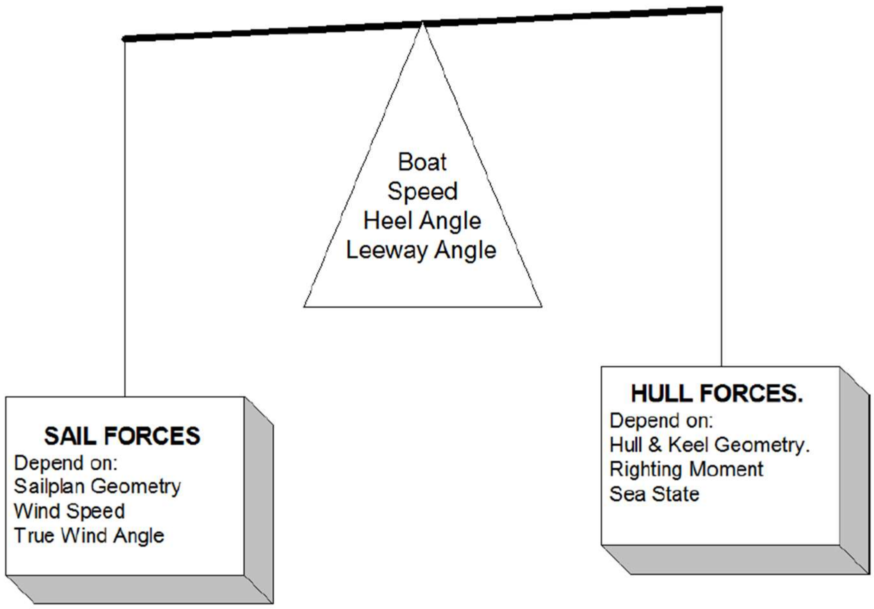

Figure 4 - Force Balance (ORC, 2024)

2.2 Velocity Prediction Program

In this chapter a broad overview of the key developments, made over the years, for velocity prediction programs and the characteristics of sailing yachts will be provided. The aim is to evaluate the various ways of predicting sailing performance, using the prior established knowledge, which will allow to a better understanding on what direction further research is important. The fundamental principles for predicting the velocity of a sailing yacht have remained consistent over time. However, the primary focus even today is on how these forces are calculated, a field where advancements are continually being achieved.

The prediction of sailing yacht performance has presented a challenge since the 1930s, when the first methods for determining aero-hydrodynamic forces and its behaviour were introduced. These early approaches laid the groundwork for modern techniques in the field and established the foundation for developing theoretical models to assess the forces involved. These models have since been incorporated into the framework of VPPs, enabling more precise performance analysis and prediction.

An early significant contribution to the field is Davidson (1936) work, where full-scale measurements of boat speeds and heel angles were conducted. These conditions were subsequently replicated in a towing tank to assess ship resistance and side forces. The combination of full-scale measurements with model results facilitated the determination of sail forces. The accuracy of the results is largely contingent upon the quality of the equipment employed and largely on the expertise and careful attention of the professionals overseeing the experiments.

In the 1970s, Kerwin's work on the "H. Irving Pratt Ocean Race Handicapping Project" resulted in the creation of the first real iteration of a VPP (Kerwin, 1975). The objective of the program was to provide a fair distribution of handicaps across several types of sailing boats, and it encompassed multiple components and achieved considerable advancements in several key areas. These advancements include the creation of a hydrodynamic force model derived from towing tank tests and an aerodynamic model to calculate sail forces at all relevant apparent wind angles. Additionally, the project introduced an iterative optimization to find the equilibrium sailing condition of forces determined by the apparent wind speed and angle with the two sail trim factors of flat and reef. It also developed new methods of race scoring that utilized handicaps, typically expressed as speeds in seconds per mile, which the VPP predicted for each point of sailing. Furthermore, the project led to the development of a hull offset measurement tool and an associated Lines Processing Program (LPP) to process hull shapes before their incorporation into the VPP. Figure 5 presents the procedure of the performance tool developed.

The original code was relatively simple, based on basic analytical models and restricted by the degrees of freedom (DOF) in which it could be solved. It is essential to acknowledge that the computational resources available at the time were a significant limitation, influencing the scope of what could be calculated. The most fundamental VPP solution focused on achieving steady-state equilibrium in Roll and Surge. Equilibrium in other degrees of freedom was assumed, and the effects on other variables were disregarded. For instance, the influence of trim angle at which this equilibrium might occur was not factored into subsequent calculations. The incorporation of additional DOF continues to significantly increase the complexity of the solver algorithm, as it must resolve a greater number of force and moment equilibrium conditions. In many cases, this simplification is valid, addressing the core of the problem and delivering sufficiently accurate results while reducing computational complexity. For this reason, it has been extensively used for conventional monohulls and remains central to the VPPs employed nowadays.

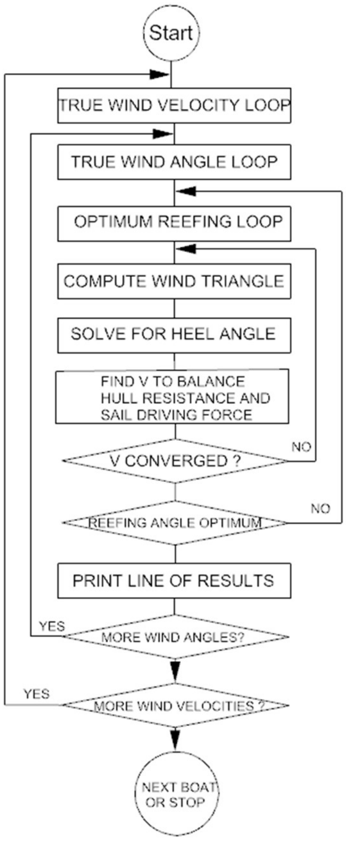

Figure 5 - Kerwin's simplified VPP flow chart (Kerwin, 1975)

Kerwin’s work ended up becoming the original Measurement Handicap System (MHS), which has evolved into the International Measurement System (IMS), when the Offshore Racing Council (ORC) decided to adopt it as its handicap system. Certain aspects of the research and core principles established in the Kerwin model have formed the basis for subsequent approaches, with improvements introduced over the years to specific components of the method. Since Kerwin's foundational work, numerous VPP tools and aerodynamic/hydrodynamic assessment methods have been developed to enhance and extend the original model’s capabilities. Some of these tools have been made commercially accessible to yacht designers, while the most advanced remain proprietary due to their strategic significance, especially in high-performance applications.

Peter Van Oossanen identified two possible approaches to determine vessel performance (Oossanen, 1993). The first approach uses Kerwin’s model that begins by calculating the driving and side force generated by the wind on the sails, then determining the boat speed, heel, and leeway angle at which aerodynamic forces reach equilibrium with hydrodynamic forces. The second approach, employed by the author, starts by assuming a specific boat speed, heel and leeway angle, then calculates the side force and resistance to derive the corresponding aerodynamic force on the sails to achieve equilibrium. This method shares the same theoretical foundation as the one established by Davidson (1936) in the tests that he has carried out.

Another improvement made by Oossanen (1993) was the inclusion of the concept of wave added resistance, which was previously neglected in most of the models available at the time. Oossanen work recognized that sailing in calm water was not representative of real-world conditions and therefore, included the wave added resistance into the models. He assumed that the wave direction always coincided with the true wind direction, which was a novel approach as only a limited number of studies had been conducted in this area at the time. The component of the resistance can only be considered when the wind direction is known. Other publications were made on this topic, by Gerritsma & Keuning et. all (1993), and later by Keuning & Sonnenberg (1998).

Later, Oossanen (1995) researched the impact of the rudder angle (to balance the yaw motion) by including an extra force-moment equilibrium, despite the previous iterations ignoring it due to the additional mathematical complexity required to solve an addition equation for rudder angles. In said research he concluded that when adding a rudder angle, the degree of flow separation is influenced, and therefore the centre of side force is seen to be shifted significantly, depending on the rudder angle. The optimum weather helm angles are perhaps smaller than often supposed.

As demonstrated, over the years, there has been a constant effort to improve the accuracy and reliability of the traditional VPPs whether by building upon past methods or creating entirely new ones based up on new testing methods. With time a different iteration urged, and new distinction came about, either traditional/conventional or dynamic. Traditional VPPs are the most used and the ones described so far. They provide a solution for steady state conditions, while the dynamic ones can model the time-varying nature of a boat's performance and consider changing wind and wave conditions as well as the boat's motion and crew actions. Dynamic VPPs are often used in racing situations where the goal is to maximize speed and can also be used in the design process to optimize a boat's performance.

2.2.1 Traditional VPPs

Traditional VPPs rely on a pre-determined database of a yacht's aerodynamic and hydrodynamic characteristics, including drag and lift coefficients as functions of apparent wind angle, to predict the yacht's performance. This database also includes coefficients to estimate hull and appendage drag. Using input values for true wind speed and angle, the VPP calculates the necessary force components and solves a system of non-linear equations to predict performance.

Aerodynamic data for the VPP is typically obtained through wind tunnel testing or numerical analysis and is stored for various sails or sail combinations, through the form of coefficients.

As for hydrodynamic data, there are two main methods. The first uses empirical regressions based on towing tank test results across a range of hull designs, often applied to custom-built yachts with limited budgets, though this approach is generally less accurate for unique hull shapes. The second method involves detailed analysis of the specific hull shape, either through physical or numerical towing tank tests, allowing for a more precise assessment of factors contributing to the vessel’s total resistance and lift. The total resistance of a sailing yacht comprises multiple components: the upright resistance, the increased resistance due to heel, induced resistance, the profile drag of the keel and rudder and added resistance from sea state (often excluded due to prediction difficulty.

Conventional VPPs typically generate polar plots of optimal boat speed as a function of true wind speed and angle. The IMS VPP, which was developed for the Offshore Racing Congress (ORC, 2024) to make handicap calculations for yachts in races and regattas, is one of the most widely used conventional VPPs. Other commercial programs like Maxsurf VPP and WinVPP are also available in the market.

2.2.2 Dynamic VPPs

In recent years, there has been a trend towards evaluating the performance of sailing yachts not only in steady-state conditions, but also in unsteady-state conditions and dynamically over time.

Unsteady motion refers to a more realistic scenario in which the boat experiences acceleration in its degrees of freedom due to changes in wind and waves over time, or because of adjusting the rudder angle, which serves as the boat system's input variable. When in motion, various actions such as forces and moments of inertia also impact the boat and must therefore be considered in the dynamic equilibrium equations. In these conditions, time is explicitly represented in the equations that govern motion, resulting in a set of differential equations (often non-linear) that must be integrated in the time domain, well described in Fossati (2013) and Böhm (2014). Dynamic VPP can be divided into two main categories:

1) Classical, coefficient based VPPs that have been extended to include manoeuvring using measured data.
2) Direct calculation approach of all time-dependent aero-hydrodynamic data.

The first approach aims to simulate the velocity losses that occur during tacking and gybing to optimize these manoeuvres. This problem has been approached from several different angles, including the tacking model developed by Keuning et al. (2005) which relies on empirical coefficients to predict manoeuvring behaviour.

The second approach improves the accuracy of performance prediction by directly calculating the actual fluid dynamic properties of the yacht over time. These predictions are still typically evaluated using a velocity polar plot or a chart showing the time difference to cover a nautical mile under different conditions. One advantage of this method is that it allows for the easy incorporation of unsteady effects. For the present study, we will only consider the steady state problem and examine the fundamental principles underlying the mathematical models used to calculate sailing boat performance.

2.3 Hydrodynamics of Yacht Hull and Appendages

2.3.1 Towing Tanks and Model Testing

The methods for assessing the hydrodynamics of yacht hulls and appendages have progressed significantly since initial insights were derived from towing tank tests. Traditionally, experiments were frequently conducted to establish foundational formulations. Today, resistance prediction relies on three methods, model testing, empirical approaches, and computational techniques, all of which are extensively used in marine design (Larsson, 2010). One of the major challenges initially, in the study of the hydrodynamic forces, has been replicating real sea conditions within the constraints of experimental facilities such as towing tanks. While towing tanks can provide valuable insights into a vessel's performance, they have some limitations. In a towing tank, the model is typically subjected to very low wind speeds, if any at all, while on open ocean the wind represents a significant force acting on the sailing vessel. As a result, the aerodynamic forces acting on the model in a towing tank may not accurately reflect those that experienced in the real sea. Current practices in international towing tanks largely adhere to the ITTC-78 procedure, which was last updated in 1984 (ITTC, 2000). Consequently, methodologies for assessing ship resistance in model testing have seen minimal change in recent years. A significant focus within model testing science remains on the accurate scaling of the various resistance components.

In 1868, William Froude provided the first comprehensive description of the mechanisms responsible for the waves formation of a hull moving through water. Froude identified two primary wave systems generated by a body at the water’s surface, known as Kelvin wave systems. These systems, originating at the bow and stern, collectively contribute to the wave-making resistance or in other terms residuary resistance. Froude’s investigations enabled the development of towing tank tests by considering gravitational forces, facilitating results that can be extrapolated to full scale. Initially, these testing methods were applied primarily to merchant vessels and warships rather than to yachts.

The first recorded experiments to try and enhance the performance of racing yachts using a towing tank occurred in 1901, performed by George L. Watson. The goal was to try improving the chances of success in the America's Cup Challenge and involving eleven yacht models. Although the results were not favourable, it was evident that the America's Cup competition amongst others would drive advancements in sailing technology (Böhm, 2014).

The first successful towing tank test was achieved in 1936, where Davidson determined the resistance of a yacht by considering the influence of sail forces on dynamic trim and sinkage. This work set the foundation for modern towing tank tests on yachts and has been further developed and improved since then (Davidson, 1936).

In 1974, researchers at TU Delft began to study the impact of different hulls on wave-making resistance. To do so, they developed new hulls based on parent hull form and changed only certain parameters. These hulls were then assessed in an upright position in a towing tank. From the results of these several tests, it was possible to estimate the influence of the hull form parameters in the upright resistance, which led to a method that empirically estimates the wave resistance of a yacht as a function of its form.

The so-called Delft Systematic Yacht Hull Series (DSYHS) is still being expanded and has undergone several iterations since its inception, including the inclusion of modern yacht lines. According to Keuning & Sonnenberg (1998), the DSYHS method focuses on analysing the bare hull without appendages to facilitate the creation and evaluation of new appendages. This includes the study of vessel's trim, leeway, and heel to calculate the ship's resistance and side force. The DSYHS is a polynomial regression based on experimental data and over fifty models were tested as bare hulls at Froude numbers ranging from 0.1 to 0.6 in three different conditions (upright, upright with trim, and heeling 20 degrees) to assess the impact of trim and heel. In towing tank tests, the three degrees of freedom considered were heave, roll, and pitch.

Later, Keuning & Katgert (2008), present updated results. The objective of this newer paper was to demonstrate that sailing yacht hulls have evolved over time, resulting in higher speeds, which required more tests. The number of tested models in the DSYHS increased to 56 in this updated version. This new iteration, known as Series 7, also expanded the range of tested speeds, reaching a Froud number of 0.75. The DSYHS is still a highly regarded tool in the field of yacht hydrodynamics and is widely used due to its reliability, flexibility, and ease of use, especially during the pre-design and early design phases. The method is well documented and has been throughout the subject of several publications, particularly by Gerritsma et. al (1993), Keuning & Sonnenberg (1998), Gerritsma et. al (1981). In addition to the formulas derived for calculating the hull's upright resistance, some more complementary formulas for determining the added resistance due to heel were derived, as well as methods for approximating the impact of the appendages on the overall resistance. The Delft Systematic Keel Series (DSKS) was developed to calculate the influence of the appendages (Beukelman & Keuning, 1975; Gerritsma & Keuning, 1985).

At the same time, other interactions were made using towing tank, Oossanen (1986) provided a detailed description on the model testing techniques used at the Maritime Research Institute Netherlands (MARIN), that made possible to predict full-scale performance more accurately than before. The detailed description published, consisted of preforming several tests, carried out at various angles of heel and yaw, using the sails centre of effort as the towing tank point. With the model acceleration a side force on the keel, rudder and canoe body is generated, which by itself induces a force momentum due to the model wanting to heel and adopt a different yaw angle. Strain gauge dynamometers fitted to the mast sense it, and counter it by lowering the vertical carriage mounted on the towing carriage and moving the tow-mast and longitudinally supporting the model. After 15 to 20 seconds, an equilibrium state is achieved, the tow-mast achieves a position where the axial force and momentum are zero in accordance with the physics of sailing.

2.3.2 Computational Fluid Dynamics

Despite all the results that derived from towing tanks and model testing, the developments in technology brought new complementary techniques to study the hydrodynamics of sailing vessels. Advancements in computing power have introduced new opportunities for applied methods, enabling computational results to achieve greater accuracy and faster processing times. Consequently, the potential for Computational Fluid Dynamics (CFDs), to eventually replace traditional tank testing in marine technology has been a topic of longstanding debate. Larsson, among others, has suggested that this transition will occur eventually (Larsson, 1998; Larsson et al, 2010). However, to date, CFD advancements have also driven improvements in tank test measurements by providing a valuable benchmark for comparison (Fossati, 2009).

The successful Americas Cup Winner Australia II, that ended the longest winning streak in sailing sporting history, used the combination of towing tanks tests and CFD to study a new vigorous design, the winged upside-down keel. The combination of the two methods eventually lead it to victory, see Oossanen (1986). The use of CFDs become widely used in yacht design in the early 1980s following Australia II success (Rosen et al, 2000, proving to be a new landmark in assessing the hull and keel hydrodynamics and been since then growing in popularity.

The techniques employed at the time used simplifications as potential flow solvers that assumed the fluid was inviscid, incompressible and irrotational (ideal) and were primarily used for the design of appendages such as keels and rudders. These assumptions allowed the problem to be transformed into a simpler algorithm, which only required discretizing the boundary of the physical domain. This made the models linear, as opposed to the non-linear full governing flow equations. The simulations can be computationally intensive, and it resulted in a significant reduction in computational cost, making CFD practical for large-scale applications at that time. As described by Larsson (1990), the availability of more powerful computers made it possible to run larger and more detailed simulations and eventually expanded to include hull design as well.

The future of CFD in marine applications appears highly promising, with an ongoing shift toward simulation-based design. A significant transformation has already taken place, as design processes now rely primarily on simulations, with physical testing reserved primarily for the final validation stages. This transition has raised new requirements for the precision and procedures of tank testing. Today, simulation is extensively applied across all aspects of hydrodynamic design, including resistance and propulsion, seakeeping, manoeuvring, stability, and capsize analysis. With continued advancements in computational power and CFD tools, computational hydrodynamics is expected to expand and become widely accessible, empowering engineers to create safer, more innovative, and cost-effective solutions to address the challenges of the 21st century (Stern et al. 2013).

Today, it is technically feasible to replace the traditional VPP solver entirely with CFD software to solve the full equilibrium of a yacht. Achieving this requires integrating both hydrodynamic and aerodynamic models within a single simulation, including multiple degrees of freedom and a moving rudder to maintain yaw stability. Substantial progress toward a fully numerical VPP has already been made, and the subject is currently under research within the sailing dynamics program at Chalmers University. A fully numerical VPP using RANS simulations for the hydrodynamic component and a panel method for aerodynamics was introduced at CSYS in 2005 (Jacquin et al. 2005). Additionally, Kristoph Böhm presented a fully coupled VPP in his PhD thesis, employing a RANS code for hydrodynamic forces and the empirical Hazen model for aerodynamic forces (Böhm, 2014).

The evolution of these methodologies has played a crucial role in enhancing the accuracy of VPP over the years. The various tests and experiments conducted have led to significant advancements in theoretical knowledge related to sailing yachts. These studies have aimed to translate practical observations and real-world performance into a solid theoretical framework. As more data has been gathered from diverse sources, the available information has improved, allowing for more accurate correlations between boat speed and design characteristics. Specifically, in this context, it has facilitated a better understanding of the relationship between hull and appendage design and the resistance or drag generated when interacting with water.

2.4 Aerodynamics of Yacht Rig and Hull

Over the years, sailors have continuously sought to enhance the design of yachts to achieve faster, more stable, and more efficient vessels. Advances in materials and construction techniques have played a crucial role in this pursuit, but the development of better aerodynamic performance stands out as the most crucial factor. The experimentation with different shapes and sizes of sails and rigging configurations has led to improved sail tune and aerodynamics, resulting in increased speed and efficiency from wind power.

The aerodynamics involved in sailing yachts is a challenging aspect of predicting performance and is considered one of the most difficult parts of the VPP theory. The aerodynamic model is responsible for determining the forces that make up the vessel's thrust, and there are various methods for obtaining these forces.

2.4.1 Full-Scale Measurements and Model Testing

For an extended period, quantifying sail forces posed a significant challenge. The first method to address this issue was described by Davidson (1936). This method involved calculating the lift and drag forces on a sail using coefficients that consider the heel, wind speed, and direction, all derived from towing tank data. Davidson initially addressed the challenge of employing scale model testing to predict upwind performance, conducting preliminary experiments in the campus swimming pool, which often perplexed his classmates. His early research efforts culminated in securing a $5,000 grant from the Research Corporation of New York, allowing him to construct an experimental towing tank equipped with sensitive dynamometers affixed to small-scale models. The testing conducted in this facility was correlated with full-scale trials under real-world conditions. The vessel “Gimcrack” was outfitted with over 70 data points and a damp-spring dynamometer capable of measuring both side force and drag. With her mast and rigging in place, Gimcrack was towed from Larchmont to City Island, New York. The results from the side force measurements of the scale model and Gimcrack were combined to create an upwind performance prediction methodology, leading to the formulation of sail force coefficients known as the “Gimcrack Coefficients.” These coefficients were instrumental in determining drag at the points where the heeling moment produced by the sails equalled the righting moment of the hull.

Davidson's approach assumed that the aerodynamic forces could be reduced to a single point of application, the centre of effort of the sails, based solely on the geometries of the rig. This single resultant sail force premise indicates the absence of an irreducible aerodynamic couple, positing that the resultant sail force vector is situated within a plane orthogonal to the mast. The state of the yacht during full-scale trials is characterized by various parameters, including the heel angle, forward speed through the water, rudder angle, relative wind speed, and relative wind direction, with the assumption that these conditions remain stationary. Notably, Davidson's initial approximation overlooked the rudder angle.

To replicate these conditions at the model scale, full-scale tests must be conducted in calm water, as measuring and reproducing the wave spectrum encountered for this specific purpose is nearly unfeasible. Moreover, minimizing fluctuations in wind velocity is critical, as ideal conditions for full-scale yacht testing are challenging to achieve. For instance, during the trials of Gimcrack, some runs at elevated wind speeds were reportedly influenced by sea waves, as noted by Davidson himself. Subsequent studies were conducted to review and refine Davidson’s “Gimcrack” Coefficients enhancing the methodology for predicting sail performance.

Following Davidson’s method, another boat submitted to this methodology was the “BayBea”, and the results demonstrated by Kerwin (1975). The Delft Shipbuilding Laboratory also directed extensive model and full-scale tests with the America’s Cup Yacht “Standfast”, and the results were published by Gerritsma & Kerwin (1975).

These tests combined full scale measurements with the corresponding model tests. Building upon the original method, the rudder angle was also included as a variable to characterize the situation of the yacht. The full-scale testing, at the time, was accomplished using sailing dynamometers. These comprehensive measurement systems are mounted on sailing vessels to accurately determine sail forces under real-world sailing conditions. Full-scale testing was acknowledged as a crucial method of investigating sail performance, as the results obtained from model testing may not accurately reflect the behaviour of full-scale systems, due to variations in size and material properties. Full-scale testing has the advantage of providing measurements in real-world conditions, accounting for wind variations, changes in yacht motion, adjustments made by the person steering the vessel, and modifications to the sails. From the two different model testing Gerritsma and Kerwin concluded that the trend observed in the “Standfast” data closely aligns with the averaged curves from “BayBea”. Data points that are significantly below the curve likely indicate unfavourable conditions. The high driving force coefficients recorded at a relative wind angle of 160 degrees occur at elevated wind speeds, which may be further amplified by surfing.

Gerritsma et. al. (1993) performed tests out in deep and calm water, to minimize the additional resistance that could be caused by shallow water waves. All parameters related to the ship's performance in wind and water were measured. From the results, they concluded that the “Gimrack” coefficient was reasonable when compared to full-scale tests and sailing upwind, specially under the wind speed range of 5-7 knots. At this range, the resistance of the vessels is typically on the steeper portion of its resistance curve, leading to a disproportionate increase in driving force with even small increments. The Davidson's method has been found to predict higher speeds than expected at higher wind speeds (approximately 20 knots), possibly due to the consideration of waves and ship motions by Gerritsma. The Gimcrack method, on the other hand, assumes all different sized foresails to have the same area value of the foretriangle under varying wind speeds, which could also contribute to such deviation. For example, the genoa area at 20 knots is about two-thirds of its area at lower speeds.

2.4.2 Wind Tunnel Experiments

The first breakthrough post Davidson's coefficients was conducted by Marchaj (1996) throughout the 70's, which had its foundations from a new oriented data, wind tunnel experiments. The experiments carried at the University of Southampton, led to important improvements in the understanding of aerodynamic loads in sailing yacht were made which helped establishing the principles of sail aerodynamics. Improvements to this investigative method were achieved through the development of specialized twisted-flow wind tunnels, which closely simulate the aerodynamic flow that a yacht encounters in real-world conditions. Hazen's aerodynamic model (Hazen, 1980) is also derived from wind tunnel testing and provides lift and drag coefficients at five different angles for each sail.

The new iteration of the wind tunnel allowed also to study the effects of vortex flow through the sails. These aimed to provide a realistic simulation of real-world wind conditions for yacht testing. They were specially designed to simulate changes in wind speed and incident angle over height caused by the movement of the yacht. The tunnels were equipped with a series of vanes or blades that were oriented to generate a swirling flow field around the test model. The speed and intensity of the flow could be controlled to simulate different flow conditions.

The first of these tunnels was built at the University of Auckland to undertake research for Team New Zealand's campaign for the 29th America's Cup in 1995, and the results were published by Flay (1996), where the author concluded that wind tunnel testing can be also useful for evaluating sail performance, and even basic wind tunnel designs can be effective as the required speed is not particularly high. The wind tunnel model described in this paper had a successful history and was used regularly to evaluate sails for several hours each day, from 1994 to 1995. Soon other facilities were also built, as described by Fossati et. al (2006), in Milan.

2.4.3 Computational Fluid Dynamics

CFDs, are also a worthy mention as they represent another possible method to assess the pressure distributions around the sails of a sailing yacht. Potential flow methods are commonly used to analyse the flow of air over sails when a boat is sailing up-wind (or close-hauled). To accurately study the behaviour of the sail, the flow of air must be combined with a structural solver that accounts for the sail's deformation and elasticity. Structural solvers used nowadays for this purpose are based on the membrane theory. These solvers may be combined with vortex-lattice methods to study the flow of fluids around the sail. When the flow of air over a sail is expected to be separated and form a turbulence, viscous flow simulation must be used to accurately understand the behaviour of the sail. This is particularly important for downwind sails, as the flow over these sails can be complex and difficult to analyse. Viscous flow simulation considers the effects of viscosity (such as friction) in the fluid, which is important in understanding the behaviour of turbulent flow. In terms of mathematical complexity, performing an analyses considering viscous flow is more demanding than potential flows. It is common to study the aerodynamics of sails using any of the mentioned methods. Full-scale tests often involve comparing the performance of two similar boats, while wind tunnel tests are used to measure aerodynamic forces, and numerical methods used to calculate the pressure on sails. In recent years, advances in technology have increased interest in full-scale and wind tunnel pressure measurements. More recently, Viola & Flay (2011), performed an investigation on the pressure distribution on sails considering the three methods: full-scale measurements, wind-tunnel measurements, and computational fluid dynamics, in which the following conclusions were made:

1) Overall, the pressure distributions calculated using the three methods were found to be in good agreement with each other. In particular, the pressures computed using numerical techniques were very similar to those measured in a wind tunnel. However, measurements taken on a full-scale downwind sail showed the largest discrepancies, likely due to the tighter sail trim used in the full-scale measurements to prevent the spinnaker from collapsing in gusty wind and wave conditions.
2) Full-scale testing considers dynamic effects like wind fluctuations, yacht movement, course corrections, and sail trim changes, resulting in a tighter trim of the asymmetric spinnaker compared to wind tunnel measurements. While upwind conditions showed good repeatability in pressure measurements, downwind conditions were unsteady, leading to low repeatability and accuracy. Both conditions indicated that pressure distributions could enhance sail trim or shape, and real-time pressure measurements could improve onboard sail trim and aid in sail design. Wind tunnel tests allow a more controlled and stable environment, where pressure measurements, forces, and flying shapes were measured simultaneously. Both rigid and flexible sails were tested in the wind tunnel. Flexible sails allowed for easy modification of sail trim, as in full-scale testing, while rigid sails provided better control of sail shape and better test repeatability. Both methods were effective in studying the effects of sail trim on pressures and aerodynamic forces.

As detailed by Böhm (2014), there are now two main approaches to describe the aerodynamic loads on a sailing yacht. The first approach uses an explicit sail shape or trim, where program must have access to all possible sail configurations and their corresponding force coefficients, which make up a test matrix. This allows the VPP to determine the optimal sail shape for a given wind condition and boat state. The advantage of this approach is that the force coefficient of each individual sail can be precisely described, including the effect of depowering due to its trim. However, sail shapes cannot be linked to their trim setting. This explicit method is used in computational fluid dynamics (CFD) applications for competitive sailing teams but is not suitable for the purpose of this text due to its level of detail. The second approach has an implicit description of sail trim, where only one optimal sail trim must be found and any effect on sail shape is accounted for by a penalty. This simplification, which basically means not linking the aerodynamics of sails to their actual shape, is simpler and suitable for preliminary design VPPs. This approach is also known as the Kerwin model.

3. OCEANVPP ARCHITECTURE

The present chapter outlines the architecture of OceanVPP, focusing on two main stages: defining the equilibrium conditions of a sailing yacht and solving them. The equilibrium conditions describe the balance of forces and moments acting on the yacht, capturing its dynamic motion under various sailing conditions. The second stage involves solving these conditions using numerical algorithms to determine key metrics, such as speed, heel, and possibly leeway angles. Together, these stages form the core of OceanVPP, enabling accurate analysis of sailing yacht behaviour. The developed tool, like any VPP, requires the user to input the desired run configuration. Parameters such as true wind speed and angle must be specified. For more detailed information on the user interface, please consult Appendix I.

3.1 Sailing Yacht Equilibrium Conditions

In this chapter, the forces and moments that act on a sailing boat will be thoroughly analysed and described. The behaviour of a sailing boat is determined by six equations, which will be dissected and explained in detail. The evaluation and understanding of these forces and moments are crucial for the design and performance of sailing boats, as they govern the stability, handling, and speed of the vessel.

The architecture of most modern sailing yachts is well described by Larsson et. al (2022) and Fossati (2013) while more technical details of its incorporation on a VPP can be found in Oossanen (1993).

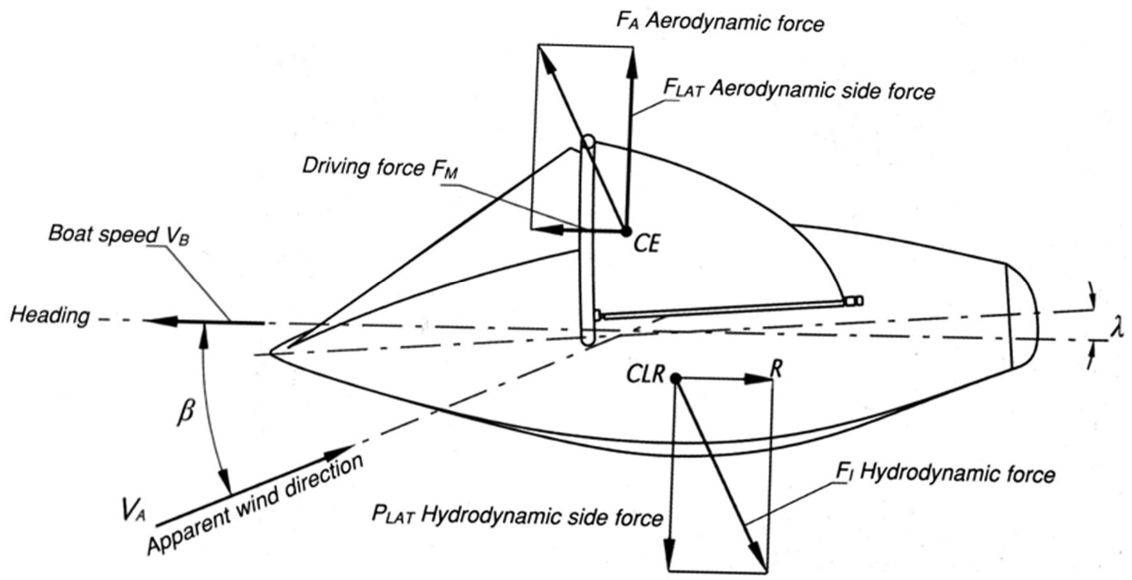

Figure 6 - Forces on sailing yacht (Fossati, 2013)

Figure 6 presents the elementary forces in play on a sailing yacht under equilibrium conditions. This top view displays the longitudinal and lateral components of the forces. For the yacht to move through water, a resistance (R) must be overcome through a driving force (F_M) from the sails. However, this generates a side force (F_{LAT}) that must be countered by a hydrodynamic side force (P_{LAT}) to maintain the balance. To ensure the roll moment under equilibrium is zero, the aero-and hydrodynamic forces must act along the same line. The leeway (λ) is the sideways range of movement caused by the wind forces acting on the sails and the hulls sideways resistance, that neglects the boat from drifting. It is therefore the result of the wind pushing the boat off course, away from its intended heading. Leeway can be a significant factor in sailing, particularly when sailing close-hauled (lower sailing angles, with the sails trimmed in tight to the wind) or in strong wind conditions. Notably, the resulting aerodynamic side force acts perpendicularly to the mast, a principle established by Davidson (1936) and subsequently adopted by all investigators in the study of sailing yacht performance

Figure 7 provides an additional perspective on force balances by illustrating the vertical and lateral components of the forces acting on the yacht. Specifically, the aerodynamic force (F_H) includes a transverse component relative to the boat, which must be considered, as it is countered by the hydrodynamic lift (P_l) generated by the submerged sections. The distance h between these two forces results in a heeling moment.

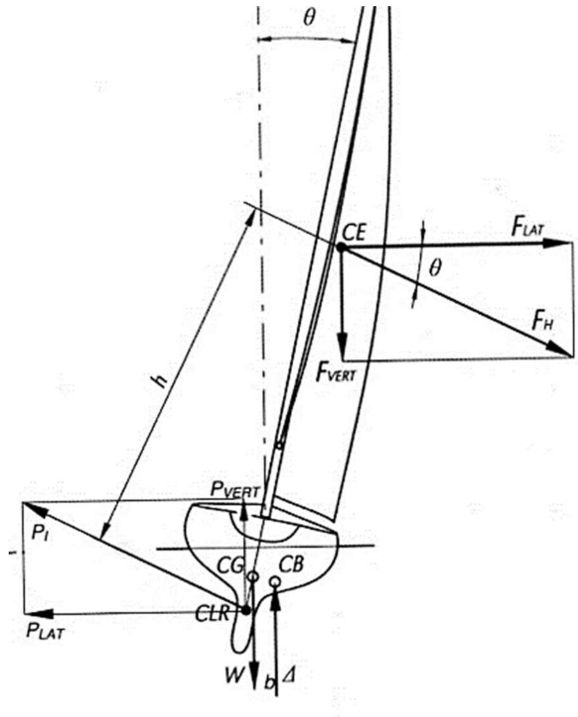

Figure 7 - Forces on sailing yacht II (Fossati, 2013)

It is relevant to revisit the application point of the aerodynamic force at the sail plan's centre of effort (COE) positioned at a specific height above the waterline. The aerodynamic heeling force exerts both a lateral force, inducing leeway, and a heeling moment that causes the boat to heel towards the leeward side. Similarly, the hydrodynamic lift acting at the centre of lateral resistance (CLR) (Chapter 4.1.3), located at a particular depth below the water’s surface, not only counteracts leeway but also contributes to the overall heeling moment. The heeling moment produced is counterbalanced by a righting moment generated by the combined effect of the yacht's weight and the buoyancy force.

The VPP depends on achieving equilibrium in both forces and moments. In more advanced VPPs, multiple equilibriums are considered, with the most critical being:

- Force equilibrium in the sailing direction (governed by speed)
- Moment equilibrium in the heel direction (governed by heel angle)
- Force equilibrium in the sway direction (governed by leeway angle)

The system of equations governs the dynamic equilibrium of a boat on the water plane under steady-state conditions, where neither boat nor the wind speed change, whether in magnitude or direction. While these conditions represent an idealized scenario, as actual sailing involves fluctuations in both wind speed and direction, leading to varying motion states and accelerations, the boat is consequently subjected to inertia forces that oppose acceleration. The steady-state motion approximates conditions such as those experienced in light wind on calm seas. To solve these, the procedure involves adjusting the free parameters until the equilibrium equations are satisfied. Once all equilibrium condition are met, the yacht is in a realistic sailing condition, known as equilibrium condition. While the number of free parameters can vary, at least speed and heel angle must be included to derive a viable solution.

The developed tool, as previously mentioned, considers two degrees of freedom to predict the final velocity and heeling angle. These degrees of freedom are thoroughly explained in Subchapters 3.1.1 and 3.1.2, with their code implementation detailed in Appendix **II**.

3.1.1 Velocity Calculation

The longitudinal force equilibrium, composed by the driving force from the sails is equal to the hydrodynamic resistance of the yacht in the direction of travel.

$$F_x = F_M - R_{tot} \tag{1}$$

The equilibrium condition in the x-direction ($F_x = 0$) determines the vessel's velocity, governed by the propulsive force generated by the wind on the sails, commonly referred to as "thrust" or driving force. Concurrently, the total hydrodynamic resistance due to the hull and its appendages acts as a counterforce, causing a reduction in velocity. In the sailing direction, force equilibrium is maintained by adjusting the yacht's speed to align the driving force from the sails with the resistance of the hull and appendages. However, since the yacht's speed depends on the driving force, direct determination of speed is not possible and must be iterated to convergence. Both the resistance and the sail forces are influenced by the heel of the yacht.

3.1.2 Heel Angle Calculation.

The heeling moment due wind acting on the sails must be matched by the righting moment from the hull.

$$M_x = M_{right} - \ M_{heel} \tag{2}$$

The righting moment, which is determined by the hull's initial stability, allows for more sail area and higher speeds. When the righting moment (M_{right}) equals the heeling moment produced by the heeling force applied at a distance (h), the heeling moment (M_x) is canceled out. Crew effects can also be factored into this equation, depending on the intended accuracy of the results. The heeling moment results from the side force of the sails. Thus, the heel, along with the speed, must be iterated to achieve equilibrium. More regarding these two moments on the following Chapter for the heeling moment and Chapter 6.1 for the righting moment.

3.1.3 Leeway Angle Calculation

The hydrodynamic side force acting on the hull, keel and rudder must equal to the aerodynamic side force.

$$F_y = F_{lat} - P_{lat} \tag{3}$$

The equilibrium condition in the y-direction ($F_y = 0$) determines the drift or leeway angle (λ) in equilibrium. The aerodynamic side force, denoted as F_{lat} is generated by the airflow over the sails and hull, acting perpendicular to the yacht's mast. Conversely, the hydrodynamic side force, denoted as P_{lat} arises from the water flow over the hull, acting in the opposite direction of the aerodynamic force. These side forces play crucial roles in yacht design and performance, impacting stability and handling.

At small apparent wind angles, the side force from the sails can exceed the driving force, potentially causing excessive sideways movement through the water. To counteract this, hydrodynamic side forces generated by the keel and rudder come into play. These forces can be produced by asymmetric foils or through an angle of attack on the hull and keel, known as the leeway angle. Although most yacht appendages are symmetrical, they still require a leeway angle to create side forces. The equilibrium of side forces is primarily controlled by the leeway angle, typically ranging from 1-5 degrees. Consequently, the side force from the sails is often considered independent of the leeway angle, allowing for direct determination.

3.1.4 Additional Equilibriums

The boat's vertical equilibrium equation is defined by its buoyancy minus the sum of the displacement and the resultant of aero-hydrodynamic vertical forces.

$$F_Z = B - (\triangle + F_{aero-hidroV}) \tag{4}$$

The buoyancy of the boat is one of the main forces acting on the boat in the vertical direction, plus the displacement of the boat, which is the water weight that the boat displaces as it floats. In addition, there may also be aero-hydrodynamic vertical forces acting on the boat. These forces are generated by the flow of air and water and can include lift and drag forces. The vertical equation of a boat considers all these forces to determine the balance of forces acting in the vertical direction.

For the moment's equilibrium, not only the magnitudes of the forces are considered but also the distances between the points of application of the forces are involved. It is considered that the aerodynamic forces are applied at the centre of effort of the sailboat, COE, and the hydrodynamic forces are applied at the centre of lateral resistance (CLR).

The heeling moment M_y results from the binary $F_M - R_{tot}$, and causes a forward dip which in turn will result in a longitudinal repositioning moment due to the longitudinal displacement of the vessel's centre of thrust.

$$M_y = F_M \cdot d - M_{Long} = 0 \quad (5)$$

The moment in the z-axis (yaw moment) is caused by the longitudinal distance, a, called "lead". This moment can be cancelled by the rudder action, which for a given λ_L, controls the longitudinal position of CLR.

$$M_z = F_H \cdot h = 0 \quad (6)$$

Despite all demonstrated moments and equations, in practice, most speed prediction programs solve only require equation (1) and equation (2), and optionally include equation (3), to solve for the leeway angle (Claughton, 1999). To reach the equilibrium conditions (1) to (6) the vessel will adopt a navigation attitude defined by the sailing velocity (V_B), the heeling (φ) and leeway angle (λ). According to Bettencourt et. al (2015) the values of these variables depend on the vessel's parameters and the environmental conditions TWA and TWS so that the following is generally true:

1. When sailing close-hauled the heeling force (F_H) is significantly higher than the driving force (F_M), so the boat will adopt a heel angle (φ) to counteract the heeling moment, produced by the sails, and a leeway angle to prevent drift. Under these conditions, the speed of the boat is relatively low because of heel and drift on the boat's resistance.
2. When sailing on a beam reach (wind perpendicular to the bow), the heeling force (F_H), and the driving force (F_{drive}) have similar orders of magnitude and although the heeling force is still high, the increase in (F_{drive}) allows the boat to reach higher speeds.
3. When sailing at TWA greater than the situation described in point 2, characterized by a decrease in the AWS and consequently the need to use a larger sail area to maintain or increase the driving force. Under these conditions, the heeling force is also reduced compared to the driving force and therefore the heeling (φ) and leeway angled (λ). will be smaller than in situation 1 or 2.

3.2 Equilibrium Condition Solver

An important part of a VPP is its solution algorithm or iterative loop. The loop solves a nonlinear problem, with the end goal of maximizing the objective variable, the sailing yacht speed. The problem requires initial guesses for the decision variables, and based on its values verifies if the result converged. When the convergence is achieved it uses the latest obtained values as inputs for the initial guesses and keeps running until the result respects the desired tolerance. In this iterative procedure, the state variable is the velocity with the reefing and flattening being decision variables, that are under constant change (for 3-DOF). When the solution is found, the software follows by calculating multiple possible combinations of different true wing angles and speeds, which leads to the VPP results often displayed in a polar plot.

There are many possibilities on which methods can be used to solve the nonlinear problem system, one of the most used is the Newton-Raphson method. This method offers several advantages. First, it converges quickly for sufficiently well-behaved functions, often requiring fewer iterations compared to other methods. Second, it allows for efficient computation of derivatives, which is crucial for nonlinear systems. Third, it provides local convergence guarantees, meaning it will converge to a solution near the initial guess under certain conditions. Lastly, it's versatile and can be adapted to handle systems of equations with different dimensions and complexities. In this work, the nonlinear system defined by the equilibrium conditions was initially solved using the Newton-Raphson method. However, the initial implementation lacked optimization, resulting in slow convergence. To address this issue, a MATLAB function was adopted. This function minimizes a constrained nonlinear multivariable function, with constraints including physical limitations such as reasonable hull speeds and heeling angles.

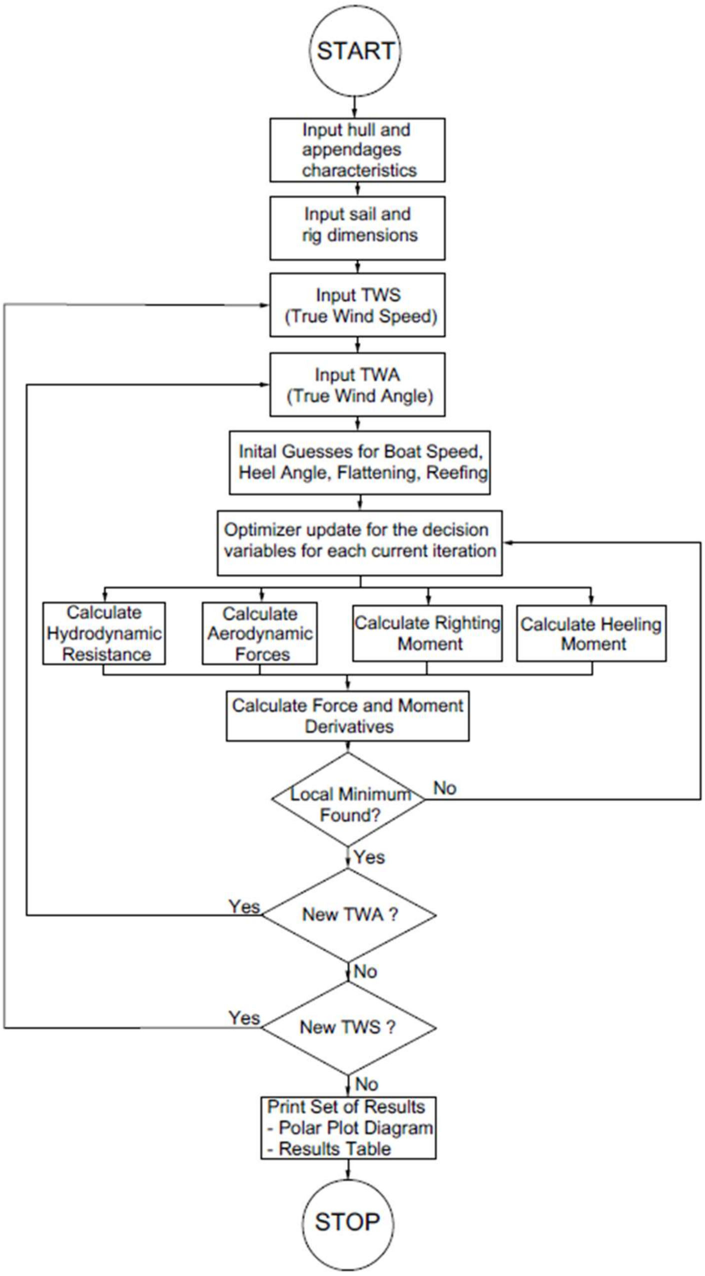

Figure 8 - OceanVPP flow diagram.

The process for performing a VPP analysis, as illustrated in Figure 8, involves a systematic sequence of steps to determine the potential speed and performance of sailing vessels under various conditions. Initially, the geometrical parameters and physical properties of the hull, sails, and rig are specified. These inputs are crucial for accurate hydrodynamic and aerodynamic calculations. Initial estimates for all decision variables, based on the first wind combination, are provided. These estimates serve as a starting point for the optimization process. An optimization algorithm then updates these decision variables based on the outputs of the current iteration. The objective is to identify the combination of variables that yields optimal performance in terms of speed and stability.

The initial guess for the velocity (V_0) is calculated based on a hull speed coefficient of 1.25, but if the TWS is less than or equal to the calculated V_0, it is adjusted to 80% of TWS. Regarding the other decision variables, the initial guess for the heeling angle is set to zero degree and the flattening and reefing of the sails is set to 1.

Using the initial estimates, the hydrodynamic and aerodynamic models calculate the forces acting on the yacht. The hydrodynamic forces include resistance caused by the hull shape and water flow around it, along with the resistances the keel and rudder, which significantly impact the overall drag in the water. The aerodynamic forces generated by the sails, driven by wind pressure, include the driving and heeling forces.

The positions of the centres of effort for both hydrodynamic (CLR) and aerodynamic (COE) forces are also assessed. The derivatives of forces and moments with respect to the decision variables are then computed to understand how small changes in these variables affect the overall performance and stability.

The optimizer checks if a local minimum in the objective function (maximum speed) has been found. If a local minimum is not found, the optimization loop continues with updated estimates. If a local minimum is found, the program checks if there is a new true wind angle to analyse. If so, the process restarts from the input of the new TWA and using the previous results as the new initial guesses. If there are no new true wind angles, the program checks for new true wind speeds to analyse and re-runs for all TWAs.

Finally, if there are no new true wind speeds to analyse, the process concludes, thereby completing the VPP analysis. This sequence provides a structured approach to simulating and optimizing the performance of sailing vessels under various wind conditions. Each step iteratively refines the estimates to achieve the most efficient configuration for sailing, considering the complex interactions between the hull, sails, rigging, and environmental factors.

4. HYDRODYNAMIC MODEL – OCEANVPP

In this chapter, the essential concepts of sailing boat mechanics and their interaction with the surrounding fluid will be presented. The present hydrodynamic model comprises the several resistance components necessary to the solution of a two DOF VPP. For additional DOF, components such as the buoyancy of the submerged body and the hydrodynamic side force need to be also assessed. A code snippet regarding the Hydrodynamic Model can be consulted in Appendix III.

4.1 Introduction

The hydrodynamic analysis of a sailing yacht requires an in-depth evaluation of each component constituting the submerged portion of the hull. Typically, this analysis is approached by isolating and examining the individual effects of each component, which allows for a more detailed examination of their specific influences on overall yacht performance. The resistance calculations for the canoe body, for example, have been well-researched and refined over the years, providing a robust framework for analysis. However, studies on the appendages, namely the keel and rudder, remain an area of evolving inquiry, as their effects on yacht dynamics continue to invite new methodologies and insights.

This approach, by focusing on each element individually, simplifies the analytical process and enables a more precise understanding of each component's unique impact. Nonetheless, the technique inherently relies on a series of approximations, which, when combined, can introduce significant discrepancies in predictive accuracy. Such limitations necessitate continuous advancements in hydrodynamic modelling techniques to reduce these approximations, ensuring that the interplay of forces acting on the yacht is as accurately represented as possible.

Alterations to the hull, keel, or rudder parameters invariably influence the yacht's performance, with the potential to either enhance speed or reduce hydrodynamic resistance. As such, ongoing research is directed at resolving ambiguities surrounding these parameters, with the overarching aim of optimizing both performance and drag reduction. The theoretical basis for the present model draw upon the foundational work of Keuning and Sonnenberg (1998). This model serves as a basis for understanding the influence of various hull forms and dimensions on hydrodynamic forces, providing a critical benchmark for evaluating modern performance prediction methods.

4.1.1 Canoe Body

The groundwork regarding the canoe body hydrodynamics has been set by the Technical University of Delft, whose work and testing facilities led to countless publications such as Keuning (1998), and Keuning & Katgert (2008), amongst many others, contributing to improvements and expansions of the DSYHS. The basis set created the sole acknowledged empirical model for predicting hydrodynamic forces. This approach relies on conducting regression analysis on a significant number of model hulls, where the hulls exhibit systematic variations in their characteristic parameters. The analysis is carried out in sets of ten model hulls, and the findings for each set have been publicly released. A standard design acts as the base hull, and several hulls are produced by modifying the characteristic parameters based on this original design.

The latest publication's polynomials are constructed using hulls that fall within the specified limits outlined in Table 1. If a hull lies outside these limits, the reliability of the method becomes uncertain.

Table 1- Range of Hull Parameters tested in the DSYHS (Keuning & Sonnenberg, 1998)

Parameter	**Min**	**Max**
Length - beam ratio $\left(\frac{L_{WL}}{B_{WL}}\right)$	2.73	5.00
Beam - draft ratio $\left(\frac{B_{WL}}{T_C}\right)$	2.46	19.38
Length - displacement ratio $\left(\frac{L_{WL}}{\nabla_C^{\frac{1}{3}}}\right)$	4.34	8.50
Longitudinal centre of buoyancy $(\boldsymbol{LCB})$ (%)	0.0	-8.2
Longitudinal centre of flotation $(\boldsymbol{LCF})$ (%)	-1.8	-9.5
Prismatic Coefficient $(\boldsymbol{C_P})$	0.52	0.60
Midship Area Coefficient $(\boldsymbol{C_M})$	0.65	0.78
Loading factor $\left(\frac{A_W}{\nabla_C^{\frac{2}{3}}}\right)$	3.78	12.67

As the method relies on polynomial fittings, even slight deviations from the data range can result in significant outcome variations.

4.1.2 Appendages

As mentioned before, there are still grey areas regarding the keel's behaviour. The appendages studies rely on the experimental data obtained from towing tank tests, and in recent years complemented with CFDs analysis and wind tunnel testing. The buffer in technology allows for more complex simulations to be made and to obtain more data on the test subjects Even still, some of the keel's most well-established principles have been set long ago from aircraft aerodynamics, the adaptation was easily made, considering the similar wing profiles, and the inherently fact that they both describe the interaction between fluids and solids. To be able to dissect and understand the impact of either the keel or the rudder on the sailing dynamics, a brief introduction needs to be made to the flow over a wing section. Figure 9 depicts the separation of inflow into two parts as it encounters the wing. One-part flows above the wing while the other below, with a dividing streamline separating them. The streamlines that run over the top part of the wing face a greater resistance or pressure upon contact. This asymmetrical pressure distribution also creates a discrepancy in velocity and two different phenoniums.

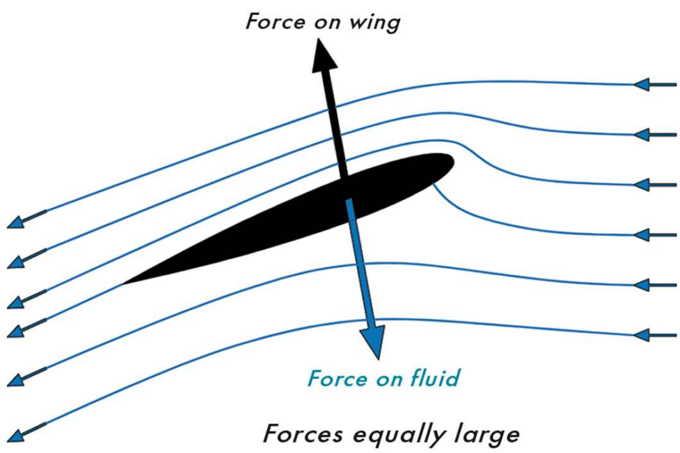

Figure 9 - Flow around a wing (Larsson et. al, 2022)

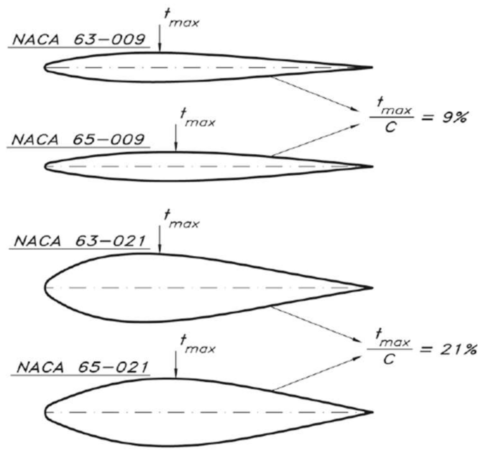

Figure 10 - NACA Profiles (Larsson et. al, 2022)

A greater pressure encounter leads to higher velocities, this difference between both sides creates a force on the fluid. As Newton's 3rd law states "If an object A exerts a force on object B, then object B must exert a force of equal magnitude and opposite direction back on object", which leads to our lifting force generated on the wing, acting upwards. The generation of the lifting force, led to the study of many new keel NACA profiles with the intent of malleablizing this force generation, while still overstating a drag reduction.

On sailing yachts, the wing profiles are generally symmetrical due to the obligation of performing well on both tacks. Figure 10 displays four different NACA profiles, they consist of different shaped wing sections, with some variations amongst them regarding their shape parameters (camber, chord length, thickness, etc).

The impact of parameters such as the thickness or camber ratios has been studied to obtain a better knowledge of the impact of shape on section characteristics. Abbott, et al. (1959) conducted comprehensive research in this field, emphasizing not only the theoretical aspects of wings and wing sections, but also providing a detailed exposition of the geometry and properties of numerous sections.

Along with new NACA profiles there has been many new different shaped keels over the years, from the plain deep keel to the winglet keel, or even the canting keel, naval architects have sought to develop the most optimum keels for yacht racing and cruising. The discrepancies of said keels, and their shapes, also led to many publications. For example, Beukelman & Keuning (1975) studied the impact of changing the fin keels sweep-back angles from 0, 20, 140 and 6 degrees. Many iterations and approaches were compiled, regarding the different configurations. To settle and regroup all the new designs into a uniform bundle, the DSKS was created.

4.1.3 Centre of Lateral Resistance

The centre of lateral resistance is a focal point on the hydrodynamics of a sailing vessel and represents the theorical point where the combined hydrodynamic forces can be applied. Over the years many approaches have been compiled to assess the correct location of it. One of the outstanding methods was proposed by Gerritsma & Keuning (1985) where they introduced a notable technique known as the extended keel method. This method involves considering the 'extended keel,' a geometric figure obtained by extending the keels and rudders leading and trailing edges all the way to the waterline. The hull's contribution is somewhat neglected, its only contribution are the areas where the keel and rudder extend to the waterline. In fact, the forebody of the hull does contribute very little to the force but unbeknownst its centre of pressure is located quite forward which lead to the results derived from this method, to a CLR too far aft. Some improvements to Gerritsma method were developed over the years, until a general "rule of thumb" was achieved.

The present VPP initially adopted the geometrical centre approach to predict the vertical position of this focal point. The contour of the yacht and the appendages was generated by incorporating various dimensions related to both objects. The keel/rudder have connecting/attaching point that allow the user to select their longitudinal position. After the overall contour was assembled the CLR was calculated considering the centroid of the generated area.

This method revealed more accurate for yachts with a centreboard keel rather than fin yacht keels. This approach was then replaced by a more recent approach, currently used in the ORC. For fin-keel yachts, it is now obtained by assuming that it lies on the 25% chord intersection with the 45% draft line. This "rule" assumes that the rudder can be neglected as its interaction with the forebody cancel each other out. For long fin keels, the most practical approach is to utilize the geometric CLR and establish an empirical connection with the sail plan (Nomoto & Tatano, 1979). The vertical position of the CLR was found through the following principle:

$$zCLR = 0.45 \cdot T_{MAX} \qquad (7)$$

As it stands, only if the sailing yacht has a centreboard, the geometrical approach will be used, for the other cases, the method represented in Equation 7.

4.1.4 Resistance components

Regarding the resistance assessment, there has been numerous approaches developed over the years. In conceptual terms, the hydrodynamic resistance encountered by sailing boats can be divided into three main categories: resistance when sailing upright, the additional resistance when heeled, and the increased resistance from wind-generated waves. This categorization has its roots in the history of hydrodynamic studies and will be further discussed in the study. The resistances developed by a boat sailing upright in calm water can be broken down into two main elements: viscous resistance and wave making or residuary resistance. Viscous resistance can then be divided into frictional resistance and form drag.

Table 2- Resistance Components acting on a sailing boat (Fossati 2013)

Hydrodynamic Resistance	Boat Upright	Residuary or Wave Making Resistance
		Viscuous (Frictional + Form Drag)
		Propeller
	Heeled Resistance	Resistance increase due to heel
		Induced or Leeway Resistance
	*Possibly	Wind-generated Waves

To determine the resistance of a yacht, the method begins with calculating the resistance of the bare hull in an upright position, including both the frictional and residuary resistance. The resistance of the keel and rudder is also calculated under the same condition and added to the total resistance. The resistance of the yacht when heeled, causes changes both in the frictional and residuary resistance of the hull, and appendages caused by the new angle of attack on the water. The wind generated waves presence can be neglected if the yacht is sailing under calm waters.

The total hydrodynamic resistance is then obtained from the following equation:

$$R_{tot} = R_v + R_{v_{app}} + R_r + R_{rk} + R_{ru} + R_{CBheel} + R_{Aheel} + R_{id} \quad (8)$$

Where:

R_{tot}	Total Resistance
R_v	Canoe Body Frictional Resistance
$R_{v_{app}}$	Appendages Frictional Resistance
R_r	Canoe Body Residuary Resistance
R_{rk}	Keel Residuary Resistance
R_{ru}	Rail Under Drag
R_{CBheel}	Canoe Body Delta Resistance Increase due to heel
R_{Aheel}	Appendages Delta Resistance Increase due to heel
R_{id}	Induced Resistance

4.2 Viscous Resistance

The viscous resistance is attributed to the influence of the water viscosity, which directly or indirectly causes this form of resistance. This resistance has two components: the friction experienced directly on the smooth surface and the pressure disparity between the fore and aft sections resulting from the boundary layer, or in other terms the form drag. Each of these components will now be examined separately. The force magnitude is generally proportional to the speed of the yacht and the wetted surface area of the hull/appendage.

4.2.1 Canoe Body

The theorical background regarding the drag created between the interaction of a solid and a fluid, shows that the frictional resistance of the hull (R_f) can be calculated as a dynamic action using the following equation:

$$R_f = \frac{1}{2} \cdot \rho \cdot V^2 \cdot S_c \cdot C_f \tag{9}$$

Which considers the yacht speed V, the fluid density ρ, the wetted surface area of the hull S_c, and lastly the skin friction coefficient C_f.The coefficient being calculated using the ITTC-57 extrapolation line and given in function of the Reynolds Number.

$$C_f = \frac{0.075}{(\log(Rn) - 2)^2} \tag{10}$$

The hull Reynolds number R_n can be determined using equation 11, that depends on the water viscosity (v) and consequently on the water temperature (i.e., at 20°C it is $1 \cdot 10^{-6}\ \frac{m^2}{s}$).

$$R_n = \frac{(V \cdot 0.7) \cdot L_{WL}}{v} \tag{11}$$

The wetted area of the hull can be computed employing an empirical formula to determine the wetted. This formula relies on the theoretical waterline length and beam, the canoe body draft, displacement, and the midship coefficient of the vessel, as demonstrated in equation 12. Remarkably, this formula yields accurate results for smooth hulls.

$$S_c = \left(1.97 + 0.171 \cdot \frac{B_{WL}}{T_C}\right) \cdot \left(\frac{0.65}{C_m}\right)^{\frac{1}{3}} \cdot (\nabla_C \cdot B_{WL})^{\frac{1}{2}} \tag{12}$$

To include the viscous pressure resistance the form factor $(1 + k)$ is introduced and multiplied on R_f:

$$R_v = R_f \cdot (1 + k) \tag{13}$$

The form factor of the hull, represented by k is typically unknown, so to account for the viscous pressure resistance, a different method is employed. According to Davidson (1936), the form factor is set to zero $(k = 0)$ and the Reynolds number in Equation 11 is adjusted by using $0.7 \cdot L_{WL}$ rather than the full waterline. This is also due to the fact, that generally the water particle does not follow the entire length of the hull.

4.2.2 Appendages

The numerical method to derive the appendage resistance follows the same methodology as the canoe body calculations. In equation 9, the wetted surface area of the hull is replaced by the appendages, that depends on its shape, and configuration. The frictional coefficient is also calculated using the ITTC-57 extrapolation line, but to calculate the Reynolds number, either the average chord length of the appendage can be used or, if the appendage is divided into segments along its span, the local chord length of each section can be employed.

4.3 Residuary Resistance

The residuary or wave making resistance is caused by the shape and configuration of the yacht and the appendages. It also depends on the sailing speed that in turn influences the Froude Number. An initial iteration was developed by Kerwin (1975), where a method was developed for speeds only up to Froude Number 0.45, and its empirical database based on the first 9 models of Series I of the DSYHS. A second iteration demonstrated in Gerritsma, et. al (1981), extended the database from 9 to 21 models, but the Froude Number range remained the same. Gerritsma et al, (1987) presented a method comprised by two different equations, one for speeds up to a Froude number of 0.45, using the entire available model range from Series 1 and 2, and one for the higher speed range ($0.475 < Fn < 0.75$) using only Series 2.

The new series aim was to use models which in shape followed the developments in the design of sailing yachts of that time more closely. The new parent hull, lead to sailing yachts attaining much higher speeds, than compared previously, so the Froude number range was extended. Up until this point, every method considered the resistance of the hull of the sailing yacht including the keel and rudder from the Standfast design used for the parent hull of the Series 1, as equipped on all models of the DSYHS. The keel and rudder designs over the years evolved towards more efficient designs, with higher aspect ratios, and therefore the automatic inclusion of these components resistance in the total resistance did not make sense and proved to be unrealistic.

To deal with this challenge Keuning et. al (1996) provided a new extensive approach that singularized the bare hull resistance (without keel and rudder) and later Keuning & Sonnenberg (1998) derived the methodology to assess the resistance of the keel and rudder individually (Keuning & Katgert, 2008). From this point onwards the total residuary resistance was obtained by the sum of all components singularized contribution.

The adopted method for the OceanVPP uses a single formulation to obtain the desired total residuary resistance, this formulation included several differences on the previous iterations, the most impactful being:

- A single expression for the whole speed range using the same database.
- All parameters of the polynomial expression are now coupled with the length/displacement ratio to be weight dependent.
- The LCB-LCF separation introduced for higher speeds to incorporate effects of trim at speed.
- The beam/draft ratio of the hull was replaced by the relation between the wetted surface and the displacement, which was a less sensitive parameter with respect to possible "exploitation".
-

4.3.1 Canoe Body

The bare hull resistance of the sailing yacht was obtained by the following polynomial regression formula, obtained from the studies published by Keuning & Sonnenberg (1998).

$$\frac{R_r}{\nabla_c \cdot g \cdot \rho} \cdot 10^3 = a_0 + \left(a_1 \cdot \frac{L_{CB\,fpp}}{L_{WL}} + a_2 \cdot C_p + a_3 \cdot \frac{\nabla_C^{\frac{2}{3}}}{A_{WP}} + a_4 \cdot \frac{B_{WL}}{L_{WL}} \right) \cdot \frac{\nabla_C^{\frac{1}{3}}}{L_{WL}} + \left(a_5 \cdot \frac{L_{CB\,fpp}}{L_{CF\,fpp}} + a_6 \cdot \frac{B_{WL}}{T_C} + a_7 \cdot C_m \right) \cdot \frac{\nabla_C^{\frac{1}{3}}}{L_{WL}} \tag{14}$$

Where:

- B_{WL} - Theoretical waterline beam
- C_m - Midship section coefficient
- C_p - Prismatic coefficient
- L_{CB} - Longitudinal centre of buoyancy (from the fore perpendicular)
- L_{CF} - Longitudinal centre of flotation (from the fore perpendicular)
- L_{WL} - Theoretical waterline length
- R_r - Wave making resistance
- T_C - Canoe body draft
- ∇_c - Canoe body displacement volume

Where the coefficients a_{0-7} are given in function of the Froude number and were obtained by interpolating the measured values, using the minimum squares technique. The coefficients used can be consulted in Table I-1.

4.3.2 Appendages

The expression used to model the appendages residuary resistance in an upright condition, derived from several experiments taken at the Delft Hydrodynamics Laboratory. The first studies to assess the impact of the appendages on the residuary resistance date back to 1975, where tests were carried out on both bare hulls, and the same hulls with appendages. The results published by Beukelman & Keuning (1975), concluded that there was a contribution that need to be considered. Thereafter, the Delft Systematic Keel Series was created, and investigations were carried out to understand the impact of certain appendages parameters on the residuary resistance, Gerritsma & Keuning (1985). After extensive publications on the subject, Keuning (1998) introduced an equation that achieved a highly satisfactory fit across all the data. This equation is derived from the correlation between the volume of the hull and keel, the taper ratio of the keel, the ratio of the hull's beam to draft, the vertical distance of the keel volume's centre of buoyancy to the free surface and the ratio of the canoe body volume to the keel volume.

$$\frac{R_{rk}}{\nabla_k \cdot \rho \cdot g} = A_0 + A_1 \cdot \frac{T}{B_{WL}} + A_2 \cdot \frac{T_C + Z_{Cbk}}{\nabla_k^{\frac{1}{3}}} + A_3 \cdot \frac{\nabla_c}{\nabla_k} \tag{15}$$

Where:

A_{0-3}	-	Empirical derived coefficients (Table I-2)
B_{WL}	-	Theoretical waterline beam
R_{rk}	-	Keel Residuary Resistance
T	-	Maximum draft of the hull including the keel
T_C	-	Canoe Body draft
∇_c	-	Canoe body displacement volume
∇_k	-	Keel displacement volume
Z_{Cbk}	-	Vertical position of the centre of buoyancy of the keel measured from the waterline.

4.4 Change in Resistance due to Heel

When the hull heels due to the side force from the sails, two resistance components develop, the induced resistance, caused by the keel and rudder generating the hydrodynamic side force and the heeled resistance. The resistance due to heel represents the change in total resistance due to heel alone, (zero side force). Since the submerged shape of the hull changes with heel, all resistance components change as well to some extent, However, most changes are negligible, and the only ones considered here are those related to:

- Hull frictional resistance
- Hull and keel residuary resistance.

The change in viscous resistance due to the heel of the canoe body is solely attributed to a change in the frictional resistance, since that the variation of the wetted surface does not imply a variation of the form factor. The calculation for the present resistance component follows the procedure described by Keuning & Sonnenberg (1998).

4.4.1 Change in Frictional Resistance

The asymmetry of the hull when heeled, results in a different distribution of the submerged volume. The effect of the former can be accounted for in the calculations by adjusting the value of the wetted surface, used in the formulas for calculating the frictional resistance.

The variation in the wetted surface given in function of the heel can be obtained by the regression formula, displayed in equation 16. The equation was obtained through the least squares interpolation of results from the hydrostatic calculations, conducted on all models in the Delft systematic series.

$$S_{wc} = S_c \cdot \left(1 + \frac{1}{100} \cdot \left(s_0 + s_1 \cdot \frac{B_{WL}}{T_c} + s_2 \left(\frac{B_{WL}}{T_c}\right)^2 + s_3 \cdot C_m\right)\right) \qquad (16)$$

The frictional resistance delta due to heel can be computed by altering in equation 9, the original wetted surface by the newly computed wetted surface given in function of the heel. The frictional resistance primarily relies on the wetted surface area. Consequently, any alteration in the wetted surface area resulting from heel also impacts the resistance. However, the appendages do not become sufficiently unsubmerged to cause a significant change in their surface area and, consequently, in resistance. Hence, this component can be disregarded

4.4.2 Change in Residuary Resistance

In alignment with the methodology demonstrated for a boat sailing without heel, the researchers from Delft proposed the following formula based on experimental outcomes obtained from a systematic series. The deltas in residuary resistance of the hull in its bare state due to heeling were determined through towing tests conducted on all the models in the DSYHS, both without heel and at a 20° heel angle. After subtracting the frictional resistance from the overall measured resistance, the discrepancy in residuary resistance at a 20° heel angle can be approximated using the subsequent polynomial expression. The delta residuary resistance difference at 20º of heel (R_{Rheel}) (as an average sailing angle) can be obtained using the following polynomial equation:

$$\frac{R_{Rheel_{\varphi=20}}}{\nabla_C \cdot 10^3 \cdot g} = u_0 + u_1 \cdot \frac{L_{WL}}{B_{WL}} + u_2 \cdot \frac{B_{WL}}{T_c} + u_3 \left(\frac{B_{WL}}{T_c}\right)^2 + u_4 \cdot L_{CB} + u_5 \cdot {L_{CB}}^2 \tag{17}$$

With the coefficients from u_{0-5} displayed in Table I-3.

The delta resistance given in function of the heeling angle, for any angle of heel, has been established using a limited set of measurement data, as described in Keuning & Sonnenberg (1998). Nevertheless, a strong correlation was found between the change in resistance and the heeling angle, with the change being proportional to the heeling angle raised to the power of 1.7. With φ in radians.

$$R_{Rheel} = R_{Rheel_{\varphi=20}} \cdot 6 \cdot \varphi^{1.7} \tag{18}$$

The change of the residual resistance of the keel due to the heel is calculated using equation 19, where C_H in the equation is found using equation 20. With φ in radians.

$$R_{Rheel_k} = \nabla_k \cdot \rho \cdot g \cdot C_H \cdot {F_n}^2 \cdot \varphi \tag{19}$$

The coefficients in equation 20 are found by a regression analysis and published by Delft.

$$C_H = -3.5837 \cdot \left(\frac{T_C}{T}\right) - 0.0518 \cdot \left(\frac{B_{WL}}{T_C}\right) + 0.5958 \cdot \left(\frac{T_C}{T}\right) \cdot \left(\frac{B_{WL}}{T_C}\right) + 0.2055 \cdot \left(\frac{L_{WL}}{\nabla_k^{\frac{1}{3}}}\right) \tag{20}$$

4.5 Induced Resistance

Since its initial introduction in 1981, an equation has been used to assess the production of lateral force by a sailing vessel, considering its leeway and heel based on findings from the Delft Systematic Yacht Hull Series (Gerritsma et. al. (1981). Substantial changes have occurred in the arrangement and configurations of appendages since then. However, the consideration of lateral force generation in relation to leeway and heel has played a relatively minor role in the current calculations of VPPs, leading to its somewhat undervalued status for several years. In recent times, there has been increased emphasis on this subject, primarily driven by the necessity to evaluate the yaw balance of (large) sailing yachts and the incorporation of manoeuvring models for sailing vessels.

In Gerritsma's original model, the calculation of the hull and appendage side forces, as well as the individual contributions of the hull, keel, and rudder, differs for upright and heeled conditions. In the upright condition, the keel and rudder side forces were calculated using the extended keel method, where the keel and rudder are virtually extended into the hull up to the waterline. The downwash angle on the rudder was set at 50% of the leeway angle, and rudder water velocity was reduced by 10% to account for the keel's wake. The total yaw moment was calculated based on the keel and rudder side forces and their distances from the ship’s centre of gravity. This method worked well for moderate aspect ratio keels but was less effective for low-aspect-ratio keels, especially when under deep hulls, and failed to accurately predict yaw moments. Limitations were also encountered when applying this approach in heeled conditions. Consequently, an alternative approach was developed for such situations. To enhance its effectiveness, the expression was further refined in 1998 by calculating new coefficients using the results from Series 1, 2, 3, and 4, encompassing approximately 50 models studied by Keuning & Sonnenberg (1998). While the assessment formula demonstrated satisfactory performance for hulls and appendages that closely matched the layout and plan form utilized in the DSYHS model series, it encountered limitations when dealing with high aspect and short chord keels. The obtained results did not align well with the experimental data available in such cases. To address this issue and simplify the calculation of the yaw moment in real-world sailing scenarios, Keuning & Vermeulen (2003) proposed a solution. They assumed that the distribution of the total side force over the keel and rudder, as EKM could also be applied in heeled conditions. This approach considered the total side force to originate from both the keel and rudder, considering the carryover effect of lift. This finding aligns with the observation that a heeled and yawed hull typically generates minimal or negligible side force on its own. Moreover, the utilization of this expression does not provide a breakdown of the individual contributions from the three distinct components: the hull, keel, and rudder. Consequently, it fails to yield conclusive findings regarding the yaw moment.

For a VPP software running in 2 DOFs, to determine the induced resistance, it is assumed that the heeling force generated by the aerodynamic forces is equal to the side force produced by the hydrodynamic forces. For 3 DOFs or more, the hydrodynamic side force needs to be computed.

$$R_I = \frac{{F_H}^2}{\pi \cdot T_E \cdot \frac{1}{2} \cdot \rho \cdot A_{lat} \cdot V^2} \tag{21}$$

The A_{lat} is the lateral surface of hull with keel, T_E is the effective draft and can be derived following a polynomial expression developed by Delft and presented in Equation 22. The equation's coefficients are documented in Table I-5 and are dependent on the heeling angle.

$$\frac{T_E}{T} = \left(A_1 \cdot \frac{Tc}{T} + A_2 \cdot \left(\frac{Tc}{T}\right)^2 + A_3 \cdot \frac{BWL}{Tc} + A_4 \cdot TR\right) \cdot (B_O + B_1 \cdot F_n) \quad (22)$$

4.6 Rail Under Drag

Rail-under drag is a mechanism used in the ORC (2024) to stop the VPP from settling on equilibrium at high heel angles and adopted in the present work. Up until 30 degrees of heel, the rail-under drag is zero. Beyond this angle, a multiplier is applied to the upright residuary resistance, which is then added to the total resistance.

$$DRU = 0.0004 \cdot (Rr + Rrk + Rrr) \cdot (\varphi - 30)^2 \quad (23)$$

In summary, the developed hydrodynamic model considers the following resistance components.

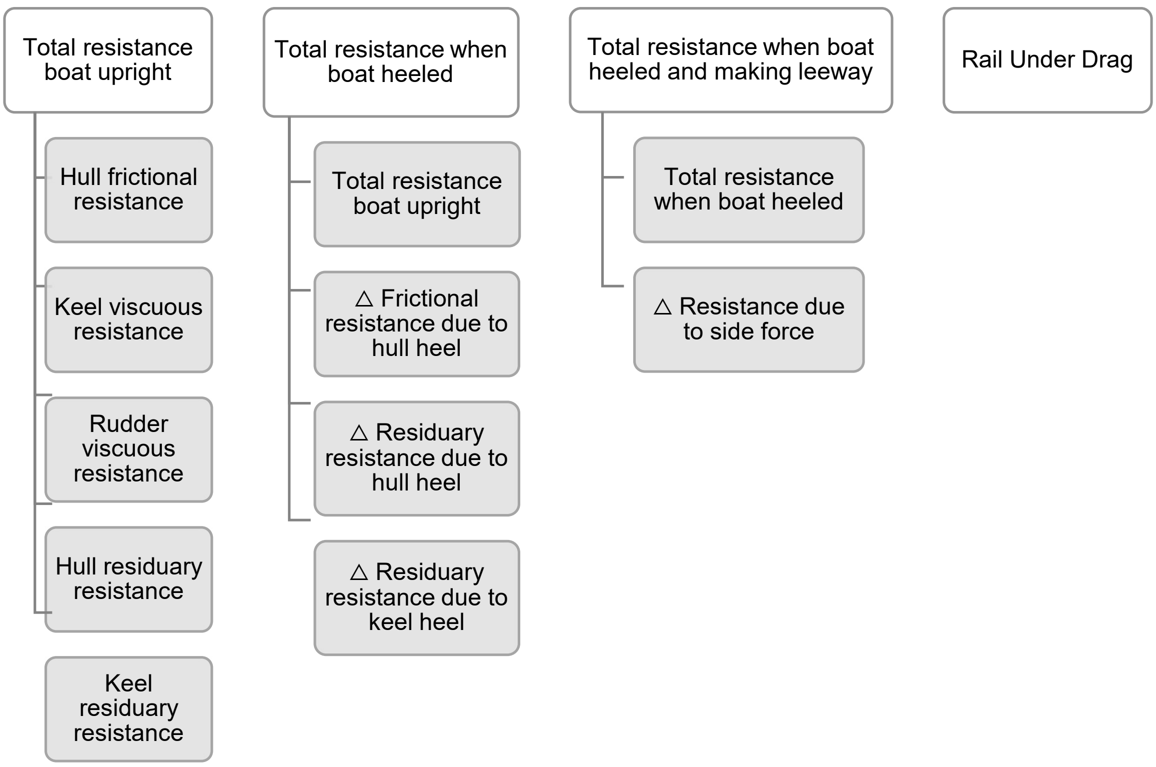

Figure 11 - Resistance components (Fossati, 2013)

4.7 Hydrodynamic Model Results

This chapter presents and validates the results obtained from the hydrodynamic model developed for the OceanVPP. The hydrodynamic model plays a critical role in determining the yacht's performance by evaluating resistance components.

4.7.1 Centre of Lateral Resistance

As previously mentioned, the centre of lateral resistance is a focal point on the hydrodynamics of a sailing vessel and represents the theorical point where the combined hydrodynamic forces can be applied. For the present VPP, since it only contemplates 2 DOF, the only parameter required of said point is its vertical position. The following results were obtained considering the two different approaches mentioned before.

Table 3- CLR results

	CLR height [m]
Geometrical centre	0.33 (above WL)
Namoto's method	0.99 (below WL)

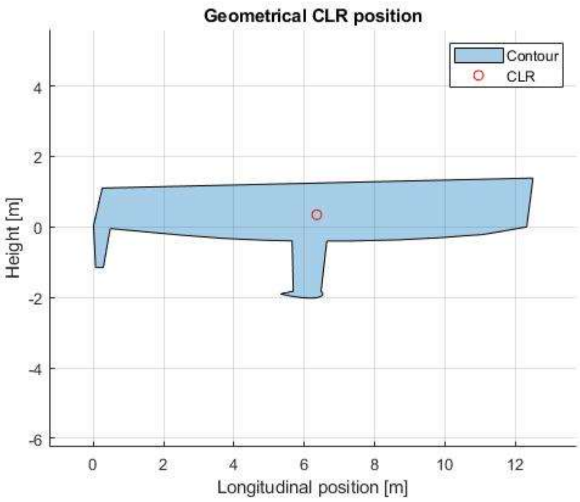

Figure 12 - Geometrical CLR position function.

In evaluating the results, a clear difference can be observed between the CLR values obtained through the initial geometrical centre approach and those determined using the newer methodology, which aligns better with fin-keel yacht configurations. The discrepancy likely stems from the limitations of the geometric centre approach, which, while suitable for long keels, tends to overestimate the CLR vertical positioning in yachts with fin keels.

The second method aligns the CLR more accurately, especially as it reduces the contribution of the rudder, which typically acts in opposition to the keel's lift force. This method, therefore, better reflects the lateral resistance distribution in fin keels, particularly for yachts with higher draft-to-length ratios, where such accuracy directly influences stability predictions.

Moreover, the placement of the CLR closer to the keel's lower sections is theoretically justified, given that these areas experience a greater lateral force concentration at increased drafts. By positioning the CLR at 45% of the draft, the approach captures the keel's predominant role, especially under typical sailing conditions where the keel's lower sections generate substantial lift.

4.7.2 Resistance Components

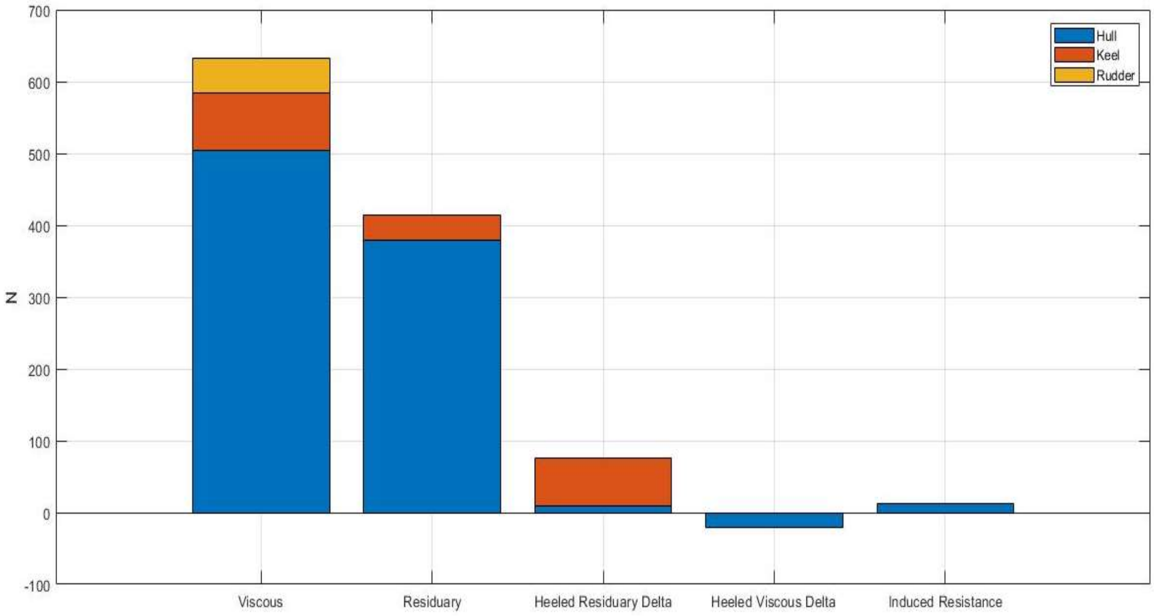

Figure 13 - Components of Different Resistance Types (V = 3.75 m/s, heel = 10º, Aero Side Force = 1000N)

The bar chart illustrates the components of different resistance types, viscous, residuary, heeled residuary delta, heeled viscous delta and induced resistance categorized by hull, keel, and rudder. Viscous resistance shows the highest overall value, with significant contributions from the hull, keel, and rudder, respectively. This high viscous resistance is primarily due to the frictional forces between the water and the surfaces of the hull, keel, and rudder. The hull, being the largest component in contact with water, experiences the most frictional drag, followed by the keel and rudder, which also contribute but to a lesser extent due to their smaller surface areas. So, for the viscous resistance the higher the area or wetted surface the higher the value obtained.

Residuary resistance follows, with the hull being the predominant contributor. This is influenced by wave-making resistance and pressure differences around the hull as it moves through the water. The keel and contributes less to residuary resistance because their streamlined shapes are designed to minimize wave creation and pressure drag. The hull's larger size and shape create more significant wave patterns, resulting in higher residuary resistance.

Heeled residuary delta indicates a significant keel resistance increase when the vessel heels (66 N) and much lower regarding the hull (10 N). Heeled viscous delta shows a small negative value for hull resistance, suggesting that heeling reduces the hull's wetted surface and consequently the viscous resistance. Regarding the induced resistance a small contribution was found considering the aerodynamical side force of 1000N.

Overall, this analysis highlights the complex interplay between different parts of the vessel and how their resistances vary under different conditions.

4.7.3 Validation

The present chapter aims to validate the developed model using two distinct comparison tools. An accurate validation on such a preliminary stage of the VPP is significantly important as it will mitigate possible discrepancies of the final velocity results. Additionally, it will simplify the results interpretation for further comparisons made.

The hydrodynamical model adopted, as described, follows the work developed under Delft University which was comprised under the DSYHS (for hull resistance estimations), the DVKS and DSKS (appendages). For the canoe body resistance study Series 4 was adopted and when possible, Series 7. Some of the new formulations developed under Series 7 use split equations for different Froude Number ranges, therefore creating small continuity and gradient changes, which affects the sequential quadratic programming algorithm adopted within the *Matlab* VPP solver algorithm. Regarding the cases where Series 4 was adopted, a linear extrapolation will be used for the Froude Numbers higher than the ones available. Table 4 summarizes the methods chosen per resistance component.

Table 4- Resistance Components adopted and theorical background

Sailing Yacht Component	Resistance Component	Method
Canoe Body	Viscous Resistance	DSYHS Series 4
Appendages		DSYHS Series 4
Canoe Body	Residuary Resistance	DSYHS Series 7
Keel		DSKS Series 1
Canoe Body	Delta Frictional due to heel	DSYHS Series 4
Canoe Body	Delta Residuary due to heel	DSYHS Series 4
Keel	Delta Residuary due to heel	DSKS Series 1
Canoe Body and Appendages	Induced Resistance	DSYHS Series 4
Rail Under Drag		ORC

The validation tool used for this assessment was sourced from NavalAPP (2024), which follows the same methodology applied in the OceanVPP hydrodynamical model and displayed in Table 4. When possible, depending on the availability, other validations tools were used.

4.7.3.1 Upright Resistance

The results displayed in Figure 14 demonstrates the results obtained for the viscous and residuary resistance per yacht component. Individual plots per yacht component (rudder, keel, canoe body) can be also found in Appendix III.

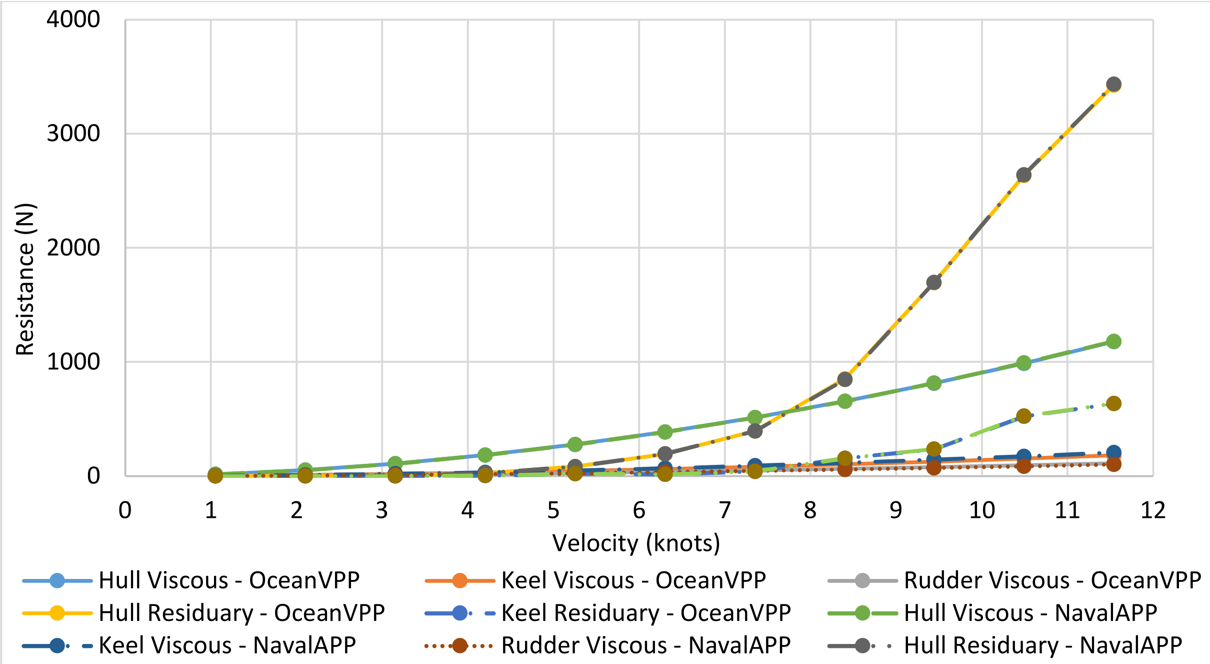

Figure 14 – Upright Resistance per Component (Viscous + Residuary)

Regarding the accuracy of the model, a strong correlation was found, the impact of velocity on the resistance is the same only contemplating some minor deviations, in some cases (1 to 6%), due to possible discrepancies in areas or surfaces computations. Interpreting the results, the hull is the biggest contributor to the yacht's total resistance, it has the most significant wetted surface (dictating the outcome of the frictional resistance) and is also the component that generates the most waves, as it needs to displace more water to propagate forwards (residuary resistance). At a lower velocity range (below 7 knots), it is the viscous (frictional + form drag) that takes the most toll, but a shift is noted around 7.5 knots (approximately) where the residuary significantly increases at a much steeper rate. This shit is also verified in the other components, keel and rudder.

The results displayed in Figure 15 demonstrate the results obtained for the total upright resistance. The validation tools for this study now includes the results derived from Maxsurf VPP. This comparison is of great significance as Maxsurf VPP will also be used to validate the results of the developed velocity prediction program.

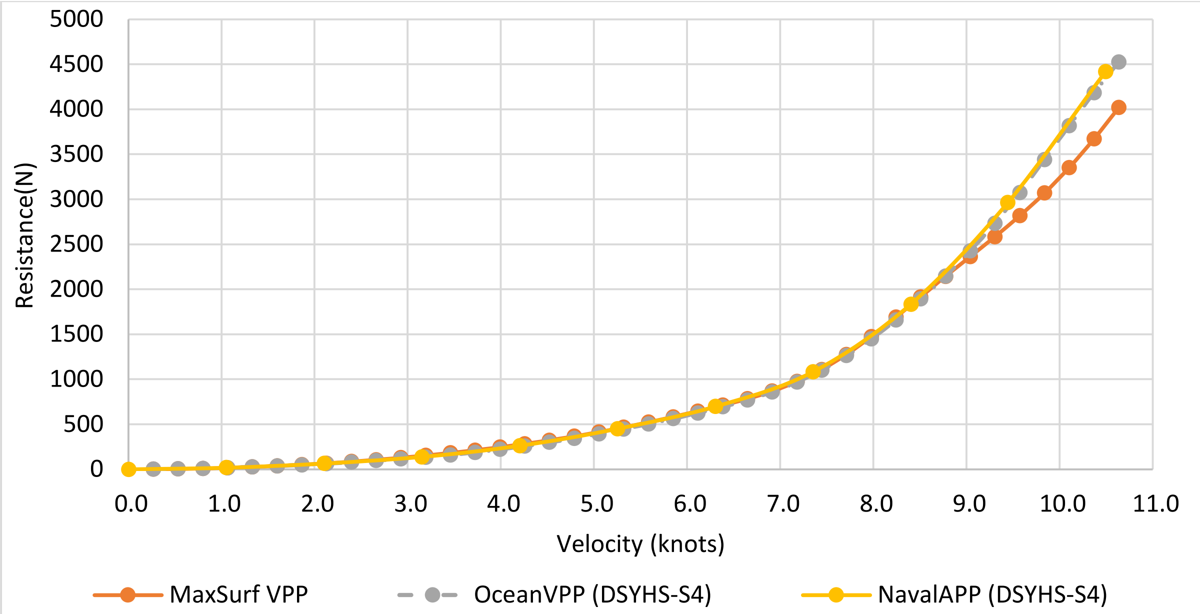

Figure 15 - Sailing Yacht Total Upright Resistance (Viscous + Residuary)

From Figure 15 it can be concluded that the agreement found between NavalAPP and OceanVPP is followed by Maxsurf VPP up until 8,5 knots (approximately). Beyond this value the start of a deviation can be observed, which steadily increases with the velocity. At higher velocities, the residuary resistance usually becomes more significant, as already stated, which could imply an underestimation of this component by Maxsurf VPP software, whose methodology adopted is unclear.

4.7.3.2 Heeled Resistance

Figure 16 shows the keels residuary resistance change per heel angle.

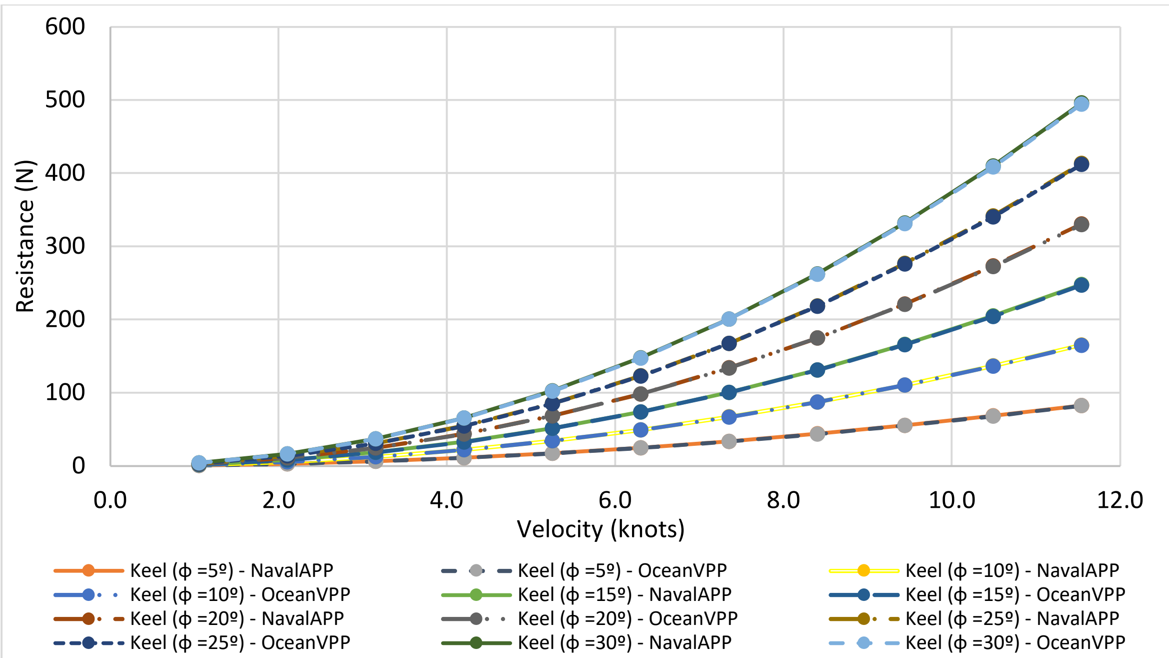

Figure 16 - Keels Delta Residuary Resistance per heel angle

The results exhibit a close correspondence attained between the two methods for the keel's delta residuary resistance. A resistance increase with the velocity can be observed for this component, especially accentuated for higher heeling angles. The viscous resistance delta is not considered due to keels being submerged for most heel angles, and therefore not having a wetted surface variation.

Figure 17 shows the total delta (viscous + residuary) for the canoe body per heel angle obtained using NavalAPP and the developed tool OceanVPP.

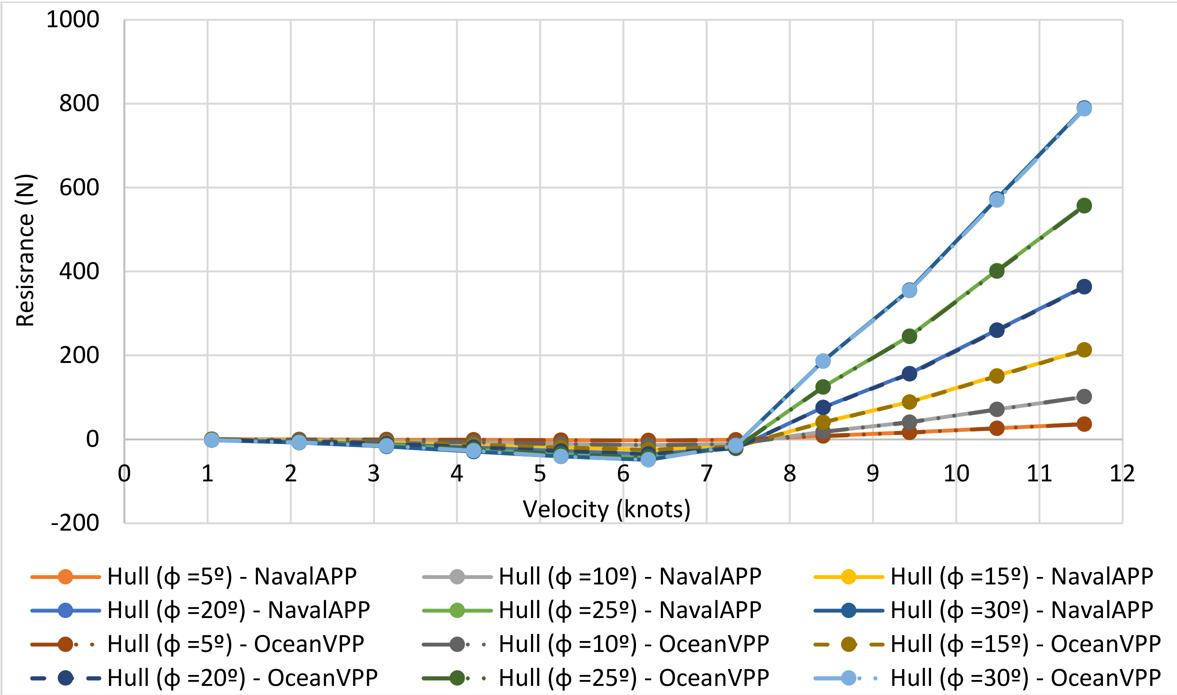

Figure 17 - Canoe Body Total Delta Resistances (Viscous + Residuary) per heel angle

The results obtained and displayed in Figure 17 shows an initial negative delta, meaning there is a decrease in the generated resistance from the hull for all heel angles up until a velocity of 7,5 knots approximately. To further understand why Figure 18 needs to be consulted, where the resistances deltas from the hull were isolated.

The negative component is associated with the decrease in the viscous resistance. This decrease in viscous resistance, observed in Figure 18, aligns with the reduction in the wetted surface area verified in Figure III-5. As the heel angle increases, there is a reduction in wetted surface area which lowers the frictional drag component of the viscous resistance. This is also verified in Keuning & Sonnenberg (1998), where some hulls tested within the DSYHS have a decrease in the wetted surface with the increase of the heeling angle.

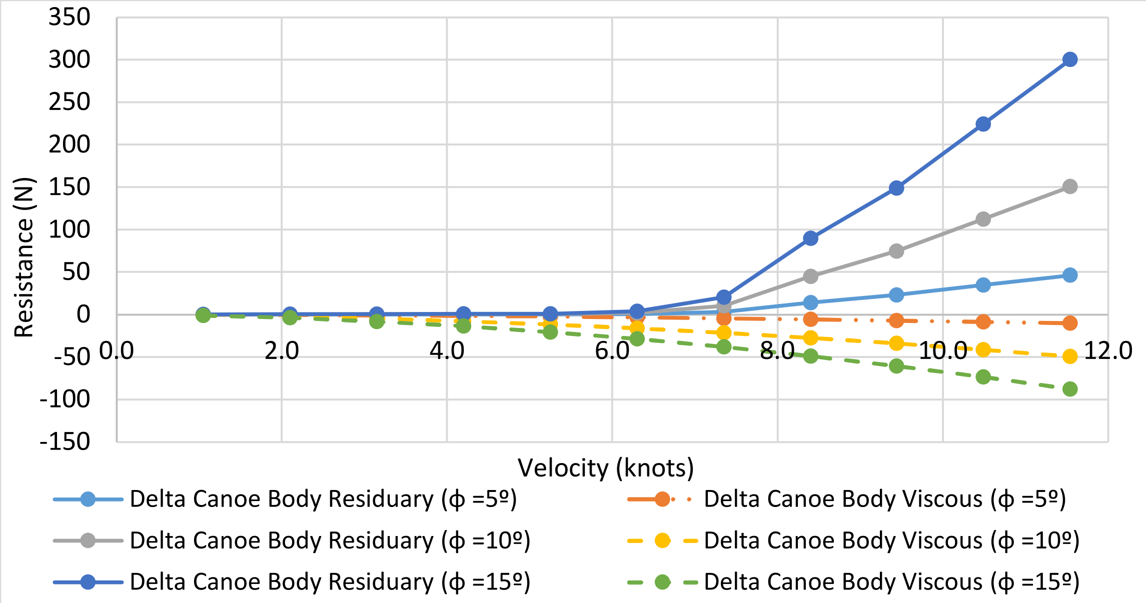

Figure 18 - Canoe Body Delta Resistances per heel angle

Figure 19 demonstrates the results obtained for the total heeled resistance (upright plus the heeled deltas) for three distinct heel angles 10°, 20° and 30° (results for further heeling angles can be consulted in Figure III-4. The validation tool for this study is once again NavalAPP as Maxsurf does not provide the heeled contributions alone. This new set of results confirms the strong coherence between the two tools, using the same methods and therefore fully validating the present hydrodynamic model.

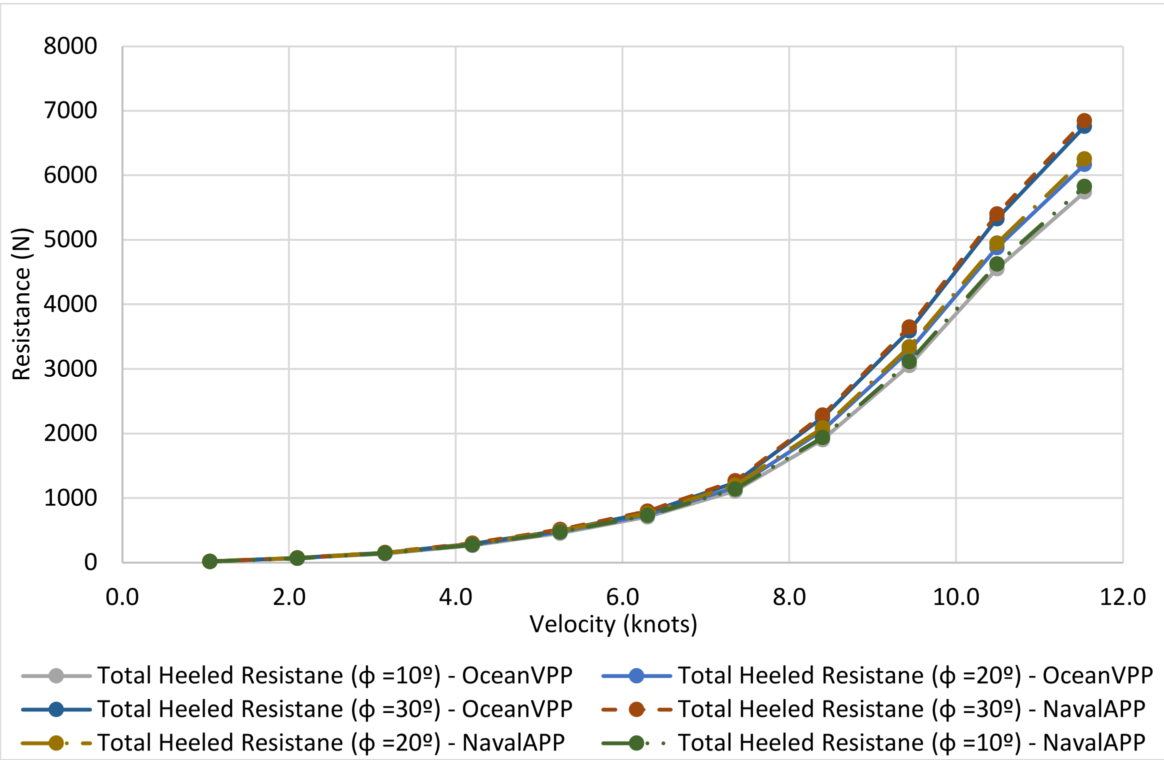

Figure 19 - Total Heeled Resistance per heel angle (10°, 20°, 30°)

5. AERODYNAMIC MODEL – OCEANVPP

In this chapter, the essential concepts of sailing yacht aerodynamics and their interaction with the surrounding air will be presented. The aerodynamic model comprises several key components: lift and drag forces generated by the sails, the aerodynamic side force, and the driving force. The aerodynamical model adopted for OceanVPP follows the work established by Hazen (1980). A code snippet regarding the Aerodynamic Model can be consulted in Appendix V.

5.1 Introduction

The aerodynamic model employed in the present VPP is designed to calculate all aerodynamic forces acting on a sailing yacht. This model considers the characteristics of the sails, the mast, and the rigging configuration. For each sail, it determines the lift and drag coefficients as a function of the apparent wind angles. These individual sail coefficients are then integrated to form a comprehensive set of sail plan coefficients, which are dependent on the apparent wind angle and have a crucial impact on the resultant forces. The primary objective of this model is to calculate the driving and side force (Figure 20). These forces are mainly derived from the lift and drag produced by the sails. While additional forces may become significant depending on the number of degrees of freedom (DOF) considered, the current VPP is configured to operate with 2 DOF.

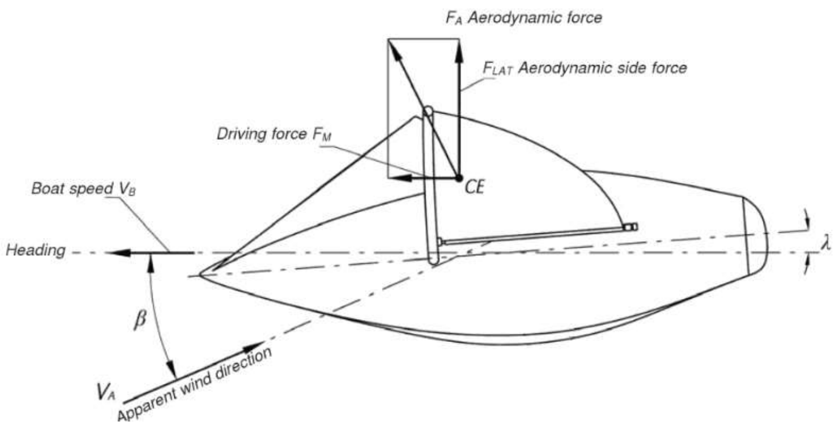

Figure 20 - Aerodynamical forces (Fossati, 2021)

To better understand the capabilities and advancements of the current aerodynamic model, it is essential to review the historical developments and improvements that have been made over the years. The following paragraphs provide a brief overview of these evolutions.

The first modern aerodynamic sail force model applied in the context of a VPP, was established by Kerwin (1975). To simulate the effect of crew trimming and changing sails, Kerwin used two parameters, "flat" and "reef" to describe the sail's shape. The flat parameter is used to simulate the reduction of lift coefficient, while the reef parameter simulates the reduction of sail area. The VPP optimizer developed adjusted these parameters to achieve the best performance for a given set of wind conditions.

Following the principle established, Hazen (1980) successfully isolated the coefficients for five sails, namely the main, jib, mizzen, and mizzen staysail, as functions of the apparent wind angle. These coefficients can now be utilized to integrate sails of varying sizes and geometries into a VPP, thereby creating a semi-empirical model.

The underlying assumption in this approach is that the interaction among the sails is such that an increase in force on one sail is offset by a decrease on another. While Hazen acknowledges that this representation does not perfectly reflect reality, the simplification gained is deemed valuable despite its slight deviation from the laws of physics. Hazen models still up to today is highly regarded in the field, his work was later admitted when the IMS VPP was developed, by the ORC,

The IMS VPP updated the coefficients for each sail, but the principle of the methodology remains, with the approach to first derive the force coefficients per sail and then to derive the final drag and lift coefficients for the whole sail plan. The ORC approach also improved the method by increasing the wind apparent angles, the original method only contemplated five angles, 27º, 50º, 80ª, 100º, 180º, meanwhile the ORC contemplates ten angles. Along with the same idea, the geometrical centres of effort are also computed, and a total reference point derived from the whole geometrical sail plan."

Between 2005 and 2007, the Offshore Racing Congress (ORC) initiated an extensive testing program at the Milan Polytechnic twisted flow wind tunnel. This program examined various rig configurations, including mainsail roach, jib overlap, and rig fractionality, to develop a more comprehensive aerodynamic database. The experimental results from these wind tunnel tests provided a clearer understanding of the aerodynamic impacts of sail plan parameters such as jib overlap, mainsail roach profile, and rig fractionality at different apparent wind angles.

To adapt to the evolving design of modern racing yachts, ORC conducted additional wind tunnel tests on Code sails in 2007. These tests were intended to model the sails in the VPP and provide accurate performance comparisons between Code O (treated as an asymmetric spinnaker) and other sails such as the genoa spinnaker. The 2008 ORC version incorporated aero coefficients specific to Code0, allowing for performance comparisons at various true wind angles. Another significant enhancement in the ORC aerodynamic model was the introduction of an updated depowering scheme (2008). This replaced the traditional depowering method, which had relied on the Reef and Flat parameters for over two decades. The older scheme, based on the Kerwin model, reduced sail area by scaling parameters such as I, J, P, and E using the Reef parameter. However, this approach did not accurately reflect real-world depowering, where sail area reduction primarily involves the headsail, especially by shortening the foot length. The new depowering process more closely mirrors real-world conditions by employing a two-stage reduction: first reducing the jib area, followed by the mainsail. For each configuration, aerodynamic data derived from wind tunnel tests, such as effective rig height and centre of pressure, can be applied. This updated scheme utilizes new VPP variables, including the "jib foot parameter" (ftj) and the "mainsail reduction factor" (rfm), alongside a new optimization parameter called the "Reduction factor" (RED), which replaces the former Reef and Flat parameters. The new method better captures the variations in aerodynamic performance due to changes in sail geometry, including induced drag and the centre of effort height, as functions of roach, overlap, and fractionality. The current aerodynamic model treats the sail plan as consisting of three different sails: the mainsail, jib, and spinnaker, with the spinnaker being either symmetrical or asymmetrical, a configuration defined by the user.

5.2 Sail Coefficients

The developed OceanVPP provides users with the flexibility to select from different sets of sail coefficients (displayed in 0), specifically the original Hazen coefficients, the IMS's and those established by the ORC. This option feature allows users to derive necessary conclusions and make comparisons with the evolution of results over time.

5.2.1 Hazen Coefficients

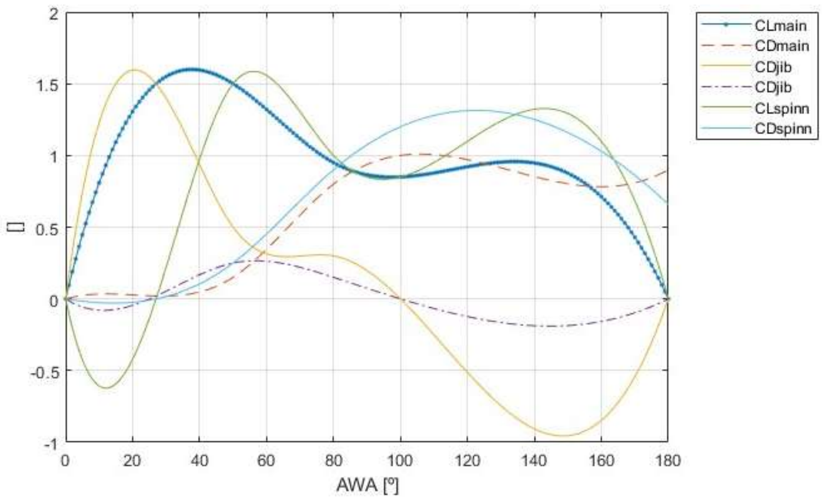

Figure 21 - Sail coefficients graphically (Hazen, 1990)

Figure 21 shows how the lift and drag coefficients for each sail with the wind angle. The jib sail lift peaks around 20° AWA and then declines, whereas its drag increases steadily. The main sail shows a lift peak around 40° AWA with a drag also steadily increasing. The spinnaker's lift and drag show significant values mainly in the range of 60° to 160° AWA, highlighting its effectiveness in broader wind angles. This comprehensive view allows for analysing the aerodynamic performance of each sail relative to wind direction.

The original model provides coefficients for only five angles: 27°, 50°, 80°, 100°, and 180°. Interpolation between these angles is expected to be performed using spline functions. Coefficients are specified for five sails: main, jib, spinnaker, mizzen, and mizzen staysail. To calculate the total lift or viscous drag (also known as parasitic drag) the area of each sail is multiplied by the respective coefficient, and the results are summed. The final coefficient is derived by dividing by a nominal sail area, which is the sum of the foretriangle, main, and mizzen areas, with all areas computed as triangular, neglecting the roach. The aerodynamic coefficients can be consulted in Table II-1.

5.2.2 IMS

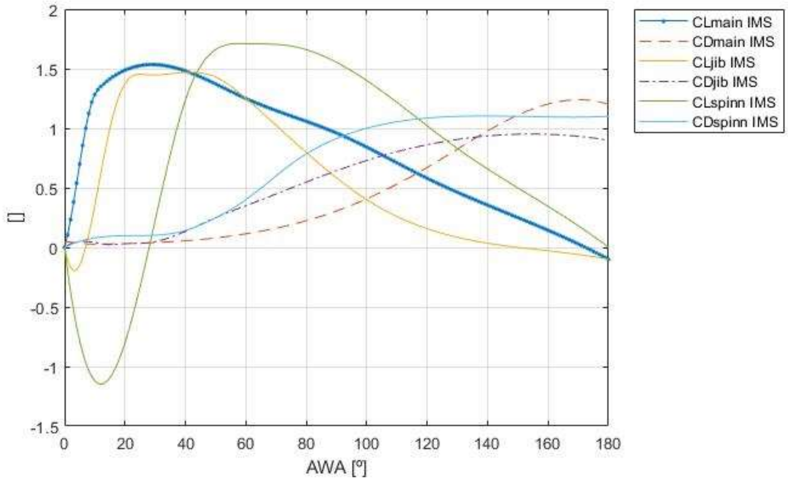

Figure 22 - Sail coefficients (Poor, 1986)

The IMS aerodynamic coefficients for the rig are derived from wind tunnel experiments conducted on two-dimensional sails. For each sail type, spinnaker, jib, or mainsail, a corresponding set of lift and drag coefficients is selected, characterized as a function of the apparent wind angle. Cubic spline interpolation must be used to the section lift and drag for the various sail types, enabling the determination of values at intermediate angles, which are then stored in arrays that span an AWA range of up to 180 degrees. Subsequently, the individual coefficients for each sail are utilized to compute a comprehensive set of coefficients for the rig. The IMS aerodynamic coefficients can be consulted in Table II-4 and Table II-5.

5.2.3 Offshore Racing Congress

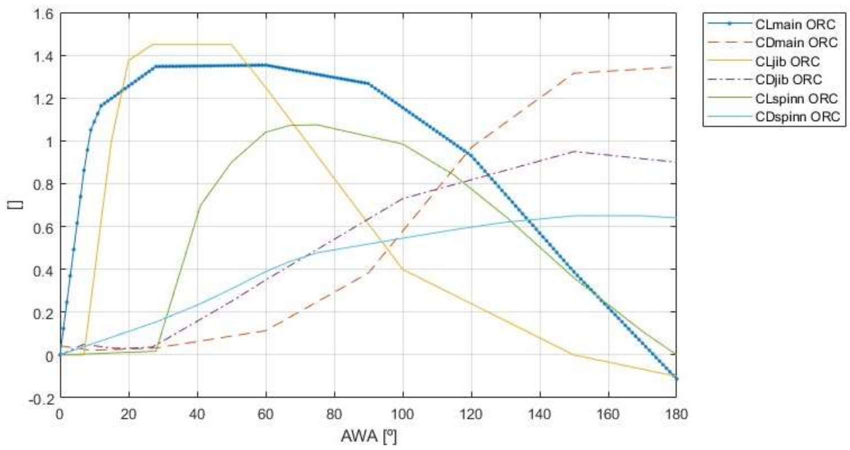

Figure 23 - Sail coefficients graphically (ORC, 2024)

Regarding ORC's coefficients, there are 2 different sets that can be used for each sail. The low lift coefficients that are associated with low mainsail adjustability and the high lift that represent high bend control. Essentially their use depends on the boats number of backstays, if one has neither a backstay nor a pair of running backstays the low coefficients are the ones to be used. The backstay controls the masts bending to counter the forestay or jib, which defines the overall sail shape, that in turn influences the amount of generated lift. For the represent work, only the low lift coefficients were used to mimic a sailboat with low control of its mast. The ORC aerodynamic coefficients can be consulted in Table II-2 and Table II-3. The spinnaker may have two different possible configurations, it can either be symmetric, derived from the sail being cut into a symmetric shape which requires a spinnaker pole, and the 2nd option, the asymmetrical, where the sail has more of a triangular shape, and has 3 distinct corners, the head, clew, and tack. Each spinnaker type has different set of coefficients to be used.

5.3 Wind Triangle

The wind triangle is a fundamental concept in navigation, particularly pertinent to sailing yachts, as it integrates the elements of true wind, apparent wind, and the yacht's velocity to provide a comprehensive understanding of sailing dynamics. In the context of a sailing yacht, the wind triangle is instrumental in determining the optimal sailing course and speed. The true wind represents the actual wind direction and speed as observed from a stationary point, while the yacht's velocity vector denotes the boat's speed and direction over the water. The apparent wind, which is the wind experienced onboard, results from the vector combination of the true wind and the yacht's motion. This apparent wind is critical for sailors as it influences the sail trim and overall performance of the yacht. Figure 24 decomposes the vectors mentioned above

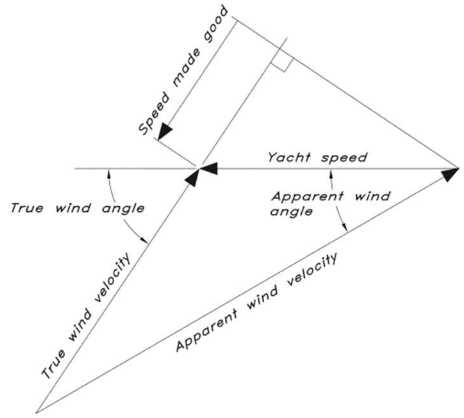

Figure 24 - Velocity triangle (Larsson, et. al. 2022)

Understanding the wind triangle allows sailors to effectively navigate and adjust their sailing strategy to maximize efficiency and safety. By analysing the relationship between the true wind, apparent wind, and the yacht's velocity, sailors can determine the most efficient course to steer, known as the course, made good, and make precise adjustments to the sail trim to harness the wind's power optimally. This analytical approach is essential for optimizing speed and achieving desired navigational outcomes, whether racing or cruising. Thus, the wind triangle not only enhances a sailor's ability to interpret and utilize wind conditions but also underscores the interplay between environmental factors and navigational techniques, which are critical for proficient sailing.

The apparent wind angle and speed can be computed quite easily, as shown in the following equations.

$$V_1 = V + TWS \cdot \cos(TWA) \quad (24)$$

$$V_2 = +TWS \cdot \sin(TWA) \cdot \cos(\varphi) \quad (25)$$

Lastly:

$$AWS = \sqrt{{V_1}^2 + {V_2}^2} \quad (26)$$

$$AWA = acos\left(\frac{V_1}{AWS}\right) \quad (27)$$

5.4 Reefing and Flattening

A noteworthy aspect of the sail model is its capability to account for reefing and flattening of the sails, both of which exert distinct effects. Reefing, characterized by the factor $Reef$, quantifies the reduction in sail height, $Reef$ is equal to 1 when the sail is unreefed. A reefed sail implies a change in the height of the centre of effort and this new height can be determined by multiplying the original height by $Reef$.

Consequently, both the lift and the viscous drag (excluding contributions from the mast and topsides) are diminished by a factor of $Reef^2$, whereas the primary reduction in the heeling arm is governed by $Reef$.

The flattening factor $Flat$ denotes the decrease in lift resulting from the flattening of the sails. This factor, which equals 1 for a standard sail, cannot be directly correlated with sail geometry; rather, it diminishes with a decrease in sail camber. It is important to note that $Flat$ does not influence the heeling arm and has varying effects on lift and drag. Since the lift is directly proportional to $Flat$, the induced drag corresponds to $Flat^2$. Thus, flattening results in a greater reduction of the drag compared, causing the resultant driving force to increase. Therefore, it is advantageous to flatten the sails prior to reefing. In most VPPs, optimal values of $Reef$ and $Flat$ are determined for various conditions, offering insights into the most effective sail settings.

5.5 Sails Geometry

As previously mentioned, the area for each sail and respective centres of effort needs to be computed. The present sub-chapter intents to demonstrate the approach considered to obtain the lift and drag coefficients to be used, with the 1st step calculating the sail areas and he respective centres of effort.

Table 5 delineates the methodology employed to calculate both the sail area and the height of the centre of effort for each individual sail. The calculations for all sail areas were conducted under the assumption that each sail is triangular, with the roach being disregarded in this context.

Table 5 - Sail areas and centre of effort

Sail	Area	Centre of effort
Main	$A_M = 0.5 \cdot P \cdot E$	$CE_M = 0.39 \cdot P + BAD$
Jib	$A_J = 0.5 \cdot \sqrt{I^2 + J^2} \cdot LPG$	$CE_J = 0.39 \cdot I$
Spinnaker	$A_s = 1.15 \cdot SL \cdot J$	$CE_S = 0.59 \cdot I$
Foretriangle	$A_F = 0.5 \cdot I \cdot J$	[-]
Nominal	$A_N = A_M + A_F$	[-]

Regarding the centres of effort, for the main this height is positioned at 39% of the luff length above the boom. For the jib, the centre of effort is at 39% of the foretriangle height above the sheer line, while for the spinnaker, it is at 59% of the foretriangle height above the sheer line. The vertical position of the entire sail plan was obtained considering the overall geometrical centre, defined by the sail combination used, as given by the following equation:

$$zCoE_{sailplan} = \frac{\sum zCoE_i \cdot Area_i}{\sum Area_{nominal}} \cdot \cos(\varphi) \tag{28}$$

5.6 Sail Lift and Drag Coefficients

The total aerodynamical drag is composed by three different components, the viscous/parasitic drag C_{D_P} , the induced drag C_{DI} and the drag of mast and topsides C_{D0}.

$$C_D = C_{D_P} + C_{DI} + C_{D0} \tag{29}$$

The inherent drag resulting from the wind resistance of the hull, spars, and rigging. The drag coefficients for the mast and topsides are established as 1.13. It is recognized that the wind near sea level tends to be less forceful than at higher altitudes (Tennekes, 1973), which raises questions about the validity of utilizing the apparent wind velocity alongside the same drag coefficients. Furthermore, recent findings from the computational fluid dynamics (CFD) era indicate that the mast contributes a substantial amount of driving force (Brummer, 2015), an aspect that is not considered in the Hazen model. Despite these observations, Hazen's model encompasses several simplifications; when applied as a whole, it has demonstrated reasonable accuracy. Consequently, no alterations are implemented regarding the drag calculations for the mast and topsides. The drag for both the topsides and the mast is computed based on the frontal area of the vessel and the mast (Pennanen, 2015).

$$C_{D0} = 1.13 \cdot \frac{(B_{MAX} \cdot FA) + (E_{HM} \cdot E_{MDC})}{A_N} \tag{30}$$

Where:

B_{MAX}	Max Beam of the yacht
FA	Average Freeboard
E_{HM}	Mast height above sheer
E_{MDC}	Average Mast Diameter

The parasitic drag of sails comprises two elements: skin friction drag, which arises from the interaction between the sail surface and the airflow, and pressure drag, which occurs due to flow separation. The parasitic drag is assumed to be unaffected by the lift force generated by the sails; nevertheless, it does vary with the sailing angle.

$$C_{D_P} = \frac{C_{DPM} \cdot A_M + C_{DPJ} \cdot A_J + C_{DPS} \cdot A_S}{A_N} \tag{31}$$

The induced drag of sails originates from the three-dimensional nature of the airflow surrounding them and the circulation loss occurring from the head to the foot of the sails. It is assumed that the induced drag varies quadratically with the lift coefficient. Additionally, a two-dimensional drag term, which depends on lift, is incorporated into the core induced drag.

$$C_{DI} = {C_L}^2 \cdot \left(\frac{1}{\pi \cdot AR} + 0.005\right) \tag{32}$$

In Hazen's model, the aspect ratio for close-hauled sailing conditions is described as a modified version of the geometric aspect ratio, where the luff length is measured from the waterline to the top of the mast. This length is then adjusted by a factor of 1.1. Since the aerodynamic planform of the sails extends down to the waterline, the model appears to assume that the sails are attached at deck level. Additionally, the factor of 1.1 suggests an end-plate effect caused by the water surface. The aspect ratio expressed as follows, where EHM represents the mast height above the sheer line, FA denotes the average freeboard height, and A_N is the sail area.

$$AR = \frac{(1.1 \cdot (EHM + FA))^2}{A_N} \tag{33}$$

For other courses:

$$AR = \frac{(1.1 \cdot EHM)^2}{A_N} \tag{34}$$

The lift coefficient is determined using a combination of coefficients and areas from various components of the sail plan. This equation combines the contributions of the mainsail, jib and spinnaker scaled by their respective areas. These values are normalized by the nominal sail area to find the overall lift coefficient. Additionally, the lift coefficient incorporates correction factors, including Flat and Reef.

$$C_L = \frac{C_{LM} \cdot A_M + C_{LJ} \cdot A_J + C_{LS} \cdot A_S}{A_N} \cdot Flat \cdot Reef^2 \tag{35}$$

5.7 Aerodynamic Forces

The model outputs the lift and drag components of sail forces. However, to make these forces practical for performance predictions, they must be converted into components parallel with and perpendicular to the direction of motion, known as driving and side forces. Figure 25 illustrates the process for transforming lift and drag into drive and side forces. An additional geometric transformation is necessary to calculate forces under heeled conditions. These forces will be used in the equilibrium conditions demonstrated in Section 3.1 of the report. They will be balanced with the hydrodynamic forces until a steady state amongst the two is achieved.

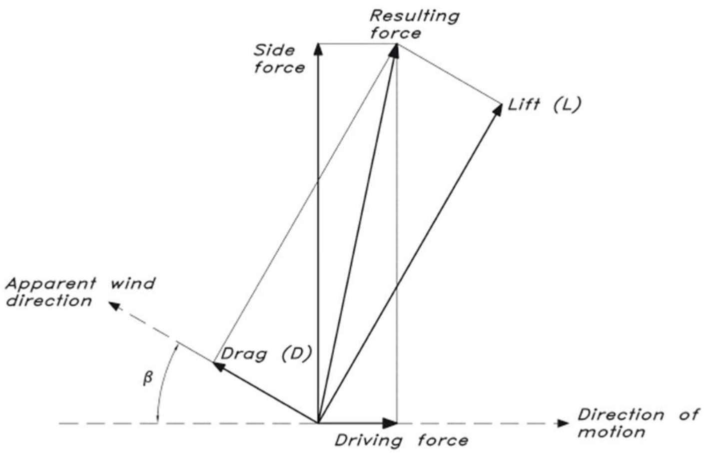

Figure 25 - Relation between aerodynamic force components (Larsson et. al 2023)

The driving force F_M is crucial for determining the yacht's velocity and overall performance, it represents the resultant force acting on the yacht “pushing” it forwards, due to wind pressure on the sails. It depends both on the lift and drag forces and can be calculated using the following equation:

$$F_M = L \cdot cos(AWA) - D \cdot sin(AWA) \quad (36)$$

Whereas the heeling force F_H or aerodynamic side force is the one responsible for the boats heel to leeward and can be obtained by the sum of the lift and drag lateral components.

$$F_H = L \cdot cos(AWA) + D \cdot sin(AWA) \quad (37)$$

This side force creates the heeling moment M_{heel}:

$$M_{heel} = F_H \cdot h \quad (38)$$

That depends on h, the vertical distance from the centre of effort height, where the sail forces are “applied” and the centre of lateral resistance (hydrodynamics).

$$h = zCoE + HBI + zCLR \quad (39)$$

The centre of efforts of each individual sail are measured above sheerline, and zCLR measured from the waterline, so the term HBI (freeboard at the base of the mast) also needs to also be accounted for.

The lift and drag forces, depend on the previously calculated coefficients, the sail plan nominal area, the sailing speed and the dynamic pressure. The lift generated by the sail, which acts perpendicular to the apparent wind, is expressed as L. In this equation, ρ represents the air density, AWS denotes the apparent wind speed, A_N the sail area, and C_L refers to the lift coefficient.

$$L = \frac{1}{2} \cdot \rho \cdot C_L \cdot A_N \cdot AWS^2 \quad (40)$$

In a similar manner, the drag components can be computed utilizing the corresponding area and drag coefficient associated with each component. All drag components are oriented in alignment with the apparent wind. The drag components are determined using the following expression, where D represents drag, ρ denotes the density of air, AWS indicates the apparent wind velocity, A_N signifies the respective area for each drag component, and C_D refers to the total drag coefficient.

$$D = \frac{1}{2} \cdot \rho \cdot C_D \cdot A_N \cdot AWS^2 \quad (41)$$

5.8 Aerodynamical Model Results

This chapter presents and validates the results obtained from the hydrodynamic model developed for the OceanVPP. The hydrodynamic model plays a critical role in determining the yacht's performance by evaluating resistance components.

This subchapter focus is the evaluation and comparison of performance outcomes associated with various aerodynamic coefficients, specifically within the context of the Hazen model.

5.8.1 Validation

To validate the aerodynamic model, NavalAPP (2024) was used. There are not many tools available that independently calculate aerodynamic forces independently or even using the same method adopted, making NavalAPP one of the only suitable choices. There are some theoretical differences in methodology: NavalAPP uses the ORC aerodynamical model, while the OceanVPP follows the Hazen method. To align results for this validation, the Hazen method was applied using ORC coefficients.

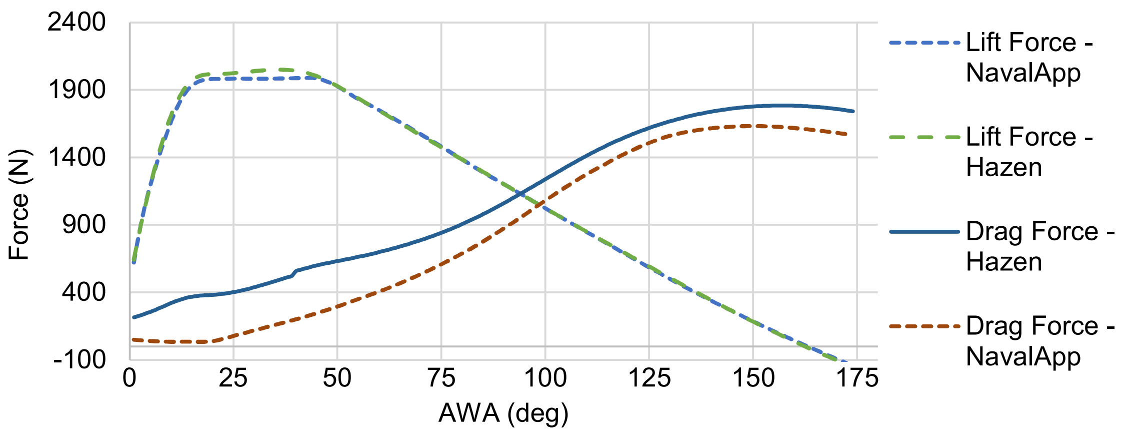

Figure 26 - Hazen Method Validation (Lift and Drag Forces Upwind)

Figure 26, comparing lift and drag forces as a function of apparent wind angle between the Hazen model and NavalAPP reveals notable distinctions.

The NavalAPP lift force model peaks at approximately 1900 N around 30 degrees AWA, while the Hazen model reaches a higher peak of approximately 2300 N around the same angle. Regarding the drag force, ORC model shows a more gradual increase with AWA, contrasting with OceanVPP's model, which increases more sharply and reaches a higher value. The drag results show the highest deviation when comparing the two force outcomes. These discrepancies arise from the different theorical foundation especially accentuated in the drag formulations.

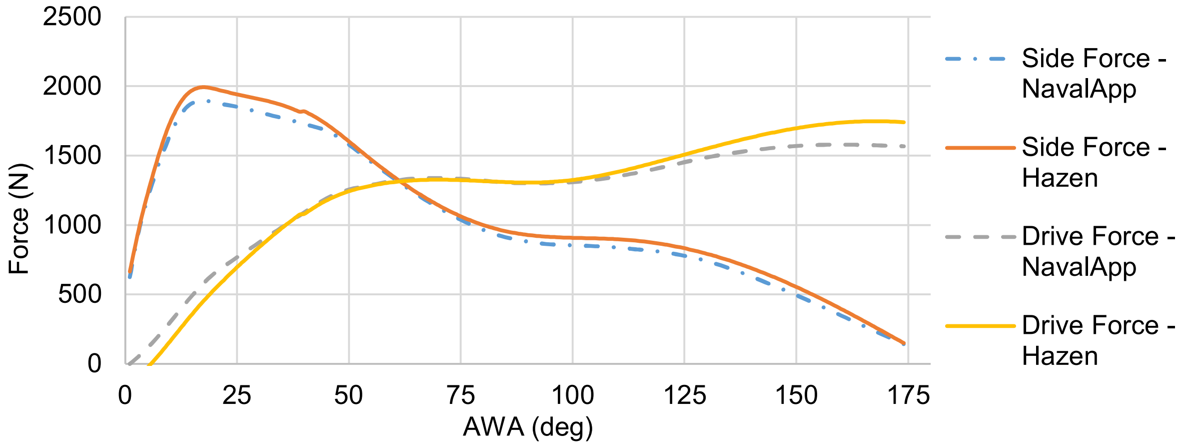

Figure 27 - Hazen Method Validation (Side and Driving Forces Upwind for AWS = 5; V = 2.57 (m/s); Heel = 0º)

Figure 27 shows the side and driving forces as functions of the AWA, the Hazen model again demonstrates a different force distribution compared to NavalApp's.

These two forces are dependent on the two examined before, so some of these results were expected. Considering the increased drag obtained previously and the lift force being relatively close, the side force would naturally be higher as it increases with the two (Equation 36). The driving force is lower at low AWA angles and higher at broader angles. This is because, at broader angles, the sailing yacht transitions from using the lift component to relying on drag. The lift forces, which are perpendicular to the AWA, do not contribute to the forward motion, while the drag forces do. Despite discrepancies in the drag, the results remain within an acceptable range

5.8.2 Sensitivity Analysis of Aerodynamical Coefficients on the Hazen Method

In this chapter, the impact of different aero coefficients on two primary forces in this model, driving force and side force, will be evaluated. To assess the results, the contributions of lift and drag, which underlie these forces, will also be presented. The following plots were obtained for a boat velocity of 5 knots, with a true wind speed of 5 knots, no heeling, and depict the variations in lift and drag forces as functions of the true wind angle.

In Figure 28, the peak lift for the main and jib, occurs around a TWA of 30 degrees across all models. The Hazen coefficients produce slightly higher peak lifts compared to the IMS and ORC indicating a steeper lift profile.

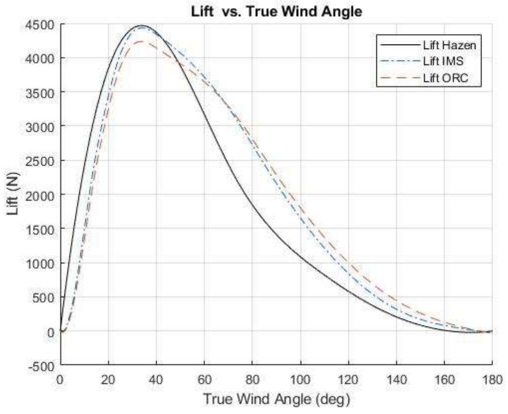

Figure 28 - Lift over TWA (Main and Jib)

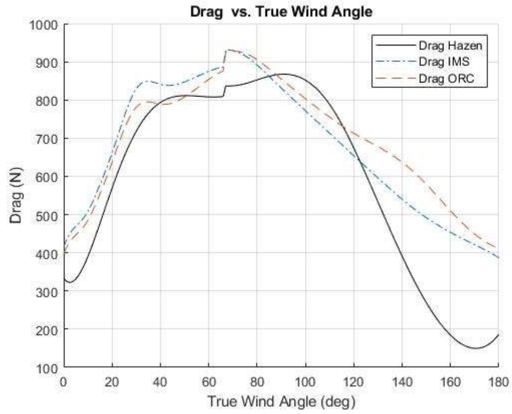

Figure 29 - Drag over TWA (Main and Jib)

Beyond the peak, lift values decline consistently across all models, although the rate of decrease varies, with the Hazen's generally decreasing with a higher degree until approximately 110 degrees, after which it converges with the IMS and ORC models. Regarding Figure 29 the drag increases with the wind angle, reaching maximum values between 70 and 80 degrees for the IMS and ORC while Hazen only around the 90 degrees. The IMS model shows the highest peak drag, followed closely by the ORC model, while the Hazen model exhibits a more moderate drag increase. As the true wind angle approaches 180 degrees, drag decreases across all models, with the Hazen model displaying a slightly lower drag profile than the IMS and ORC models, suggesting potentially reduced resistance at broader wind angles.

Figure 30 and Figure 31 depict the same results but now using a spinnaker for the downwind configuration. Both lift and drag forces increase significantly with the transition to a downwind sail, due to the sail area increase, as the jib area is 45 m2 and the spinnaker's 105 m2.

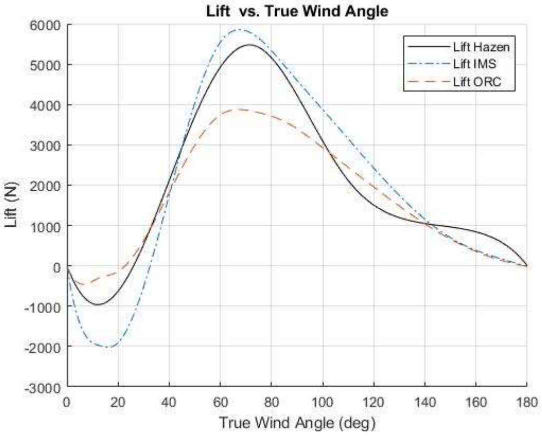

Figure 30 - Lift over TWA (Main and Spinnaker)

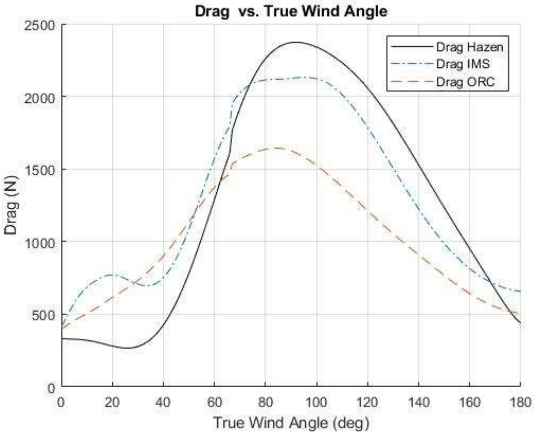

Figure 31 - Drag over TWA (Main and Spinnaker)

The lift forces peak values in the downwind case, shift from 30º to 80º, an increase as expected (Figure 30). The IMS coefficients lead to higher values, followed by Hazen and ORC's. A significant change was the fact that the ORC produce the lowest values, contrary to the previous case. This change can be validated by analysing the Aerodynamic Coefficients in Appendix II, where the ORC does, in fact, have the lowest spinnaker sail coefficients.

Regarding the drag (Figure 31), the peak drag occurs around 50 to 60 degrees of TWA across all models, with the Hazen coefficients showing the highest drag profile, followed by the IMS model, and the ORC model consistently exhibiting the lowest drag values.

Overall, the inclusion of downwind sails amplifies both lift and drag forces without altering the fundamental characteristics of each model's response across varying wind angles. The ORC downwind coefficient led to lower force magnitudes, contrary to the upwind case.

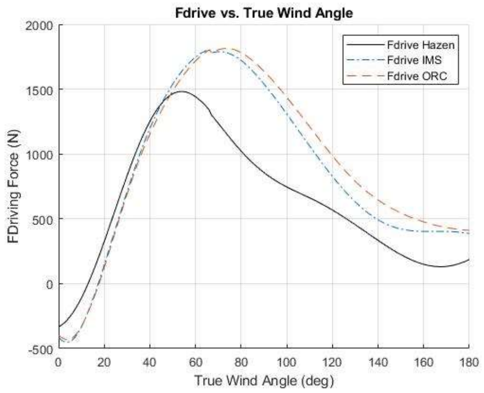

Figure 32 - Driving force over TWA (Main, Jib)

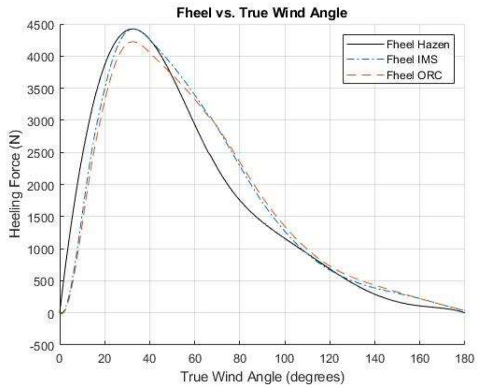

Figure 33 - Heeling force over TWA (Main, Jib)

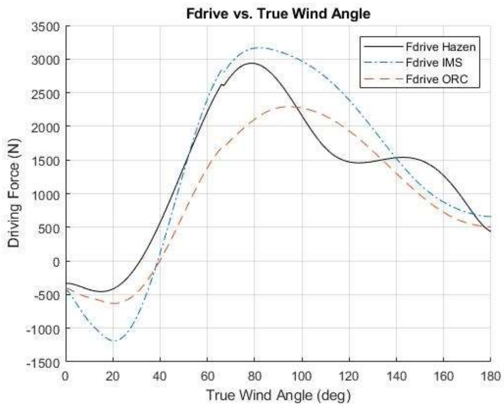

Figure 34 - Driving force over TWA (Main, Spinnaker)

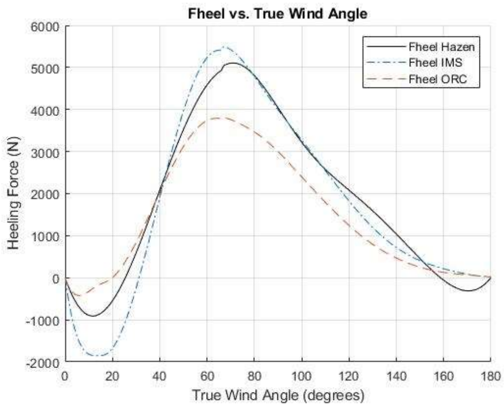

Figure 35 - Heeling force over TWA (Main, Spinnaker)

Regarding the impact on the driving force upwind (Figure 32 and Figure 33), the Hazen coefficients exhibit a lower peak driving force, reaching its maximum at approximately 50 degrees and declining sharply thereafter. Conversely, both the IMS and ORC models achieve higher driving forces, peaking slightly beyond 70 degrees and maintaining elevated levels over a wider range of wind angles. This indicates that the IMS and ORC will derive higher driving forces and therefore velocities across varying wind conditions compared to Hazen. As for the heeling force, it remains reasonably close to the three obtained results for main and jib sail combinations.

As mentioned earlier, the ORC coefficients result in the lowest lift and drag force values. Since the driving and heeling forces depend on these two components, the expected outcome occurred, as shown in Figure 34 and Figure 35.

5.8.3 Impact of Reef and Flat on Sail Forces

This chapter delves into the aerodynamic principles underlying sail performance, focusing on the effects of reefing and flattening on the driving force of a sail. Adjusting reefing, which reduces sail area by lowering sail height, and flattening, which decreases the sail's camber, optimizes the sail's aerodynamic efficiency for varying wind conditions.

Figure 36 illustrates the impact of the reefing factor on the driving force across a range of apparent wind angles, with the flat factor fixed at 1.0. As the reef factor decreases, there is a denoted reduction in driving force across all AWAs. The peak driving force diminishes progressively with lower reef values, reflecting the reduction in sail height and, consequently, the centre of effort. This leads to a proportional decrease in both lift and viscous drag, as reefing directly reduces the aerodynamic load on the sail.

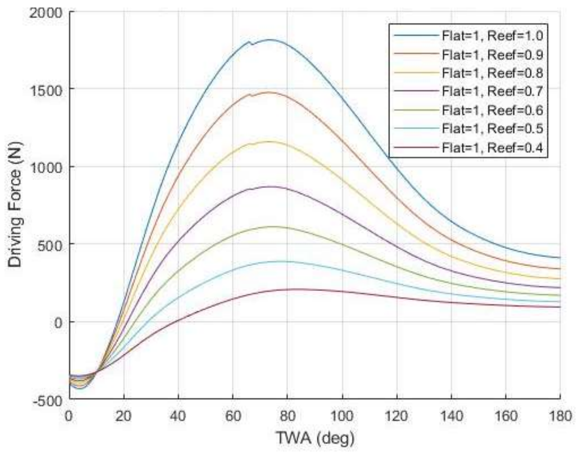

Figure 36 - Reefing Impact on the Driving Force (for TWS = 5; V = 2.57 (m/s); Heel = 0º)

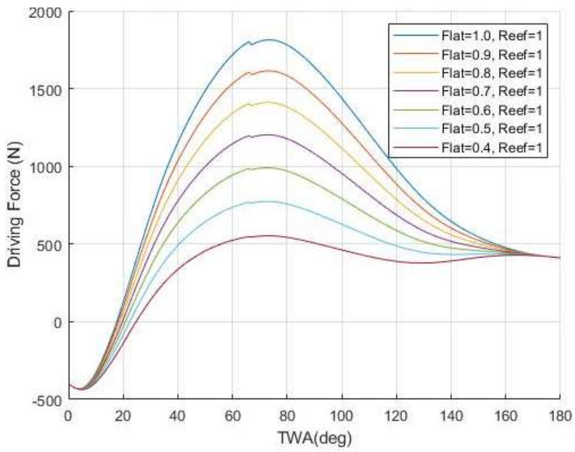

Figure 37 - Flattening Impact on the Driving Force (TWS = 5; V = 2.57 (m/s); Heel = 0º)

In Figure 37 a similar reduction in driving force is observed with decreasing flat values. However, the reduction pattern shows a different patter as flattening primarily influences lift without affecting the heeling arm. This reduction in lift is accompanied by a more pronounced decrease in the induced drag due to the relationship of drag with the squared flat factor. Thus, flattening generally retains more of the driving force than reefing, especially at moderate AWAs.

In conclusion, reefing results in a more uniform reduction in driving force across all angles by lowering the sail's centre of effort, while flattening achieves a more targeted reduction in drag relative to lift. This analysis reinforces the principle that flattening the sail should precede reefing to optimize driving force at moderate wind angles.

6. HYDROSTATICS AND STABILITY MODEL - OCEANVPP

The perceptions of the ideal yacht shape have undergone numerous transformations. These changes are influenced in part by evolving regulations and, more recently, by an enhanced understanding of the physical principles governing yacht behaviour.

Hydrostatics and stability are arguably one the most crucial aspects of yacht design, as they determine a yacht's ability to carry weight and resist heeling from sails. The larger the initial stability of a sailing yacht, the better it can withstand aerodynamic forces, allowing the designer to project a larger sail area for the rig. It is important to note that stability knowledge primarily pertains to static conditions without waves on the water surface (Gerr, 2007). In the 1990s, a technical committee of the International Standards Organization (ISO) developed a standard for evaluating the stability of pleasure craft up to 24 meters in length, which encompasses sailing vessels (Oossanen, 1997). This standard sufficiently addressed the stability assessment of small sailing yachts (Izaguirre et. al, 2008).

The resilience of a sailing yacht against to withstand the wind generated forces is represented by its righting moment curve. Key stability parameters for sailing yachts also include the area under the righting moment curve up to the angle of vanishing stability, the righting lever at a 90-degree heel, and the down flooding angle (Oossanen, 1997). Various stability criteria generally specify minimum thresholds for these parameters. For traditional assessment methods, specific vessel characteristics are required alongside the righting moment curve, such as displacement under various loading conditions, sail area, and configurations with and without sails. For more detailed analyses, computational CFD simulations can be employed to model the yacht's behaviour under various conditions, including large angles of heel as it provides a comprehensive understanding of the flow around the hull and the resulting forces and moments, allowing for precise stability assessments.

Additionally, empirical methods can also be used, especially when detailed hull geometry data is not available. These methods rely on historical data and established formulas to estimate stability characteristics based on key parameters such as length, beam, and displacement. This approach, while less precise than numerical or CFD methods, offers a practical solution for preliminary design assessments. In the VPP context, stability is reflected directly in the righting moment, The OceanVPP software requires the user to input the GZ results in function of the heeling angle.

6.1 Righting Moment

Defined as the moment that acts to restore a yacht to its upright position after being heeled by external forces, the righting moment is essential for ensuring the vessel's safety and efficiency. The hull geometry of a sailing yacht significantly influences its righting moment. The centre of buoyancy (CB), which is the centroid of the submerged volume of the hull, shifts as the yacht heels. The relationship between the hull shape and the movement of the CB is a primary determinant of the righting moment.

The distribution of ballast within the yacht also affects the centre of gravity (CG). The vertical and horizontal positions of the CG relative to the CB determine the righting moment, by developing the righting arm (GZ). Additionally, the weight distribution within the yacht influences the centre of gravity

The righting moment calculations heavily depends on the results the large angle stability. Mathematically, this righting moment can be expressed as:

$$Mhull_{RM} = \nabla \cdot \rho \cdot g \cdot \mathrm{GZ} \quad (42)$$

Where ∇ is the total displacement volume of the yacht, ρ is the density of water, g is the acceleration due to gravity, and GZ represents the righting arm, which is the horizontal distance between the CG and the CB at a specific heel angle. The static stability curve illustrates the righting moment across different heel angles.

6.2 Crew Righting Moment

The crew righting moment on a sailing yacht pertains to the righting moment generated by the strategic positioning and movement of the crew members. Unlike the inherent righting moment derived from hull geometry and ballast distribution, the crew righting moment is a dynamic and adjustable factor, crucial in competitive sailing and heavy weather conditions. As the yacht heels due to wind forces, the crew shifts their weight to the windward side, effectively increasing the lever arm distance between their collective centre of gravity and the heeling axis. This action creates a counteracting moment that opposes the heeling moment induced by aerodynamic forces on the sails. The effectiveness of this technique depends on the crew's weight, their ability to move efficiently, and their coordination in response to changing conditions. By maximizing the crew's righting moment, the yacht can maintain an optimal heel angle, thereby improving hydrodynamic efficiency and enhancing speed and manoeuvrability. This active stabilization method is integral to performance sailing, where quick, precise adjustments by the crew can make significant differences in racing outcomes and overall vessel control in adverse conditions. Consequently, understanding and optimizing the crew righting moment is essential for both safety and competitive advantage in sailing. This methodology adheres to the IMS (Poor, 1986) for calculating the crew's restoring moment on the vessel. When the waterline length exceeds 16 feet, the crew is assumed to be positioned along the deck edge, distributed symmetrically around the vessel's centre of gravity. To determine the movable crew weight contribution to the restoring moment, IMS defines two conditions based on LWL:

$$CW_{rail} = \begin{cases} (0.7 \cdot LWL - 1.33) \cdot 170 & if\ LWL < 16 \\ (0.375 \cdot LWL - 3) \cdot 170 & if\ LWL > 16 \end{cases} \quad (43)$$

The restoring moment created by the crew (M_{CREW}), is then obtained by multiplying the crew weight on the rail by a moment arm factor

$$M_{CREW} = (C_{ARM} \cdot CW_{rail}) \cdot \cos(\varphi) \quad (44)$$

Here C_{ARM}, represents the crew's moment arm, calculated as follows:

$$C_{ARM} = 0.475 * (\mathrm{B}_{max} - 1) \quad (45)$$

To refine this calculation, a corrective parameter, $M_{CREWeff}$, accounts for the boat's heel angle, and matches the crew's moment to it. For small heel angles (under 6°), where both righting and heeling moments remain "low", the crew's restoring moment can overwhelm the convergence, which may affect the stability calculations within the VPP. In such cases, the crew is positioned closer to the centreline, reducing their leverage effect.

To achieve a smooth transition of the crew's stabilizing influence, R_{MAUG} is scaled to be zero at zero degrees heel and gradually reaches the full crew restoring moment on the rail at angles above 6°.

If $\varphi < 6$ º

$$M_{CREWeff} = M_{CREWeff} \cdot \sin(15 \cdot \varphi)^2 \cdot sign(\varphi) \tag{46}$$

6.3 Dynamic Righting Moment

The term RMV is used to represent the discrepancy between the hydrostatic righting moment calculated and the actual righting moment generated by the hull when it moves through water.

$$RMV = \frac{5.955 \cdot 10^{-5}}{3} \cdot disp \cdot LWL \cdot \left(1 - 6.25 \cdot \frac{B_{cb}}{\sqrt{AMS_{CB}}} - 2.1\right) \cdot SLR \cdot \varphi \tag{47}$$

Where:

AMS_{CB}	=	Maximum section area of canoe body
B_{cb}	=	Canoe body beam
$disp$	=	Displacement
LWL	=	Waterline Length
SLR	=	Speed length ratio

6.4 Appendages Heeling Moment

The hydrodynamic heel, referred to as HydroHeel, represents the heel effect caused by the lift forces on the underwater appendages. This value is calculated as the product of the distance from the waterline to the CLR and the aerodynamic heeling force.

$$HydroHeel = CLR \cdot F_H \tag{50}$$

6.5 Results

Figure 38 shows the GZ-curve for the YD–41 model.

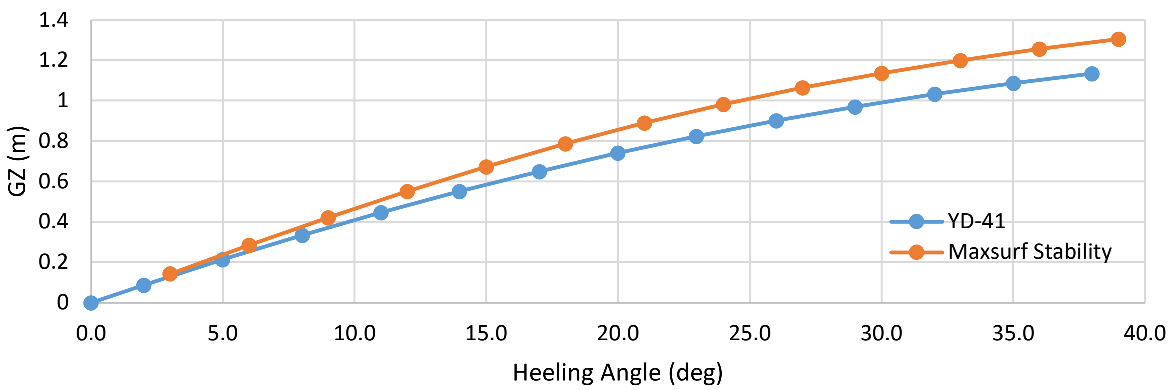

Figure 38 - YD-41 GZ Curve

The plot compares the righting arm (GZ) values in meters versus the heeling angle in degrees for two stability assessment methods: YD-41 (Larsson et. al, 2022) and Maxsurf Stability (using the developed benchmark model). Both curves display a similar trend, with GZ values increasing as the heeling angle increases. However, the *Maxsurf Stability* curve consistently yields higher GZ values across the heeling angles, suggesting greater righting arm. The discrepancy between the two methods becomes more pronounced at higher angles, with the *Maxsurf Stability* curve maintaining a steeper gradient. This divergence likely reflects differences in modelling assumptions or computational approaches between the two stability analysis tools.

7. BENCHMARK YACHT MODEL

This chapter presents the benchmark yacht model developed to use as an input for MaxsurfVPP, tool who's going to be used to compare its results with OceanVPP. By using a well-documented and widely studied yacht, the YD-41 leverages extensive hydrodynamic and aerodynamic data, providing a solid foundation for validating its accuracy. The following sections detail the model main design variables, data sources, and specific parameters applied in the validation process.

7.1 Forsatio YD-41 Sailing Yacht

The hull lines for YD-41 (Yacht Design 41-footer) were obtained from Principles of Yacht Design by Larsson et al. (2023), which enabled the construction of a 3D model from the documented lines. Using this model, large-angle stability curves were generated to support the stability model, and the hull to run the VPP simulation on other software's. The following Figure 39 illustrates the 3D model and key views of YD-41, showcasing its design features and dimensional accuracy based on the referenced hull lines. These views provide insight into the model's structural and stability characteristics. It is worth noting that the keel bulb design was not included in the model, as the hydrodynamic method selected for this study does not account for keel bulbs. To ensure compliance with established standards, the YD-41's design parameters were compared with the DSYHS guidelines to confirm the suitability of the proposed assessment method.

Table 6 - YD-41 compliance with DSYHS thresholds (Keuning & Sonnenberg, 1998)

Parameter	Min	Max	YD-41
Length - beam ratio (LWL / BWL)	2.73	5.00	3.74
Beam - draft ratio (BWL / Tc)	2.46	19.38	7.95
Length - displacement ratio (LWL / disp^1/3)	4.34	8.50	6.53
Longitudinal centre of buoyancy (%)	0.0	-8.2	-4.2
Longitudinal centre of flotation (%)	-1.8	-9.5	-7.3
Prismatic Coefficient	0.52	0.60	0.56
Midship Area Coefficient	0.65	0.78	0.715
Loading factor	3.78	12.67	8.05

Table 6 outlines the key geometric and hydrostatic properties, demonstrating the model's alignment with the hydrodynamic method and therefore solidating the choice. The YD-41 model meets essential design criteria within acceptable ranges, thereby affirming its suitability for the hydrodynamical method selected. A rigorous design process is essential to ensure the VPP model provides accurate and reliable predictions. Yacht performance prediction is highly sensitive to parameters like hull shape, keel geometry, and sail configuration, meaning even minor inaccuracies can skew results.

Precision in modelling these elements allows for realistic forecasts of speed, stability, and handling, closely reflecting real-world behaviour.

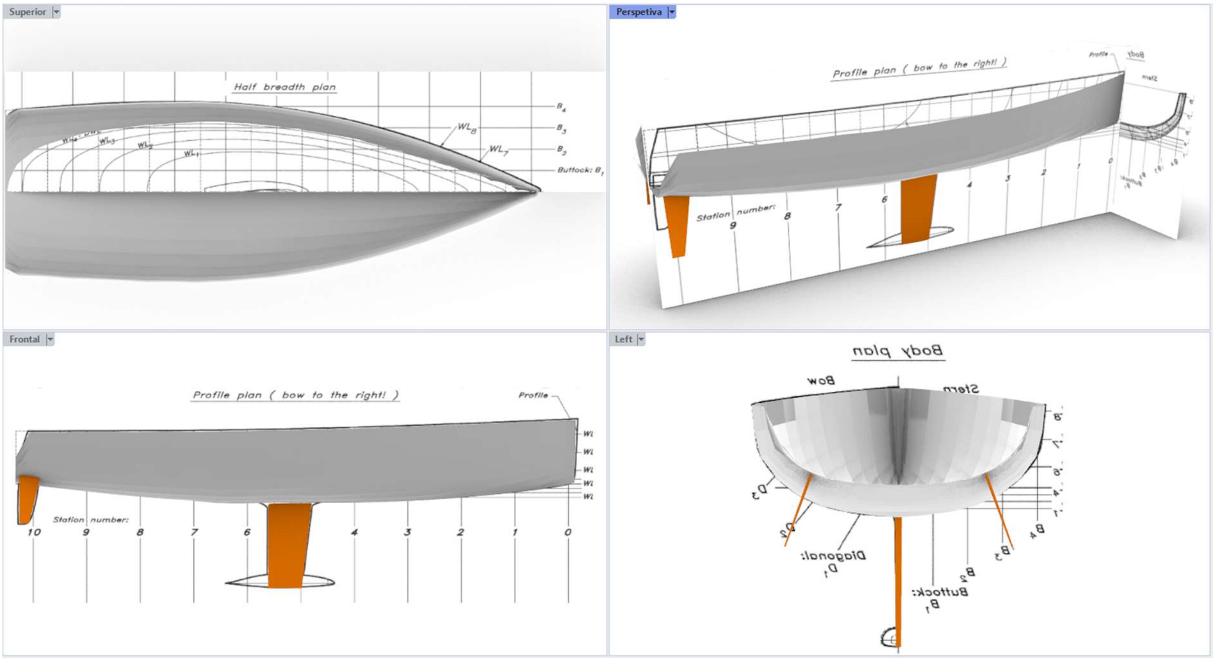

Figure 39 - YD-41 test model developed

7.2 3D Model Validation

To validate the model created from the hull line drawings, a comparison will be conducted between the original design parameters and the values derived from the *Maxsurf* own analysis of the model. This validation needs to be performed to ensure that no discrepancies derive alone from development of a 3D hull model. Maxsurf VPP requires the model to interpret the surfaces and derive measurements for calculating hydrodynamic forces and VPP results. These possible minor discrepancies in dimensions will reflect the transition from the original 2D design intent to the 3D model's geometric interpretation, where small variances can influence the final hydrodynamic calculations and performance predictions.

Table VI-2 presents a comparison between the initial design variables and the results from Maxsurf analysis, highlighting minor discrepancies across most parameters. Regarding the length parameters, the L_{oa} shows a slight increase of 1.1%, while L_{WL} demonstrates a minor decrease of -0.4% in the *Maxsurf* output. Both the beam measurements, B_{WL} and B_{MAX} are almost aligned, with only -0.6% and 0.7% deviations, respectively. Draft values show no discrepancies, while depth (D) also remains unchanged. The waterplane area (A_W) presents a slight reduction of -1.2%, and the volume parameters, such as ∇_{cb} and $\triangle_{cb}$, are also closely matched, with minor discrepancies of -0.5%. However, larger deviations are noticeable in the longitudinal centre of buoyancy (L_{CB}) and the longitudinal center of flotation (L_{CF}), both showing an increase of 2.9%. As for the coefficients, the block coefficient (C_b) remains virtually identical with a 0.4% difference. However, the prismatic coefficient (C_p) and midship coefficient (C_m) exhibit greater variations, with C_p increasing by 1.4% and C_m by 3.5%. Some minor discrepancies were anticipated due to limitations in design scrutiny, the lack of resolution in the drawing lines from the source led to occasional line overlapping, which limited the accuracy. Additionally, the deviation is also influenced by Rhinoceros' internal algorithm for creating surfaces from a set of lines.

This algorithm may introduce slight variations as it interpolates between the lines to generate surfaces, further contributing to the observed discrepancies. In summary, most parameters show minor, expected deviations, with the larger discrepancies mainly related to coefficients, particularly C_p and C_m, making the developed model suitable for benchmarking results across different softwares.

8. OCEANVPP RESULTS

In this chapter, the results obtained from the developed OceanVPP are presented and analysed to assess the performance and reliability of the model in predicting sailing yacht speeds. Using YD-41 as a benchmark model, the VPP’s accuracy is evaluated across a range of conditions, with particular attention to the influence of the wind, hull characteristics, and sail configurations on the predicted velocities. This analysis not only verifies the VPP’s capability to forecast yacht performance under diverse scenarios but also highlights any limitations and areas for improvement. To validate and contextualize the results generated by the developed VPP, the outputs are compared with those from two established resources: MaxsurfVPP (2023) and the ORC certificate results.

8.1 VPP Outputs

The two common methods to present VPP results are polar plots and table formats, both relevant to inspect and visualize different parameters. For more detailed information on the possible outputs, please consult Appendix I.

8.1.1 Table Format

While polar plots are an excellent tool for visualizing velocity results across different sailing angles and wind speeds, they primarily provide a graphical summary. This makes them particularly useful for quickly identifying trends and overall performance characteristics. However, a table format complements this by offering a detailed breakdown of the data, enabling a more comprehensive evaluation of multiple variables simultaneously. The output table contemplates key parameters such as boat speed, true wind angle, true wind speed, heel angle and the outputs form each aero-hydro model can be analysed in depth. This detailed representation facilitates cross-referencing values, performing specific checks, and identifying potential discrepancies or patterns that might be less apparent in the polar plot.

For a complete breakdown of the OceanVPP results, including all relevant variables, consult Table VII-1 and Table VIII-1. These two tables consolidate the raw outputs from the simulation and serves as a critical reference for comparisons and further analysis.

8.1.2 Polar Plot

VPP results are often presented as polar plots, offering a clear visual representation of yacht performance across various wind conditions. Figure 40 illustrates the VPP output for the YD–41 yacht, where each solid line represents yacht speed at a specific true wind speed. The yacht's speed can be interpreted by measuring the distance from the centre of the plot to each point along the curve, across a range of true wind angles. The vertical axis reflects boat speed, while each individual line corresponds to a different TWS, showing how the yacht performs at increasing wind strengths.

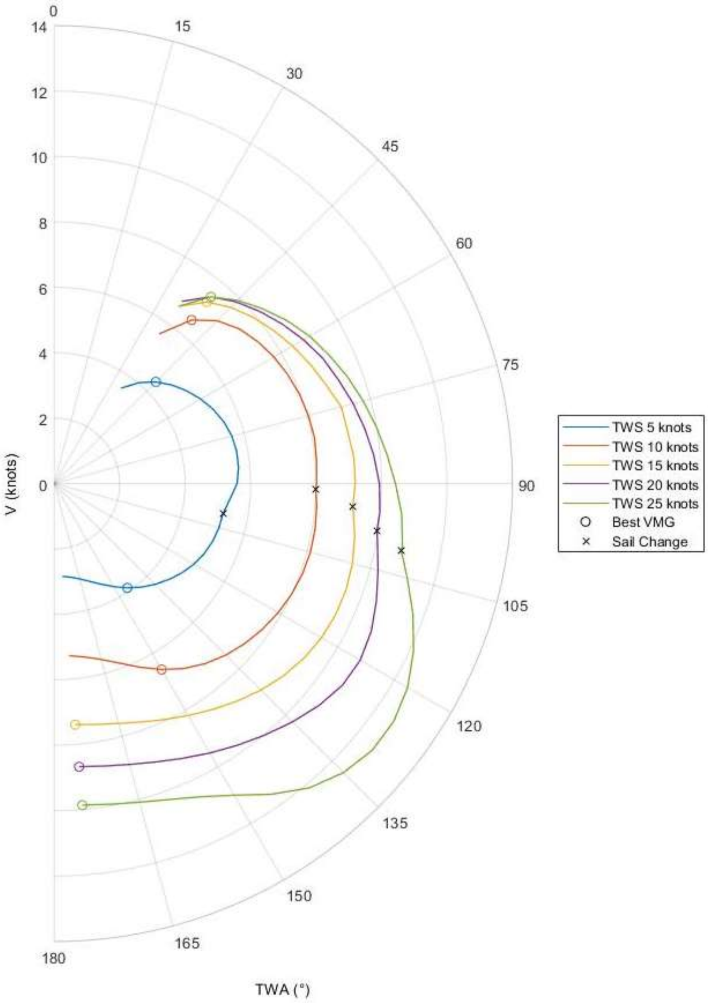

Figure 40 - YD-41 polar diagram (using ORC coefficients)

Key points of interest include the two points on each curve (marked by circles), which denote the yacht's optimal upwind and downwind performance, also known as the best Velocity Made Good (VMG). These points indicate the angles and speeds at which the yacht achieves maximum efficiency when sailing upwind and downwind. Additionally, a small cross symbol on the plot marks the recommended point for sail changes, providing guidance on when to switch sails to maintain optimal performance under changing wind conditions. This polar plot format is invaluable for understanding the yacht's handling and performance capabilities, allowing designers and sailors to make informed adjustments for improved speed and efficiency.

8.2 OceanVPP Validation

The present subchapter will compare and validate the results obtained in OceanVPP with two other VPP tools, Maxsurf VPP and ORC VPP. Before establishing any comparison there needs to be an assessment on the methodologies each VPP software uses. It is important to note that there are different theorical backgrounds in each of the comparison software's. The table below summarizes the differences amongst the different methods chosen by each VPP.

Table 7- VPP software theorical backgrounds

	Maxsurf VPP	OceanVPP	ORC VPP
Aerodynamical model	IMS (Poor, 1986)	Hazen (1980)	ORC (2024)
Aero Coefficients	IMS (Poor, 1986)	Hazen / IMS / ORC	ORC (2024)
Hydrodynamical model	IMS (Poor, 1986)	Keuning et. al 1998*	ORC (2024)
Large Angle Stability	LPP	Outsourced	LPP
Hydro Required Inputs	Hull shape	Design variables	Hull Shape
Aero Required Inputs	Rig measurements	Rig measurements	Rig measurements
Number of DOF	2	2	2
***Some of the resistances follow more recent approaches outside of the paper published by Keuning et. al 1998**			

As shown in Table 7, the two comparison models differ from the VPP under analysis, despite sharing some similarities. One of main differences that conditions the accuracy of the results is the use of an internal lines processing plan (LPP) by both the IMS and ORC. The LPP, in its essence, is a hydrostatic program that processes offset data defining the hull shape and its results are the hull data necessary for the VPP to run. The results can contemplate hull/appendages measurements, large angle stability, fore and aft girth station locations, freeboard measurements, amongst other.

8.2.1 Maxsurf and OceanVPP Hydrodynamical Model

As presented in Table 7, the Maxsurf hydrodynamic method operates within the IMS framework (Poor, 1986), yet its foundation is rooted in the work developed by Delft University based on towing tank experiments, as documented by Gerritsma et al. (1981) and later in Gerritsma et al. (1991). The current version applied in the OceanVPP is a more recent evolution of these earlier methods for estimating hull and appendages drag. There are some commonalities in principle, particularly in the equations used for resistance calculations.

The differences in method pertain to the heeled resistance calculations. The IMS model computes the total change in resistance based on the total upright resistance, applying a correction factor that correlates with the heel angle. In contrast, the more recent Delft series calculates the changes independently for each resistance component, residuary or frictional, subject to alteration. The change in the canoe body frictional resistance, for example, follows the change of the hulls wetted surface. Additionally, the IMS does not account for changes in the drag component of the appendages.

While there are additional changes, these two represent the most significant discrepancies. It is worth noting that although these methods were updated in subsequent years, there is no reference that Maxsurf updated the algorithm. Additionally, MaxsurfVPP has its own LPP, and uses its measurements to calculates the outputs of the hydrodynamical model. Poor (1986) summarizes the IMS methodology extensively.

8.2.2 Maxsurf and OceanVPP Aerodynamical Model

Regarding the aerodynamic method, it is important to note that both models are based on the initial work developed by Kerwin, which was later improved upon by Hazen. The IMS aerodynamic model, however, incorporates significant advancements beyond Hazen's original iteration.

The IMS aero model introduces a more comprehensive approach by accounting for sail parameters that were not considered in the earlier version. These enhancements include factors such as sail roach, the blanketing effect between sails, different method to estimate sails centre of effort, previously defined as the geometrical centre of the sail plan and now given as a function of apparent wind directions and the rig characteristics. Additionally, the IMS model places greater emphasis on sail flattening, resulting in more accurate performance predictions. By integrating these parameters, the IMS model provides a more precise evaluation of aerodynamic forces acting on the vessel, reflecting the impact of sail shape and interaction with wind conditions more thoroughly than previous iterations. These improvements enable more refined simulations, particularly in varying wind conditions and complex sail configurations.

8.2.3 ORC and OceanVPP Aerodynamical Model

The primary differences between the ORC and OceanVPP models reflect a similar pattern to the discrepancies observed between the IMS and OceanVPP. In essence, the ORC model incorporates a broader range of sail parameters to account for sail shape, surpassing those considered in the IMS, through the inclusion of additional sail functions such as twist, shape, and power.

The twist function is a mechanism designed to represent the decrease in the height of the centre of effort as the sails are depowered. It correlates the vertical position of the centre of effort with the amount of flatness applied. Wind tunnel experiments indicated that this reduction was proportional to the degree of fractionality. Additionally, the centre of effort height is further diminished through jib foot reduction, which is reflected in the reef parameter, ranging from 1.0 to 0.5. While the twist function is associated with the flat parameter, the reduction in centre of effort height during jib reefing also modifies the boat’s aerodynamic profile. The shape function was introduced to address the inefficiency of large spinnakers in light wind conditions. This inefficiency led to a trend favouring smaller spinnakers. To counter this, a power loss factor was developed for larger sails, reducing the effective area of spinnakers exceeding a defined a "reference area." The current formulation, adopted in 2012, considers the available space for the spinnaker based on ISP and J (sail dimensions), and the type of pole or bowsprit used. The power function was developed to provide a more equitable handicap adjustment in sailing competitions, specifically for variations in spinnaker pole and bowsprit lengths relative to different sail types, including spinnakers, gennakers, and code zero sails. Its primary goal is to ensure that the effective reference area corresponds appropriately with the apparent wind angle, facilitating fair comparisons across different sail configurations. By linking the power function to the length of the spinnaker pole and applying necessary correction factors, the function aims to create a balanced performance evaluation, particularly addressing the differences between deep running symmetrical sails on heavier boats and asymmetrical sails on lighter vessels.

This allows for a more nuanced representation of the overall sail shape conditioning. Furthermore, the ORC model employs a distinct set of aerodynamic coefficients and introduces specific sail coefficients for asymmetrical spinnakers, whether tacked on the pole or centreline, alongside a newly refined depowering scheme, as outlined in Chapter 5.1. Additionally, the ORC method provides more accurate calculations for both individual sail areas and centres of effort, enabling more precise modelling of aerodynamic forces. Moreover, the ability to opt from of high and low lift coefficients further enhances the accuracy by reflecting the boat’s ability to adjust sail configurations. For instance, lower lift and drag coefficients are applied in scenarios where a backstay or running backstays are absent, or in cases where only one pair of running backstays is present. These refinements ensure that the ORC model more accurately represents the boat's performance across a wider range of sailing conditions and boat configurations while still offering enhanced prediction capabilities when compared to earlier models.

8.2.4 ORC and OceanVPP Hydrodynamical Model

This comparison represents one of the most significant evaluations of model discrepancies, given the substantial variations it reveals. The ORC model relies on direct measurements from its own LPP output for both the hull and appendages. For the hull, it provides metrics such as second moment length (lsm), hull coefficients, effective dimensions, and various ratios. The appendages are analysed through strip-wise segmentation, enabling the calculation of wetted surface area, volume, and basic dimensions, including draft and chord length. These measurements are then integrated to develop the hydrodynamic model.

In addition, the ORC model is continually refined, with recent updates reflecting progress in hydrodynamic modelling techniques. The latest formulation for residuary resistance now depends exclusively on the beam-to-effective draft ratio (BTR) and length-volume ratio (LVR), utilizing a methodology that evaluates variations in residuary resistance (Rr) for each Froude number in relation to a baseline boat with LVR and BTR both equal to 6. This updated approach incorporates a series of neural networks, allowing for precise determination of resistance coefficients across a broader design spectrum. Moreover, modifications have been made to the length model to enhance the representation of the vessel's dynamic length. The formulation for viscous resistance has also been revised to more accurately reflect the appropriate reference length, particularly for modern canoe body shapes

Whereas in the canoe body viscous resistance, the same principle remains but some small adjustments were made, the form factor from 1 to 1.05 (2013) and the reference length from 0.7 to 0.85.

Heeled resistance has been a focal point of ORC improvements over the years. The updated hydrodynamic model introduces a new formulation for heeled drag, calculating both heeled viscous and residuary resistance components. These calculations utilize the same parameters, wetted surface area, beam-to-effective draft ratio, and length-volume ratio, but are specifically adjusted to account for the boat's heeled condition.

The procedure for calculating induced resistance within the ORC's velocity prediction program involves several critical stages. It begins by dividing the applied aerodynamic side force dynamic pressure, resulting in the required total coefficient of lift area (tcla). This value is then used to determine the leeway angle, which represents the vessel's angle of drift due to lateral forces. Once the leeway angle is established, the individual lift contributions of the hull and appendages are calculated separately at this specific angle. Next, the induced drag components for both the canoe body and appendages are derived from their respective effective spans. The effective draft of the canoe body, along with the mean hull span distance (MHSD), serves as the effective draft value within the applied equation. This approach ensures that the calculation accurately accounts for the hydrodynamic behaviour of the hull and appendages under sail. In contrast to other methodologies that may calculate multiple induced resistances, the method employed in OceanVPP simplifies the process by calculating a single induced resistance based on the total lateral surface area of the hull and keel combined.

8.2.5 Maxsurf VPP

The subsequent comparison was conducted utilizing the data inputs detailed in Table 8. This analysis aims to evaluate two distinct software's with different initial methodologies, as outlined in the previous chapter, so an approximation of the running conditions across the different platforms was made. The OceanVPP software provides a flexible framework that allows users to modify the aerodynamic coefficients and the GZ results for each simulation, facilitating straightforward adjustments to the run configurations. This capability enhances the ability to explore various performance scenarios and assess how changes in parameters impact overall vessel behaviour.

Table 8 - VPP run configuration 1 (Maxsurf and OceanVPP)

Inputs	Maxsurf VPP	OceanVPP
Hull and appendages	LPP measurements from YD-41 test model	Design Variables
Rig data	Rig dimensions (Appendix V)	Rig dimensions (Appendix V)
Aerodynamical coefficients	IMS (Appendix II)	IMS (Appendix II)
Vertical CG	0.26 (m) (below WL)	0.26 (m) (below WL)
Large Angle Stability	*Internally calculated*	*Outsourced by Maxsurf Stability*

Table 8 outlines the different inputs for the same VPP configuration between Maxsurf VPP and OceanVPP. Maxsurf VPP internally processes the results obtained from LPP assessment of the provided YD-41 test model, while OceanVPP requires the design variables to be inputted manually. Both the rig dimensions and vertical centre of gravity are identical in both systems and are manually defined. Instead of comparing Hazen coefficients with those of IMS, the same IMS coefficients were used to evaluate the outcomes using consistent aerodynamical data. Large angle stability is also calculated internally in Maxsurf VPP, whereas OceanVPP outsources this task from Maxsurf Stability.

Table 9 details the results obtained in this first comparison made. It is highly important to denote that the values demonstrated are the average relative error, given in percentage, across all the TWAs for each TWS. For example, for a TWS of 5 knots, the average error over the selected TWA (in this case, from 35º to 110º, with increments of 5º) is -4%, and so on, for the rest of scope. Further data regarding the OceanVPP upwind results can be consulted in Table VII-1.

Table 9 - Upwind discrepancy between OceanVPP and Maxsurf VPP

TWS	V	Heel	Fdrive	Fside	Reef	Flat	Mheel	Hydro Heel	Hull RM	Crew RM
5	-2%	3%	0%	-5%	0%	0%	5%	-4%	12%	-7%
10	-3%	-6%	1%	-6%	0%	0%	3%	-5%	10%	-8%
15	-4%	-21%	9%	-2%	-5%	13%	2%	-5%	9%	-8%
20	-2%	-23%	21%	5%	-3%	11%	2%	-6%	8%	-9%
25	0%	-24%	32%	13%	-1%	9%	1%	-6%	7%	-9%

At lower wind speeds, differences in the sailing speed and heeling are minimal, showing close alignment between the two models. As wind speed increases, OceanVPP predicts slightly higher speeds and reduced heeling. The driving force (Fdrive) and side force (Fside) differences are notable, particularly at higher wind speeds, where the developed VPP shows significantly higher values. The balance achieved between the two moments (Mheel/Mright) are relatively consistent between the two VPPs. Hydrodynamic heeling differences are small, while the OceanVPP predicts slightly increased contributions from hull and crew righting moments at higher wind speeds.

Figure 41 and Figure 42 show the stated discrepancies associated with Table 9. The upwind polar plot shows differences between the performance predictions generated by OceanVPP and MaxSurf under various true wind speeds. These discrepancies can be observed across a range of true wind angles, highlighting the variations in predicted velocities between the two VPP tools, particularly at higher wind speeds.

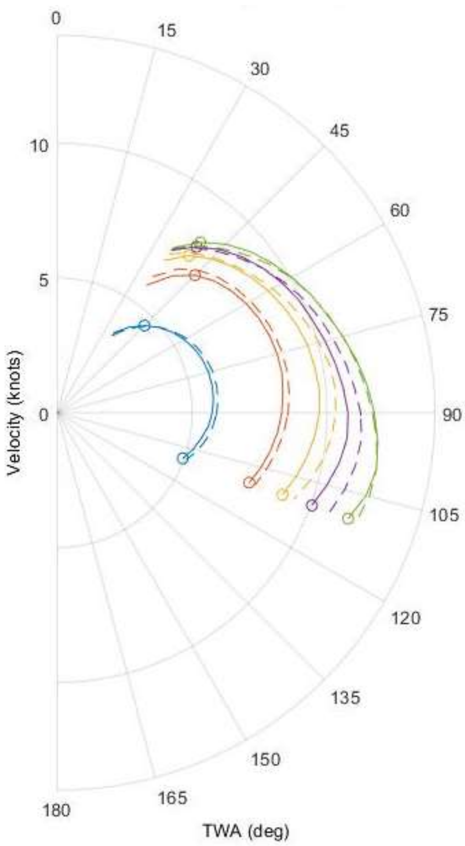

Figure 41 - Upwind polar plot, OceanVPP and Maxsurf

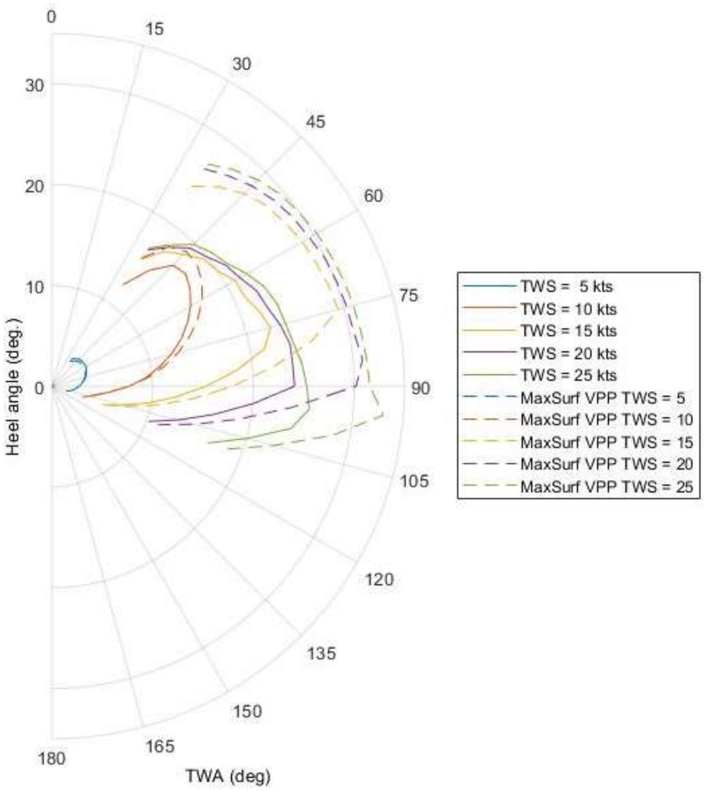

Figure 42 - Upwind polar plot, OceanVPP and Maxsurf (Heeling Angle)

Regarding the velocity, and as demonstrated in Table 9, there is a strong agreement between the two software's. A slight underestimation by OceanVPP happens across the first four wind speeds (5,10,15 and 20 knots), while for a TWS of 25 knots the results converged. The results derived at this last wind speed, are already beyond the Froud Number (0,6 ≈ 12.4 knots for the YD-41) studied in the DSYHS Series 4. The hydrodynamic model results are therefore using the linear extrapolation mentioned which ended up causing this change on the underestimation pattern.

The heeling angle polar indicates that the heeling angle exhibits greater deviations between the two models. For the first two TWS values, the results are reasonably similar. In the developed OceanVPP, the heeling angle is a constrained variable within the optimization loop and is limited to 35º. In contrast, Maxsurf manages this constraint internally, making it unclear what maximum heeling angle is applied. However, the results suggest that Maxsurf leads to significantly higher heeling angles. This discrepancy becomes evident in Figure 42, where the difference is relatively minor at lower wind speeds but increases notably as wind intensity rises.

There's three possible reasons for this deviation happening:

- Different sail depowering scheme

There is a difference in the depowering scheme, as OceanVPP constantly prioritizes the reefing over the flattening, contrary to the Maxsurf VPP, more on this topic later in the present subchapter.

- Possibly lower heeled resistance prediction by Maxsurf

As mentioned in Chapter 4, the heeled resistance prediction is not available within the Maxsurf results, and if there is a lower prediction in this component, the MaxsurfVPP will not find any constraint or consequence when trying to find equilibrium at higher heel angles.

- Higher Hull Righting Moment

As summarized in Table 9 there is a slight deviation (7-12%) in the obtained hull righting moment, which can also impact the heeled results. With a higher Hull RM the boat can sustain the sails induced heeling moment better therefore leading to smaller heeling angles.

Figure 43 and Figure 44 illustrate the discrepancies in driving force and righting moment, respectively, as referenced in Table 9. Figure 43 compares the OceanVPP driving force (equal to total resistance, as equilibrium has been reached) with the results from Maxsurf. Figure 44 presents a similar comparison but for righting moment/heeling moment.

Figure 43 shows the equilibrium obtained between the driving force and total resistance for the two software's. The attained results demonstrate a strong correlation for lower wind speeds, while increasing significantly for higher speeds. For the VPP to achieve equilibrium in higher values than expected, the resistance must match the driving force or the contrary. One of these two terms is conditioning the equilibrium, by forcing the convergence to occur at higher values.

As examined in Sub-Chapter 5.8 and demonstrated in Figure 15, there is a discrepancy between the two hydrodynamic models. Beyond 8,5 knots (approximately) Maxsurf underestimates the resistance, which causes a lower equilibrium convergence between the driving force and the total resistance.

Regarding the moment's equilibrium (Figure 44), there are some discrepancies within the smaller contributors, but a good agreement between the two major components, Mheel and Mright. The heeling moment comprises the sails heeling moment and the hydrodynamic heel caused by lift generated by the appendages, whereas the righting moment the hull and crew righting moment.

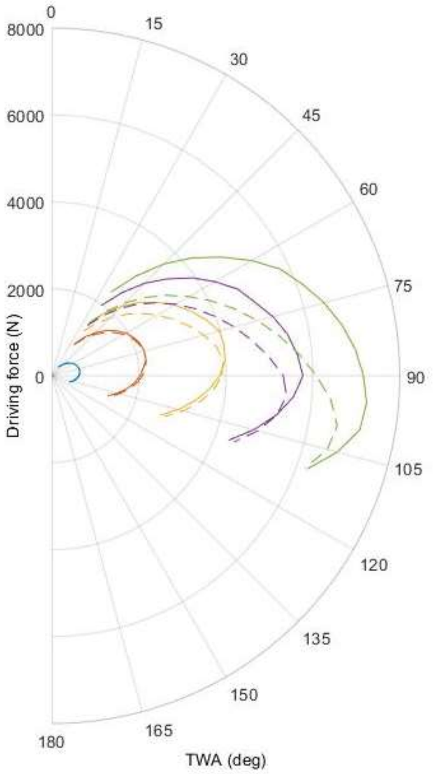

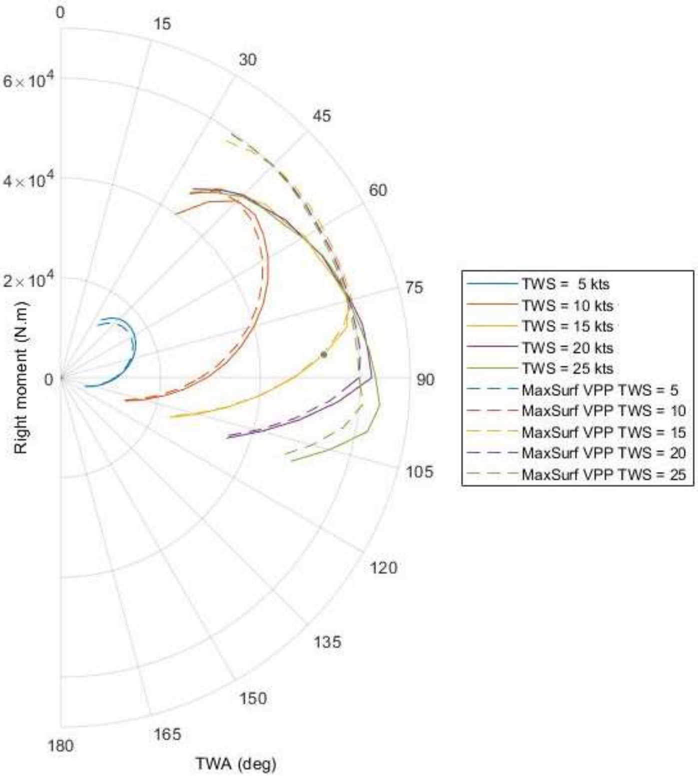

Figure 43 - Upwind polar plot, OceanVPP and Maxsurf (Driving Force)

Figure 44 - Upwind polar plot, OceanVPP and Maxsurf (Righting/Heeling Moment)

Figure 45 and Figure 46 illustrate the discrepancies on the sail shape parameters reefing and flattening.

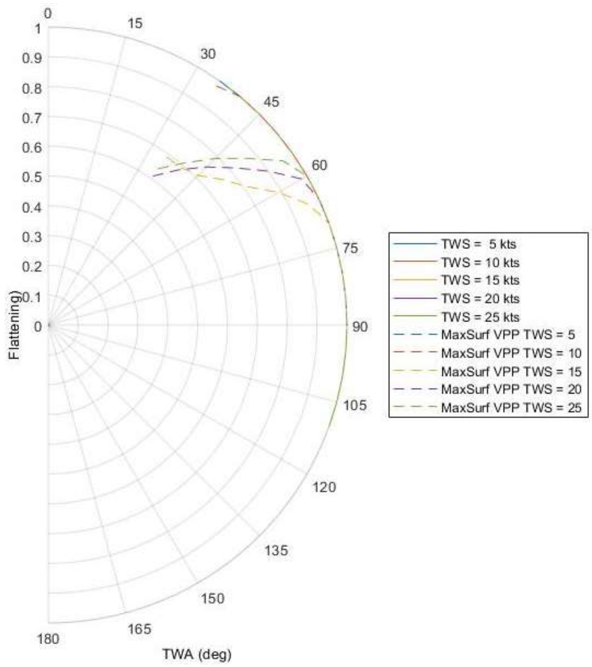

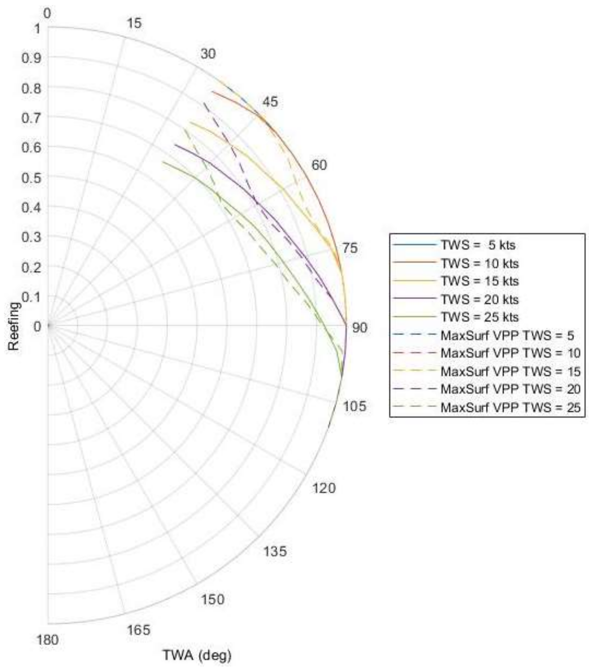

Figure 45 - OceanVPP and Maxsurf Upwind polar plot, (Sails Flattening)

Figure 46 - OceanVPP and Maxsurf Upwind polar plot, (Sails Reefing)

The OceanVPP solutions consistently prioritize changing the reefing values instead of flattening. Figure 45 shows how in this simulation the equilibrium is achieved by not using the sails flattening variable, while in MaxSurf the flattening is used for lower sailing angles (between 35º to 65º). This sailing angles most of the time require some sail tunning to limit the heeling angle and avoid the resistance increase with it. In OceanVPP the developed tool controls the heeling angle by adjusting the reefing values, as depicted in Figure 46. Compared to the Maxsurf results, it is possible to denote that the lack of flattening use, is followed by an excessive reefing use. This occurrence in fact contradicts the common real-world practice, but the implemented Hazen model coupled with the *Matlab* bult-in function fmincon consistently prioritize reefing, as it has more weight on the equations than the flattening. Overall, the upwind results obtained display the satisfactory results when compared to Maxsurf, with the most significant discrepancy being the heeling angle.

Table 10 details the results obtained in this first comparison but for the downwind condition.

Table 10 - Downwind discrepancy between OceanVPP and Maxsurf VPP

TWS	V	Heel	Fdrive	Fside	Reef	Flat	Mheel	HydroHeel	HullRM	McrewRM
5	1%	8%	1%	-3%	0%	0%	10%	-1%	15%	-2%
10	-2%	-4%	3%	-4%	-1%	0%	5%	-3%	10%	-8%
15	-3%	-11%	11%	0%	-2%	5%	4%	1%	8%	-8%
20	0%	-11%	19%	6%	0%	2%	6%	8%	12%	-7%
25	7%	-13%	22%	12%	1%	1%	6%	14%	14%	-7%

OceanVPP predicts slightly higher speeds at 5 and 25 knots, while Maxsurf shows higher speeds at mid-range TWS. Heeling angles are consistently higher in OceanVPP, peaking at 13% on average at 25 knots. The driving force (Fdrive) is significantly higher in OceanVPP, especially at higher TWS, while the side force (Fside) and reefing remain close, except for a 12% reefing difference at 25 knots. Moment discrepancies (Mheel, HydroHeel) grow at higher TWS, with HydroHeel reaching 14% at 25 knots. Hull righting moments are consistently higher in OceanVPP, while crew righting moments are slightly lower.

Figure 47 and Figure 48 illustrate the stated discrepancies associated with Table 10.

Regarding the downwind velocity polar plot shown in Figure 47, the same patterns observed in the upwind conditions are present here as well. A notable discrepancy is that the difference at a TWS of 25 knots is much larger than in the upwind case. Downwind sailing generally results in higher speeds, as the force vectors are more aligned with the driving force. Consequently, the linear extrapolation beyond 12.6 knots has a greater impact than in the upwind case.

For the heeling angle, the same curve patterns appear in Figure 48, but with smaller magnitudes in OceanVPP. As with the upwind conditions, the discrepancies are lower, as downwind sailing tends to produce smaller heeling angles.

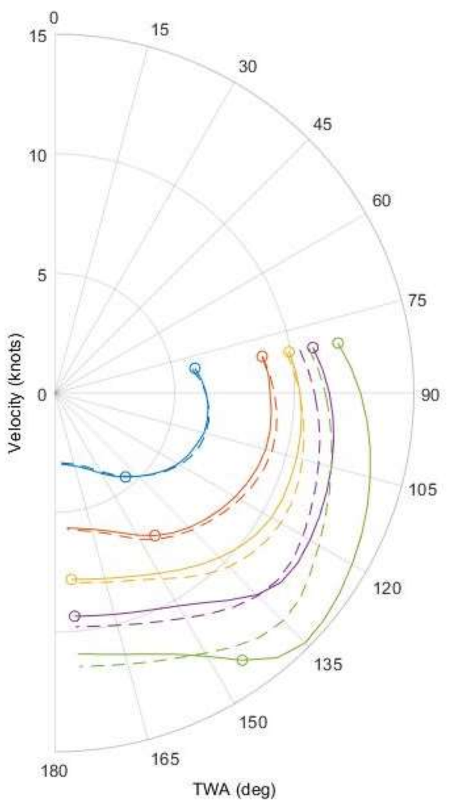

Figure 47 - Downwind polar plot, between OceanVPP and Maxsurf

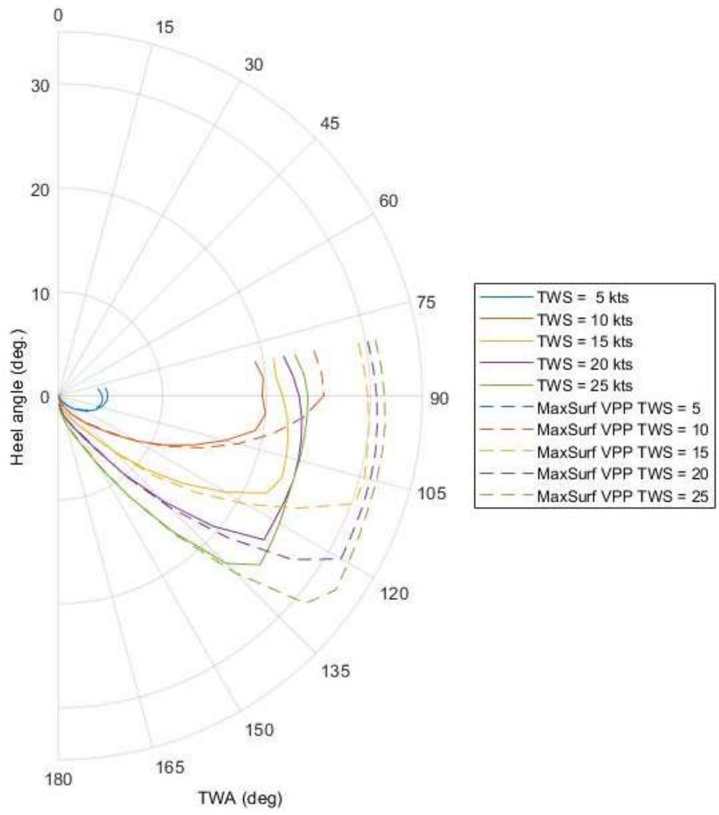

Figure 48 - Downwind polar plot, between OceanVPP and Maxsurf (Heeling angle)

Figure 49 and Figure 50 illustrate the discrepancies in driving force and righting moment, respectively, as referenced in Table 10.

Figure 49 illustrates the equilibrium between the driving force and total resistance for both software programs. The results show a strong correlation at lower wind speeds, with a significant increase at higher speeds. For the VPP to reach equilibrium at higher values than expected, the driving force and resistance must balance. One of these factors dictates the equilibrium, forcing the convergence to occur at higher values. This same behaviour is observed in the downwind conditions as well.

Regarding the Righting/Heeling Moment (Figure 50), there are some discrepancies within the smaller contributors, but a good agreement between the two major components, Mheel and Mright. The heeling moment comprises the sails heeling moment and the hydrodynamic heel caused by lift generated by the appendages, whereas the righting moment the hull and crew righting moment.

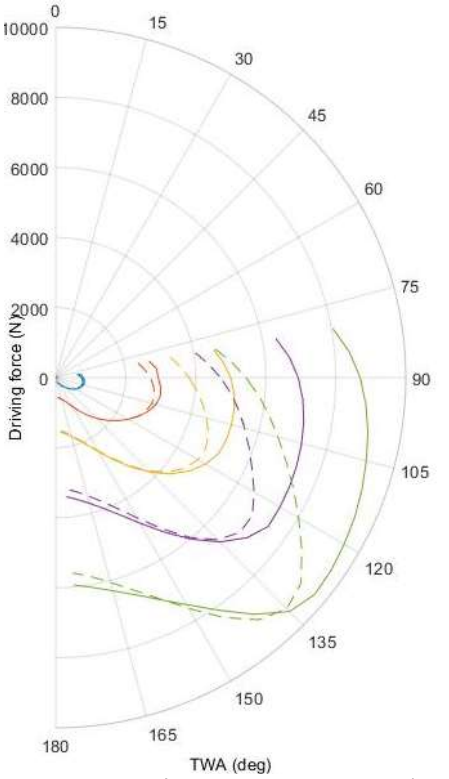

Figure 49 - OceanVPP and Maxsurf (Driving Force)

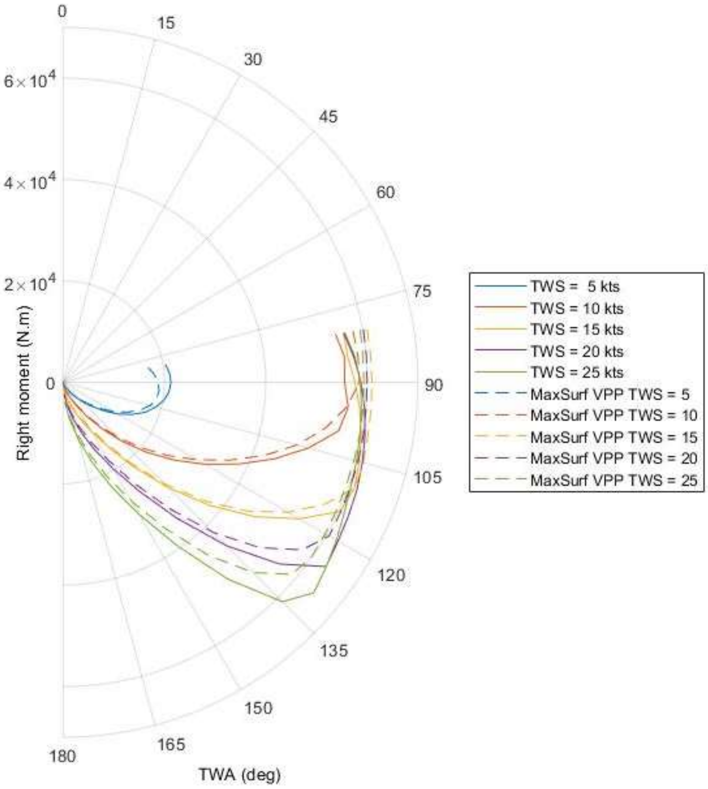

Figure 50 - OceanVPP and Maxsurf (Righting Moment)

Figure 51 and Figure 52 illustrate the discrepancies on the sail shape parameters reefing and flattening.

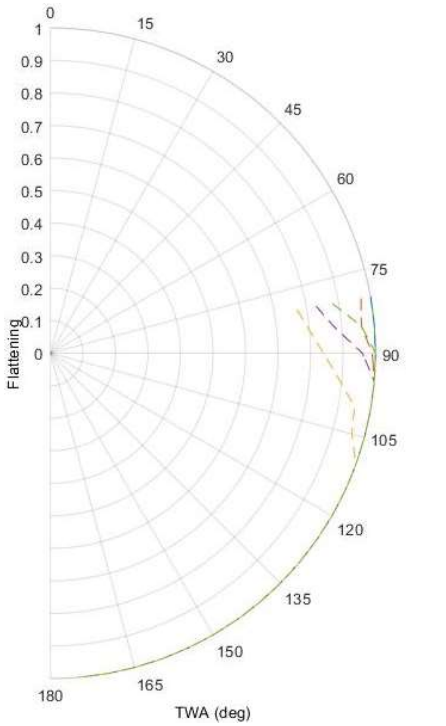

Figure 51 - OceanVPP and Maxsurf Downwind polar plot, (Sails Flattening)

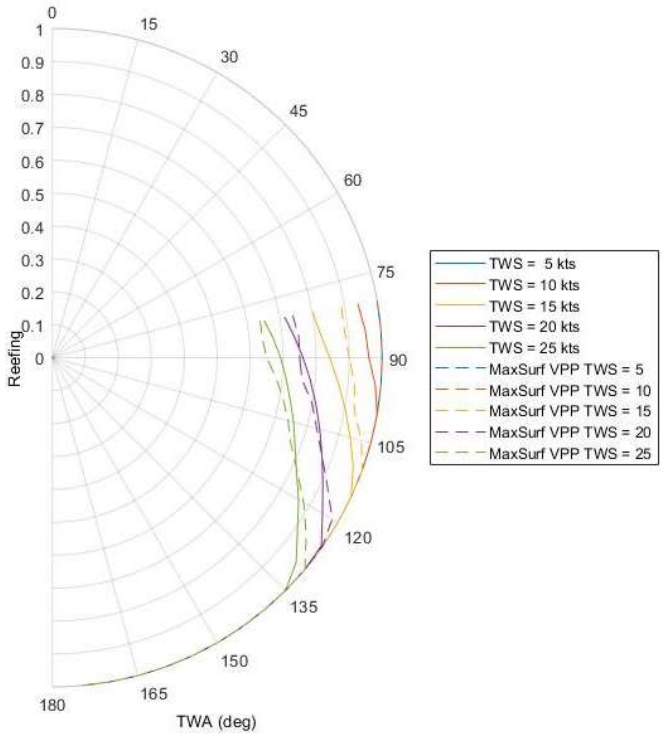

Figure 52 - OceanVPP and Maxsurf Downwind polar plot, (Sails Reefing)

The OceanVPP downwind solutions also consistently prioritize changing the reefing values instead of flattening for the downwind sailing as well.

8.2.6 Offshore Racing Congress

The subsequent comparison was performed using the input data presented in Table 11. Unlike the previous analysis, which utilized Maxsurf software, ORC software cannot be employed here, as it is proprietary and not open source. Therefore, this comparison relies on an examination of ORC certificates for the test model vessel, available for reference in the Appendix IX or through the ORC database (https://orc.org/sailors/active-certificates-database). When interpreting these results, it is essential to consider that the ORC's output table presents optimal results achieved with various sail combinations available on the vessel, without specifying which combination was used in each case. To address this and ensure consistency, given that OceanVPP currently supports only main, jib, and spinnaker sail configurations, two distinct ORC certificates were consulted: one certificate excluding the spinnaker and another including all three sails. The table highlights the input variations for the same VPP configuration between ORC and OceanVPP.

Table 11 - VPP run configuration 2 (ORC and OceanVPP)

Inputs	ORC	OceanVPP
Hull and appendages	*LPP measurements internally calculated*	Design Variables
Rig data	Rig dimensions (Appendix E)	Rig dimensions (Appendix E)
Aero coefficients	ORC	ORC
Vertical CG	0.26 (m) (below WL)	0.26 (m) (below WL)
Large Angle Stability	*Internally calculated*	*YD-41 GZ results (Larsson et. al 2023)*

The ORC results without the use of the official software are very limited to derive many conclusions, only the velocity results are provided across a limited true wind angle and wind speeds. The following table summarizes the main discrepancies between the OceanVPP results, and an ORC YD-41 certificate without contemplating any spinnaker, main and jib sail only.

Table 12 - ORC and OceanVPP comparison (non-spinnaker).

TWS/TWA	6kt	8kt	10kt	12kt	14kt	16kt	20kt	24kt
52º	0%	1%	1%	2%	4%	6%	10%	14%
60º	2%	2%	2%	3%	5%	7%	11%	15%
75º	4%	3%	4%	5%	6%	7%	10%	15%
90º	5%	3%	3%	4%	5%	5%	7%	11%
110º	3%	2%	-1%	-2%	-2%	-3%	-5%	-1%
120º	-3%	-6%	-7%	-7%	-7%	-7%	-10%	-14%
135º	-13%	-15%	-16%	-14%	-12%	-10%	-11%	-14%
150º	-10%	-11%	-11%	-10%	-8%	-6%	-4%	-4%

Table 12 demonstrates the relative error, given in percentage, across all the TWAs combination with different TWS. For example, for a TWS of 6 knots, the relative error with a TWA of 52º is 0%, and so on, for the rest of scope. Also, a positive value indicates higher results obtained from OceanVPP relative to the ORC. From the results depicted, it is possible to identify several notable trends in the relative error across various TWA and TWS combinations.

With increasing TWA for each fixed TWS, the relative error initially increases, up until 90º, and then the OceanVPP velocity results decrease at a much greater rate than those derived from ORC. For instance, at 6 knots, the error rises from 0% at 52º to a maximum of 5% at 90º, before dropping to -10% at 150º. The OceanVPP therefore initially slightly overestimates the velocity up until the 90-100º mark to only underestimate beyond these angles.

Conversely, when analysing the effects of the wind speed increase at fixed angles, the relative error generally grows. For each TWA, larger wind speed values tend to correspond to higher relative errors. At 52º, for example, the error increases consistently from 0% at 6 knots to 14% at 24 knots. This trend, however, is less uniform at broader angles, where values become more erratic; negative errors prevail between 120º and 150º.

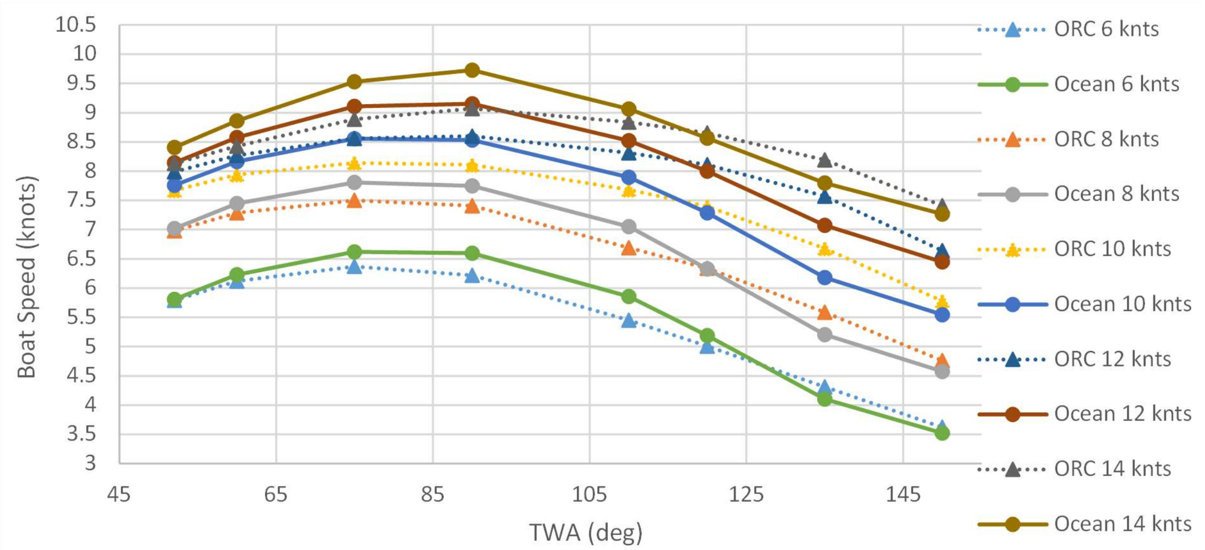

Figure 53 - ORC and OceanVPP comparison (non-spinnaker)

The current comparison, as mentioned, is only considering main and jib sail combination, and from Figure 53 it is possible to visualize that around 125º is when the OceanVPP starts underestimating results. These sailing angles are already in the downwind domain, where the spinnaker is leveraged to benefit from the increase in the drag forces and decrease in the lift. It is possible that the ORC has more parameters to account for sail adjustments due to using the incorrect sail plan for this configuration. Also, higher angles usually mean better sailing angles as the driving component increases and there is less heeling. Higher wind speeds, in turn produce greater aerodynamic forces, as shown in Chapter 5.7, where the dependence on the apparent wind speed was established. This increase results in an elevated final velocity. Exceptions arise when a significant increase in wind speed induces excessive heeling. In such cases, the OceanVPP will adjust reefing or flattening parameters to mitigate this effect, reduced the lift or the sail area, and end up reducing the higher equilibriums. The problem arises from the mentioned as the ORC method adopts a different depowering scheme, it will first change the flattening up until the minimum allowed value is reached, to start only then reducing the jib area, and only then the main. This discrepancy alone can lead to such deviations, without mentioning all the different parameters that differ in principle (more on Chapters 8.2.3 and 8.2.4).

The following table summarizes the main discrepancies between the OceanVPP results, and an ORC YD-41 certificate contemplating the total sail plan, main, jib and spinnaker.

Table 13 - ORC and OceanVPP comparison (Main, Jib and Spinnaker).

Wind Velocity	6kt	8kt	10kt	12kt	14kt	16kt	20kt
52º	3%	2%	1%	2%	5%	7%	3%
60º	4%	2%	2%	4%	6%	9%	4%
75º	5%	5%	5%	7%	8%	10%	5%
90º	15%	9%	10%	11%	10%	10%	15%
110º	12%	5%	6%	8%	9%	11%	12%
120º	9%	2%	2%	3%	3%	5%	9%
135º	1%	-1%	-2%	-1%	-1%	-4%	1%
150º	-5%	-5%	-5%	-4%	-2%	-2%	-5%

Considering the results obtained and displayed in Table 13, for the total sail plan, (Main, Jib and Spinnaker), the following conclusions can be derived. The same pattern as examined in the non-spinnaker results, is present, initially this model increasingly overestimates the velocity up until the 125-130º mark to only underestimate beyond these angles. Figure 54 illustrates the discrepancies obtained for the velocity.

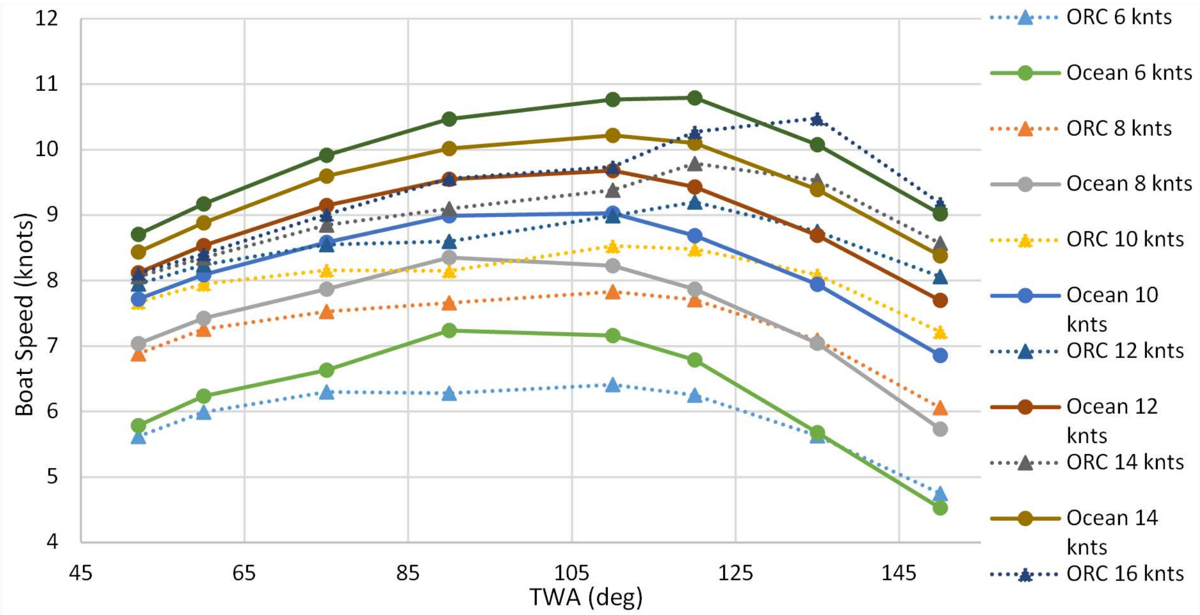

Figure 54 - ORC and OceanVPP comparison (Main + Jib + Spinnaker)

At the 90º mark, a significant increase in deviation between the two predicted velocities is observed. As mentioned, the ORC certificate only reports the best performance for each sail configuration, while the present tool allows for tracking the timing of sail changes. In this case, the change occurs precisely at 90º. The YD-41 uses an asymmetrical spinnaker, which is important for reaching angles (90º to 150º) and beneficial at lower wind speeds. Although the sail change occurs early, it is not an unusual timing. The ORC results, however, show more stable velocities throughout the study range, without indicating any velocity increase due to the sail change.

9. CONCLUSIONS AND FUTURE WORK

9.1 Conclusions

The primary aim of this project was the development of a velocity prediction program for sailing yachts. The developed tool exhibits accurate results for low wind speeds and some discrepancies as the wind speed arises, but in general the results can be considered satisfactory.

The hydrodynamic model presented predicts the same resistance increase with the velocity as the one used in NavalAPP who shares the same theoretical background. When compared to Maxsurf a deviation arises, particularly at speeds above 9 knots approximately which impacts some of the results in the developed software. In these cases, the aero model outputs, specifically the driving force and side force, are higher than those predicted by Maxsurf. The increase in resistance beyond this speed causes the aerodynamic model to converge to higher values to maintain equilibrium between the driving force and the total resistance. One limitation of the hydrodynamic model is the use of the DSYHS Series 4, whose formulations are only derived for Froude numbers of 0.6. The decision to linear extrapolate beyond this value affected the accuracy at higher sailing speeds and, consequently, the VPP results for true wind speed of 25 knots.

The Hazen method despite limited, provided a straightforward approach for assessing aerodynamic forces. However, its coefficients, calculated for only five fixed angles, introduce potential interpolation deviations across intermediate angles. The outputs of the Hazen model closely align with ORC results, especially the lift force. The three set of available aerodynamical coefficients play a large role in the outcome of the forces as demonstrated in the Chapter 5.8.2. The use of the Hazen coefficients lead to smaller driving and heeling forces upwind and were surpassed by the IMS and the ORC's. In the downwind case, ORC the lowest, Hazen's second and IMS the highest values. With years of accumulated data and better investigation techniques the ORC is expected to produce the most accurate results.

When compared to Maxsurf the velocity results showed great agreement between the two software's and for both sailing conditions. The heeling angle comparison reveals significant deviations between the developed OceanVPP and Maxsurf models, particularly as wind speeds increase. The results are reasonably similar for lower true wind speeds, but as the wind speed increases Maxsurf produces notably higher heeling angles, likely due to differing modelling approaches. The developed OceanVPP constrains heeling angles to a maximum of 35º within its optimization loop, whereas Maxsurf's approach to heeling angle limits remains unclear. This discrepancy can also be attributed to three potential factors. Differences in sail depowering schemes, with the developed VPP favouring reefing over flattening, a potentially lower heeled resistance prediction by Maxsurf, which may allow higher heel angles without consequence, and deviations in the hull righting moment, as the developed VPP shows a 7-12% higher value, incrementing its capacity to counteract sail-induced heeling moments and therefore reducing heeling. These factors collectively explain the increasing divergence in heeling angle predictions between the two models.

When comparing OceanVPP with the ORC, a clear pattern emerges in the velocity predictions. Regarding the comparison made with the ORC non-spinnaker certificate, OceanVPP tends to overestimate velocity, up to approximately 120º TWA, with this trend persisting at higher wind speeds, though less pronounced. Beyond 120º TWA, OceanVPP generally underestimates velocity, particularly in the downwind domain (120-180ª). Upwind, relative errors increase with TWA until 90º, peaking around 5% at this angle before dropping sharply to -10% at 150º. Similarly, at fixed angles, higher wind speeds amplify relative errors, with OceanVPP overestimating at lower angles and showing erratic behaviour with predominantly negative errors at broader angles. Discrepancies arise from differences in depowering schemes and sail plan adjustments. The ORC method applies a distinct sequence for reducing sail area, whereas OceanVPP employs a combined approach of reefing and flattening. Downwind, OceanVPP initially overestimates velocity until 125-130º TWA, after which it underestimates. The ORC results are more stable, showing less sensitivity to sail changes or wind speed variations. These deviations underscore the importance of parameter selection and sail adjustment strategies in achieving accurate velocity predictions.

In conclusion, this report provides a comprehensive overview of a velocity prediction program. A VPP is not merely a tool for predicting the velocity of sailing yachts, it integrates and connects all components of a sailing yacht. This includes the effects of the wind acting on the sails, the water on the hull and appendages, initial stability, weight distributions, sail trimming, and crew actions. To evaluate these parameters, it is necessary to select appropriate methods for predicting forces and moments, followed by developing an algorithm to solve the nonlinear constraints. The OceanVPP serves as a tool for predicting a sailing yacht velocity addressing the increasing demands of the market.

9.2 Future work

The developed OceanVPP exhibits discrepancies in certain cases, indicating a need for refinement. A thorough analysis of these inconsistencies will facilitate improvements in the model's accuracy and reliability.

While the comparisons made with ORC and Maxsurf VPP provide valuable insights into the accuracy of the proposed tool, the ultimate test of any VPP lies in its correlation with real-world sailing data. Validation through full-scale sailing trials would establish greater confidence in the predictions made by the program. Future efforts could focus on collecting data from full-scale sailing trials under controlled conditions, where parameters such as wind speed, wind angle, boat speed and heel angle can be measured and compared directly to the VPP outputs. An alternative approach might involve using publicly available datasets from yacht races or historical performance logs of specific yacht designs. These datasets could offer diverse validation scenarios without the logistical challenges of conducting dedicated trials. If full-scale validation proves challenging, simplified case studies could be explored, such as model-scale experiments conducted in wind tunnels or towing tanks. Although these are not fully representative of real-world sailing conditions, they could serve as a stepping stone toward empirical validation. Incorporating real-world validation into future studies would enhance the credibility of the developed VPP and help identify areas for further refinement, ensuring its robustness and applicability across a broader range of scenarios.

The current model allows for reefing values to range from 0 to 1, which does not accurately reflect practical sail handling. Future work should implement fixed reefing values that correspond to the established reefing points of sails, typically defined in quarters of the mainsail luff. This adjustment will enhance the model's realism and applicability in real-world sailing scenarios. Incorporating the windage effects of the hull and sails is essential for a more detailed analysis of yacht performance. Additionally, increasing the number of degrees of freedom within the VPP will allow for a more complex representation of sailing conditions and vessel behaviour. This enhancement will result in additional equilibrium equations to be solved, thereby improving the model's accuracy, robustness and complexity.

The current Hazen model does not consider many sail shape parameters such as twist, overlap, blanketing, amongst others. This inclusion provides a more nuanced understanding of how these factors influence and condition the performance under various wind conditions. A solution would be adopting either the IMS or ORC aerodynamic model, as it would also facilitate comparisons with established standards. The new ORC depowering scheme should be prioritized, as it offers a more accurate reflection of the common sail practice.

Hydrodynamically additional resistance components, such as the bulb and propeller, can be incorporated and adopting a new method to predict the keels residuary resistance for higher Froud Numbers.

Future iterations of the OceanVPP should also integrate a crew position optimizer, making the crew arm one of the decision variables and outputting the recommend crew arm position and weight transversely. This optimization will enable more effective weight distribution and crew positioning strategies, which are critical for maximizing performance. Lastly, preparing the VPP to accommodate multihull input, rather than being limited to monohull configurations, represents a significant opportunity for future research.

Overall, this adaptation will broaden the applicability of the developed software, catering to a wider range of vessels and enhancing its relevance in diverse sailing contexts. Addressing these identified areas will significantly enhance the accuracy and applicability of the VPP.

REFERENCES

Bettencourt, J.P.H., Fonseca, N. & Guedes Soares C. (2004). Programa Para a Previsão De Velocidade de Embarcações à Vela.

Beukelman, W., & Keuning, L. (1975). The influence of fin keel sweep back on the performance of sailing yachts. In TU Delft, Faculty of Marine Technology, Ship Hydromechanics Laboratory, Report No. 445-P, HISWA Symposium, Amsterdam, The Netherlands.

Böhm, C. (2014). A Velocity Prediction Procedure for Sailing Yachts with a hydrodynamic Model based on integrated fully coupled RANSE-Free-Surface Simulations. Ph.D. Dissertation. Technische Universiteit Delft, 2014.

Brummer, M. (2015). Aerodynamics of the Mast/Sail Combination. Finnfare, April 2015.

Claughton, A. (1999). Developments in the IMS VPP Formulations. In SNAME 14th Chesapeake Sailing Yacht Symposium, Annapolis, Maryland, USA.

Davidson, K. S. (1936). Some experimental studies of the sailing yacht. Stevens Institute of Technology, Experimental Towing Tank, Hoboken, New Jersey, Presented at The Society of Naval Architects and Marine Engineers.

EU Commission (2023). Importance of the recreational craft sector. Available at: https://single-market-economy.ec.europa.eu/sectors/maritime-industries/recreational-craft-sector_en) (consulted on 12/12/2022).

Emirates Team New Zealand (2024). Available at: https://emirates-team-new-zealand.americascup.com/en/news/743_LOOKING-TO-THE-FUTURE-BY-BUILDING-ON-THE-SUCCESS-OF-BARCELONA.html (consulted on 12/01/2024).

Flay, R. G. (1996). A twisted flow wind tunnel for testing yacht sails. Journal of Wind Engineering and Industrial Aerodynamics, 63(1-3), 171-182.

Fossati, Fabio (2013). Aero-hydrodynamics and the Performance of Sailing Yachts: The Science Behind Sailing Yachts and Their Design. Bloomsbury.

Fossati, F, Muggiasca, S & Viola (2006). Wind tunnel techniques for investigation and optimization of sailing yachts aerodynamics 2nd High Performance Yacht Design Conference, Auckland, New Zealand, 14/02/06 - 16/02/06 pp. 105-113.

Gerr, D. (2007). Basic criteria for Powerboat stability. The Masthead, 1(4), 9.

Gerhardt, F. C., Le Pelley, D., Flay, R. G. J., & Richards, P. (2009). Tacking in the Wind Tunnel.fi 19th Chesapeake Sailing Yacht Symposium, Annapolis, MD, March 20–21, pp. 161–175

Gerritsma, J. (1973). The seakeeping performance and steering properties of sailing yachts. In TU Delft, Faculty of Marine Technology, Ship Hydromechanics Laboratory, Report No. 366.

Gerritsma, J., J.E. Kerwin, & G. Moeyes (1975). Determination of sail forces based on full scale measurements and model tests. In TU Delft, Faculty of Marine Technology, Ship Hydromechanics Laboratory, Report No. 444-P, 4th HISWA Symposium, Amsterdam, The Netherlands.

Gerritsma, J., Keuning, J.A., & Onnink, R. (1981). The Delft Systematic Series II experiments. International Ship Building Progress, Vol. 28, No 328.

Gerritsma, J., Onnink, R., & Versluis, A. (1981). Geometry, resistance, and stability of the Delft systematic yacht hull series. International Shipbuilding Progress, 28(328), 276-297.

Gerritsma, J., & Keuning, J.A. (1985). Further experiments with keel hull combinations. In TU Delft, Faculty of Marine Technology, Ship Hydromechanics Laboratory, Report No. 699-P, The 1st Bay Sailing Yacht Symposium, Florida, USA.

Gerritsma, J., Keuning, J.A., & Versluis, A. (1993). Sailing yacht performance in calm water and in waves. In SNAME 11th Chesapeake Sailing Yacht Symposium. SNAME

Grand View Research (2024). Sailboat Market Size, Share & Trends Analysis Report by Hull Type. Available at: https://www.grandviewresearch.com/industry-analysis/sailboat-market-report (Consulted on 05/01/2024)

Hazen, G. S. (1980). A model of sail aerodynamics for diverse rig types. New England Sailing Yacht Symposium. The Society of Naval Architects and Marine Engineers, SNAME, March 22, 1980.

ITTC (2000). Performance, Propulsion, 1978 Performance Prediction Method. International Towing Tank Conference, Recommended Procedures

Izaguirre Alza, Patricia, Pérez Rojas, Luis and Zamora Rodriguez, Ricardo (2008). Stability Criteria for Sailing Vessels. In: "III Simposio Internacional de Diseño y Producción de Yates de Motor y Vela. MDY 2008", 26/06/2008 - 27/06/2008, Madrid, España. pp. 123-137.

Jacquin, E., Roux, Y. & Allessandrini, B. (2005). Toward Numerical VPP with the Full Coupling of Aerodynamic and Hydrodynamic Solvers for ACC Yachts. In SNAME Chesapeake Sailing Yacht Symposium. SNAME.

Kamola-Cieślik, M. (2021). Changes in the Global Shipbuilding Industry on the Examples of Selected States Worldwide in the 21st Century. European Research Studies, 98-112.

Keuning, J. A., & Katgert, M. (2008). A bare hull resistance prediction method derived from the results of the Delft systematic yacht hull series extended to higher speeds. In International conference innovation in high performance sailing yachts, Lorient, France (pp. 13-21). RINA.

Keuning, J. A., & Sonnenberg, U. B. (1998a). Developments in the velocity prediction based on the Delft systematic yacht hull series. In International conference on the modern yacht (pp. 1-16).

Keuning, J. A., & Sonnenberg, U. B. (1998b). Approximation of the hydrodynamic forces on a sailing yacht based on the Delft Systematic Yacht Hull Series. In 15th International symposium on Yacht Design and Yacht Construction, Amsterdam, 16 November 1998: proceedings (pp. 99-152).

Keuning, J. A., & Vermeulen, K. J. (2003). The yaw balance of sailing yachts upright and heeled. In SNAME 16th Chesapeake Sailing Yacht Symposium.

Keuning, J. A., Vermeulen, K. J., & De Ridder, E. J. (2005). A generic mathematical model for the manoeuvring and tacking of a sailing yacht. In SNAME 17th Chesapeake Sailing Yacht Symposium.

Keuning, J. A., & Verwerft, B. (2009). A new Method for the Prediction of the Side Force on Keel and Rudder of a Sailing Yacht based on the Results of the Delft Systematic Yacht Hull Series. In SNAME 19th Chesapeake Sailing Yacht Symposium.

Keuning, L. J., Onnink, R., Versluis, A., & Van Gulik, A. A. M. (1996). The bare hull resistance of the Delft systematic yacht hull series. In TU Delft, Faculty of Marine Technology, Ship Hydromechanics Laboratory Report No. 1102-P, 14th International Symposium on Yacht Design and Yacht Construction, HISWA, Amsterdam, The Netherlands.

Kerwin, J. E. (1975). A procedure for sailing performance analysis based on full scale log entries and towing tank data. Massachusetts Institute of Technology, MIT, Department of Naval Architecture and Marine Engineers, USA, Report No. 74-17, NAYRU Ocean Race Handicapping Project.

Kerwin, J. E. & Elliot, J. (1978). A velocity prediction program for ocean racing yachts. The Society of Naval Architects and Marine Engineers, SNAME, Report 75-17 Massachusetts Institute of Technology, MIT, Department of Ocean Engineering, Ocean Race Handicapping Project,

Larsson, L. (1990). Scientific methods in yacht design. Annual Review of Fluid Mechanics, 22(1), 349-385.

Larsson, L. (1998). Will computational fluid dynamics completely take the role of model testing. In Proceedings of the 11th WEMT International Conference: The West European Maritime Industry in the Global Challenge of the Next, Century, Rotterdam, The Netherlands (pp. 12-14).

Larsson, L. (2010). Ship resistance and flow. Published by The Society of Naval Architects and Marine Engineers, SNAME, The Principles of Naval Architecture Series, ISBN: 978-0-939773-76-3.

Larsson, L., Eliasson, R., & Orych, M. (2022). Principles of yacht design. Bloomsbury Publishing.

Marchaj, C. A. (1996). Sail Performance–Theory and Practice. Adlard Coles Nautical. ISBN: 0-7136 4123 1.

Maxsurf VPP (2023). Maxsurf VPP Program & User Manual. Bentley Systems,

NavalAPP (2024). Available at: https://navalapp.com/calculations/ (Consulted on 15/02/2024)

Nomoto, K., & Tatano, H. (1979). Balance of helm of sailing yachts-A ship hydrodynamics approach on the problem. In Osaka University, Department of Naval Architecture, Japan, Presented at: Proceedings of the 6th Symposium on developments of interest to Yacht Architecture, HISWA'79, Amsterdam, The Netherlands.

Oossanen, P. V. (1986). Use of the Towing Tank in the Design of Racing Sailing Yachts. In: SNAME 12th Chesapeake Sailing Yacht Symposium.

Oossanen, P. V. (1993). Predicting the speed of sailing yachts. SNAME, Transactions: 101(12): 337-397.

Oossanen, P. V. (1995). Improvement of Sailing Yacht Performance Prediction by Including Force-Moment Equilibrium for the Calculation of Helm Angle in a Velocity Prediction Program. In SNAME Chesapeake Sailing Yacht Symposium. SNAME.

Oossanen, P. V. (1997). Development of Proposed ISO 12217 Single Stability Index for Mono-Hull Sailing Craft. In: SNAME Chesapeake Sailing Yacht Symposium

ORC (2024). ORC VPP Documentation 2024. Offshore Racing Congress.

Pennanen, M. (2015). Optimal sailor position on an Olympic dinghy. Master Thesis. Aalto University.

Poor, C.L. (1986). VPP Algorithm description. Appendix to Description of IMS VPP and LPP Algorithms. IMS.

Rosen, B., Laiosa, J., & Davis, Jr, W. (2000). CFD design studies for America's Cup 2000. In 18th Applied Aerodynamics Conference (p. 4339).

Stern, F., Yang, J., Wang, Z., Sadat-Hosseini, H., Mousaviraad, M., Bhushan, S., & Xing, T. (2013). Computational ship hydrodynamics: Nowadays and way forward. International Shipbuilding Progress, 60(1-4), 3-105.

Tennekes, H, (1973). The Logarithmic Wind Profile. Journal of the Atmospheric Sciences. Vol.30, No.2, pp.234-238.

The Ocean Race (2023). The Ocean Race ends an epic 2023 on a high note. Available at: https://www.theoceanrace.com/en/news/14667_The-Ocean-Race-ends-an-epic-2023-on-a-high-note (consulted on 12/01/2024).

Turner J. (2015). Record numbers. Available at: https://archive.theoceanrace.com/en/news/9157_Record-numbers.html (consulted on 12/01/2024).

Viola, I. M., & Flay, R. G. (2011, March). Pressure Distributions on Sails Investigated Using Three Methods: On-Water Measurements, Wind-Tunnel Measurements, and Computational Fluid Dynamics. In SNAME Chesapeake Sailing Yacht Symposium. SNAME.

Y. Masayuma, T. Fukasawa, And H. Sasagawa (1995). Tacking Simulation of Sailing Yachts - Numerical Integration of Equation of Motion and Application of Neural Network Technique. In 12th Chesapeake Sailing Yacht Symposium, Annapolis, MD, USA, 1995. 14

Appendix I. OceanVPP User Interface

```
% True wind speed            [knts]
TWS = 5: 5: 25;
% Upwind True wind angles     [deg]
TWAd_up = 35 : 5 : 110;
% Downwind True wind angles   [deg]
TWAd_dw = 80 : 5 : 175;

%% Sailing Conditions:
condi = 3;
%(1) Upwind:   Main + Jib
%(2) Downwind: Main + Spinnaker (Sym or Asym)
%(3) Both results displayed

%% Aerodynamical Model and option to choose from coefficients to be used
AeroModel = 1;
%(1) Hazen method (1980 Hazen's Aero Coefficients)
AeroCoeffs = 3;
%(1) Hazen method (1980 Hazen's Aero Coefficients)
%(2) ORC          (2023 ORC Aero Coefficients)
%(3) IMS          (Revised October 1986)

%% Hydrodynamical Model
HydroModel = 1;
%(1) Delft (Series 4 and 7)

% Rig checkstays (Boats ability to adjust Main & Jib sail camber)
checkstays = 3; % Only works for ORC Aero Coefficients
%(1) Equipped with boom vang, backstays, etc. -> HIGH LIFT
%(2) No adjustability                         -> LOW  LIFT
%(3) Medium, check ORC table 5.5

% Spinnaker type
spinnset = 2;
%(1) Symmetrical
%(2) Asymmetrical
spintack = 2; % For Asymmetrical Spinnakers
%(1) Tacked on centreline
%(2) Tacked on a pole

%% Intended Outputs:
config = 1;
%(1) Polarplot only
%(2) Results Table only
%(3) Plots and Results Table
%(4) ORC Results Format only

plotOUTPUT = 9; % Polarplot output
%(1) V vs TWA
%(2) Heel vs TWA
%(3) Mheel vs TWA
%(4) Fside vs TWA
%(5) Fdrive vs TWA
%(6) Reef vs TWA
%(7) Flat vs TWA
%(8) HydroHeel vs TWA
%(9) Mcrew vs TWA
```

Appendix II. OceanVPP Equilibrium Conditions Definition

```
function [c,ceq] =
vpp_mycon(X,TWS,TWA,hulldata,sailsdata,spinnset,sailset,checkstays,AeroMode
l,HydroModel,condi,AeroCoeffs,GZ_method,spintack)

% Aerodynamical Forces & Moments
switch AeroModel
    case 1 % Following Hazen's model
        [Fdrive,Fheel,Flat,Mheel] =
Calc_SailsHazen(X,TWS,TWA,sailset,spinnset,sailsdata,checkstays,hulldata,Ae
roCoeffs,spintack);
    case 3 % Following IMS model
        [Fdrive,Fheel,Flat,Mheel,HydroHeel] =
Calc_SailsIMS(X,TWS,TWA,sailset,spinnset,sailsdata,checkstays,hulldata,Aero
Coeffs,spintack);
    case 2 % Following ORC 2023 Guidelines
        [Fdrive,Fheel,Flat,Mheel,RED,rfm,ftj] =
Calc_SailsORC(X,TWS,TWA,sailset,spinnset,sailsdata,checkstays,hulldata,cond
i,spintack);
end

switch HydroModel
    case 1 % Delft Hydrodynamical Force & Moments
[Rtot,Mright,MhullRM,McrewRM,HydroHeel]=Calc_HydroDelft(X,Fheel,TWS,hulldat
a,GZ_method);
    case 2 % IMS  Hydrodynamical Forces & Moments
[Rtot,Mright,MhullRM,McrewRM] = Calc_HydroIMS(X,Fheel,hulldata,GZ_method);
End

%% Inequalities(Degrees of Freedom)
%-------------------------- Linear Motions----------------------------------
% SURGE: Linear motion along its longitudinal (x) axis
deltaFx = Fdrive - Rtot;    % Along direction of motion (drivingF - Resist)

%---------------------- Rotation along axis------------------------------
% ROLL: Rotation around its longitudinal (x) axis
deltaMx = Mheel - Mright; % Sails heeling moment = Hulls Rightning Mom.

% Equalities
c   = [];

% Inequalities
ceq = [deltaFx
       deltaMx];
```

Appendix III. OceanVPP Hydrodynamical Model

```
function
[Rtot,Mright,MhullRM,McrewRM,HydroHeel]=Calc_HydroDelft(X,Fheel,hulldata,GZ
_method)  % Hydrodynamical Model

V      = X(1);
phi    = X(2);

%% Resistances calculations

% Auxiliary
Sc   = Calc_Sc(hulldata);           % Upright wet surface of canoe body[m2]

% --------------------   Resistances Upright  -----------------------------
% Frictional
Rf     = Calc_Rf(V,Sc,hulldata);          % Canoe Resistance
Rfkeel = Calc_Rfkeel(V,hulldata);         % Keel Resistance
Rfrudd = Calc_Rfrudd(V,hulldata);         % Rudder Resistance

% Residuary or Wave making Resistance
Rr     = Calc_Rr(V,hulldata);             % Canoe Body Resistance
Rrk    = Calc_Rrk(V,hulldata);            % Keel Resistance
Rru    = Calc_Rru(phi,Rr);                % Rail Under Drag

% Heeled Deltas
Rrh    = Calc_Rrh(V,phi,hulldata);        % Delta Canoe Body Residuary
Rfh    = Calc_Rfh(V,phi,Sc,hulldata);     % Delta Canoe Body Frictional
Rrkh   = Calc_Rrkh(V,phi,hulldata);       % Delta Keel Resistance

% Induced Resistances
Ri = Calc_Ri(V,phi,Fheel,hulldata);

%% RIGHTNING MOMENT

[MhullRM,McrewRM,Mright,HydroHeel]=Calc_Mright(X,hulldata,GZ_method,Fheel);

%% ------------------------ Total Resistance  -----------------------------
Rtot  =  (Rf + Rfkeel + Rfrudd*2 + Rr + Rfh + Rru + Rrk + Rrkh + Rrh + Ri);
```

Appendix IV. Hydrodynamical Coefficients

Table IV-1: Coefficients for Residuary Resistance of Bare Hull (Keuning & Katgert, 2008)

Fn	0.1	0.15	0.2	0.25	0.3	0.35	0.4	0.45	0.5	0.55	0.6	0.65	0.7
a0	-0.0005	-0.0003	-0.0002	-0.0009	-0.0026	-0.0064	-0.0218	-0.0388	-0.0347	-0.0361	0.0008	0.0108	0.1023
a1	0.0023	0.0059	-0.0156	0.0016	-0.0567	-0.4034	-0.5261	-0.5986	-0.4764	0.0037	0.3728	-0.1238	0.7726
a2	-0.0086	-0.0064	0.0031	0.0337	0.0446	-0.1250	-0.2945	-0.3038	-0.2361	-0.2960	-0.3667	-0.2026	0.5040
a3	-0.0015	0.0070	-0.0021	-0.0285	-0.1091	0.0273	0.2485	0.6033	0.8762	0.9661	1.3957	1.1282	1.7867
a4	0.0061	0.0014	-0.0070	-0.0367	-0.0707	-0.1341	-0.2428	-0.0430	0.4219	0.6123	1.0343	1.1836	2.1934
a5	0.0010	0.0013	0.0148	0.0218	0.0914	0.3578	0.6293	0.8332	0.8990	0.7534	0.3230	0.4973	-1.5479
a6	0.0001	0.0005	0.0010	0.0015	0.0021	0.0045	0.0081	0.0106	0.0096	0.0100	0.0072	0.0038	-0.0115
a7	0.0052	-0.0020	-0.0043	-0.0172	-0.0078	0.1115	0.2086	0.1336	-0.2272	-0.3352	-0.4632	-0.4477	-0.0977

Table IV-2: Coefficients for Polynomial: Residuary Resistance of Keel (Keuning & Sonnenberg, 1998)

Fn	0.20	0.25	0.30	0.35	0.40	0.45	0.50	0.55	0.60
A0	-0.00104	-0.00550	-0.01100	-0.00713	-0.03581	-0.00470	0.00553	0.04822	0.01021
A1	0.00172	0.00597	0.01421	0.02632	0.08649	0.11592	0.07371	0.00660	0.14173
A2	0.00117	0.00390	0.00069	-0.00232	0.00999	-0.00064	0.05991	0.07048	0.06409
A3	-0.00008	-0.00009	0.00021	0.00039	0.00017	0.00035	-0.00114	-0.00035	-0.00192

Table IV-3: Coefficients s0 - s3 determined as a function of heel angle, hull wetted surface (Keuning & Sonnenberg,1998)

θ	5º	10º	15º	20º	25º	30º	35º
s0	-4.112	-4.522	-3.291	1.850	6.510	12.334	14.648
s1	0.054	-0.132	-0.389	-1.200	-2.305	-3.911	-5.182
s2	-0.027	-0.077	-0.118	-0.109	-0.066	0.024	0.102
s3	6.329	8.738	8.949	5.364	3.443	1.767	3.497

Table IV-4: Coefficients for heeled residuary delta (Keuning & Sonnenberg,1998)

Fn	0.25	0.3	0.35	0.4	0.45	0.5	0.55
u0	-0.0268	0.6628	1.6433	-0.8659	-3.2715	-0.1976	1.5873
u1	-0.0014	-0.0632	-0.2144	-0.0354	0.1372	-0.1480	-0.3749
u2	-0.0057	-0.0699	-0.1640	0.2226	0.5547	-0.6593	-0.7105
u3	0.0016	0.0069	0.0199	0.0188	0.0268	0.1862	0.2146
u5	-0.0070	0.0459	-0.0540	-0.5800	-0.1006	-0.7489	-0.4818
u5	-0.0017	-0.0004	-0.0268	-0.1133	-0.2026	-0.1648	-0.1174

Table IV-5: Coefficients for the Polynomial: Effective Span

Φ	0	10	20	30
A_1	3.7455	4.4892	3.9592	3.4891
A_2	-3.6246	-4.8454	-3.9804	-2.9577
A_3	0.0589	0.0294	0.0283	0.0250
A_4	-0.0296	-0.0176	-0.0075	-0.0272
B_0	1.2306	1.4231	1.5450	1.4744
B_1	-0.7256	-1.2971	-1.5622	-1.3499

Appendix V. OceanVPP Aerodynamical Model

```
function [Fdrive,Fheel,Flat,Mheel] =
Calc_SailsHazen(X,TWS,TWA,sailset,spinnset,sailsdata,checkstays,hulldata,AeroCoeffs
,spintack) % Aerodynamical Model

V    = X(1);
phi  = X(2);
flat = X(3);
reef = X(4);

[AWS,AWA,AWAd] = Calc_WindTri(TWS,TWA,V,phi); % Output AWA in rad

%% Sail areas

A_main = 0.5 * P * E;                    % [m^2] Mainsail area, factor 1.1 accounts
A_jib  = 0.5 * sqrt(J^2 + I^2) * LPG;    % [m^2] Jib area
A_fore = I * J * 0.5;                    % [m^2] Fore Triangle area
A_spi  = 1.15 * SL * J;                  % [m^2] Spinnaker area
A_nom  = A_main + A_fore;

%% Centre of efforts of each individual sail measured above sheer
zCoE_main = 0.39 * P + BAD;
zCoE_jib  = 0.39 * I;
zCoE_spi  = 0.59 * I;

switch AeroCoeffs
    case {1,3} % Hazen
        [CLmain, CDmain, CLjib, CDjib, CLspinn, CDspinn] =
Calc_SailCoeffHazen(AWA,AeroCoeffs);
    case 2 % ORC2023 Coeffs
       [CLmain, CDmain, CLjib, CDjib, CLspinn, CDspinn] =
Calc_SailCoeffORC(AWA,checkstays,spinnset,spintack,sailsdata);
end

zCoE   = ((zCoE_main .* A_main + zCoE_jib .* A_jib + zCoE_spi .* A_spi) ./ (A_main
+ A_jib+ A_spi));

switch sailset
    case 1  %  Main and Jib
        CLift  = (CLmain  .* A_main + CLjib  .* A_jib) ./ (A_nom);
        CDp    = (CDmain  .* A_main + CDjib  .* A_jib) ./ (A_nom);
        zCoE   = ((zCoE_main .* A_main + zCoE_jib .* A_jib) ./ (A_main + A_jib));
    case 2 % Main and Spinnaker
        CLift  = (CLmain .* A_main + CLspinn .* A_spi) ./ (A_nom);
        CDp    = (CDmain .* A_main + CDspinn .* A_spi) ./  (A_nom);
        zCoE   = ((zCoE_main .* A_main + zCoE_spi .* A_spi) ./ (A_main + A_spi));
end

zCoE = zCoE * reef * cos(phi);

%If sailing close hauled (AWA<45°) the aspect ratio requires new formulation
if AWA <= deg2rad(45)
    ARatio = (1.1*(EHM + AvgFB)).^2./A_nom;
 else % Other courses
    ARatio = ((1.1*EHM).^2) ./A_nom;
end

%% ----------------- AERODYNAMIC COEFFICIENTS ----------------------------
% Lift Coefficient adjustment due to Flattening Factor
CL  = CLift .* flat .* (reef.^2);

% Viscous/Parasitic drag
CDp = CDp .* (reef).^2;

% Induced Drag
CDi = CL.^2 .* ((1/(pi*ARatio)) + 0.005);
```

```
% Drag of mast and topsides
CDo = 1.13 *((Bmax*AvgFB)+(EHM*EMDC)) ./(A_nom);

% Total Drag Coefficient
CD  = CDp + CDi + CDo;

%% -------------------- AERODYNAMIC FORCES ---------------------------------
% Drag and Lift Forces
q       = 0.5* rhoA .* AWS .* AWS;    % Dynamic head
FDragA =  q .* CD * A_nom;
FLiftA =  q .* CL * A_nom;

% Heel and Side Force
Fdrive = FLiftA .* sin(AWA) - FDragA .* cos(AWA);
Fheel  = FLiftA .* cos(AWA) + FDragA .* sin(AWA);
Flat   = Fheel  .* cos(phi);

h = (zCoE + HBI + zCLR)*reef;

HydroHeel = 2.3 * 0.43; % Eff Draft * 0.43, usually called RM4
HydroHeel = HydroHeel * Fheel;

% Rig Heeling Moment
Mheel = Fheel * h + HydroHeel;
```

Appendix VI. Aerodynamical Coefficients

Table VI-1: Sail coefficients (Hazen, 1980)

AWA [º]	27	50	80	100	180
Main CD	0.02	0.15	0.80	1.00	0.90
Main CL	1.50	1.50	0.95	0.85	0.00
Jib CD	0.02	0.25	0.15	0.00	0.00
Jib CL	1.50	0.50	0.30	0.00	0.00
Spin CD	0.00	0.25	0.90	1.20	0.66
Spin CL	0.00	1.50	1.00	0.85	0.00

Table VI-2: Individual sail coefficients (ORC, 2023)

Sail	0º	7º	9º	12º	28º	60º	90º	120º	150º	180º
main-CDlow	0.043	0.026	0.023	0.023	0.033	0.113	0.383	0.969	1.316	1.345
main-CLlow	0.000	0.862	1.052	1.164	1.347	1.353	1.267	0.931	0.388	-0.112
main-CDhi	0.034	0.017	0.015	0.015	0.026	0.113	0.383	0.969	1.316	1.345
main-CLhi	0.000	0.948	1.138	1.250	1.427	1.383	1.267	0.931	0.388	-0.112
jib-CDlow	0.000	0.050	0.032	0.031	0.037	0.250	0.350	0.730	0.950	0.900
jib-CLlow	0.000	0.000	1.000	1.375	1.450	1.450	1.250	0.400	0.000	-0.100
jib-CDhi	0.000	0.050	0.032	0.031	0.037	0.250	0.350	0.730	0.950	0.900
jib-CLhi	0.000	0.000	1.100	1.475	1.500	1.450	1.250	0.400	0.000	-0.100

Table VI-3: Spinnaker coefficients (ORC, 2023)

AWA [º]	28º	41 º	50º	60º	67º	75º	100º	115º	130º	150º	170º	180º
sym-CD	0.182	0.267	0.337	0.417	0.465	0.506	0.588	0.615	0.636	0.650	0.650	0.640
sym-CL	-0.024	0.660	0.861	0.992	1.026	1.026	0.920	0.805	0.635	0.360	0.110	0.000
asym-CD	0.154	0.239	0.309	0.389	0.436	0.477	0.545	0.566	0.475	0.352	0.290	0.262
asym-CL	0.017	0.698	0.899	1.040	1.072	1.075	0.985	0.805	0.372	0.100	0.020	0.000

Table VI-4: Sail coefficients (Poor, 1986)

Sail	0º	7º	9º	12º	60º	90º	120º	150º	180º
Jib CL	0	1	1.375	1.45	1.43	1.25	0.4	0	-0.1
Jib CD	0.05	0.023	0.031	0.037	0.25	0.35	0.73	0.95	0.9
Main CL	0	1	1.22	1.35	1.25	0.96	0.58	0.25	-0.1
Main CD	0.05	0.03	0.027	0.027	0.114	0.306	0.671	1.11	1.2

Table VI-5: Spinnaker coefficients (Poor, 1986)

Sail	28º	41º	46º	60º	75º	100º	130º	150º	180º
Spin CL	0	1.31	1.56	1.71	1.69	1.4	0.83	0.5	0
Spin CD	0.1	0.15	0.2	0.4	0.7	1	1.1	1.1	1.1

Appendix VII. Hydrodynamic Model Results

Table VII-1: Upright Resistance Results per Component

Speed [Knots]	Hull Viscous [N]	Keel Viscous [N]	Rudder Viscous [N]	Hull Residuary [N]	Keel Residuary [N]
1.05	14.6	2.5	1.6	0	0
2.1	51.5	8.4	5.4	0	0
3.15	108.1	17.4	11	0.7	0
4.2	183.2	29.1	18.4	24.8	4.2
5.25	276	43.5	27.3	81.3	19.4
6.3	386	60.5	37.8	193.2	15.5
7.35	512.6	79.9	49.8	395.2	39.9
8.4	655.7	101.7	63.3	851.7	156.5
9.44	813.2	125.7	78	1693.9	233.7
10.49	987.9	152.2	94.3	2634.8	524.1
11.54	1178.2	181	111.9	3426.5	634.3

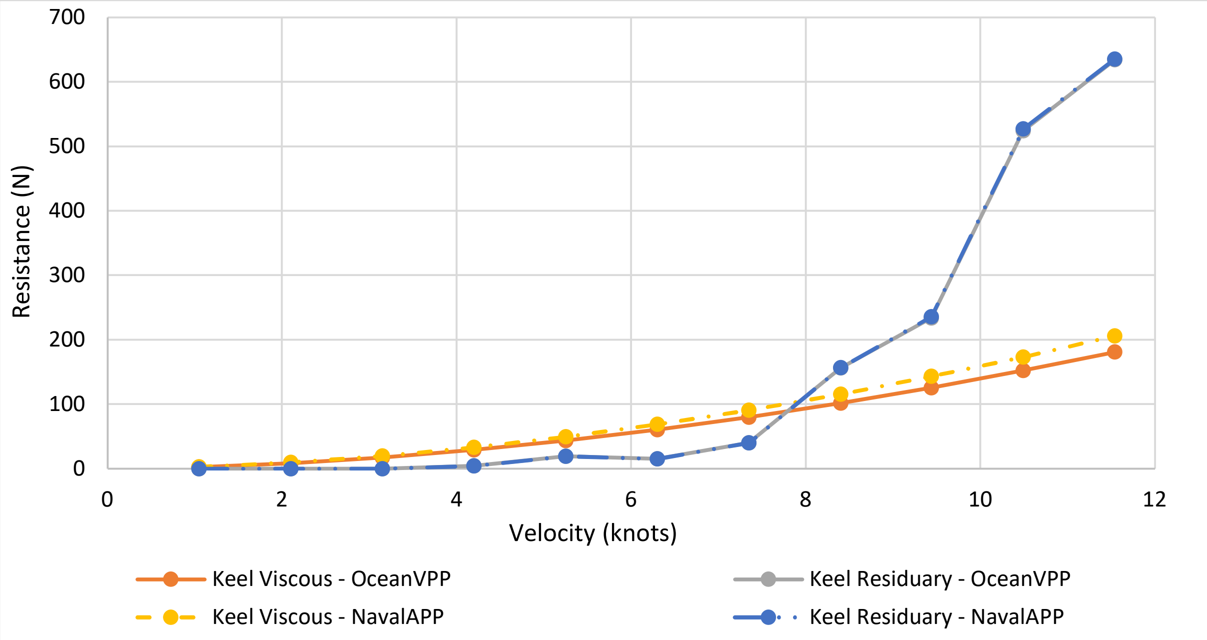

Figure VII-1: Keel Upright Resistance

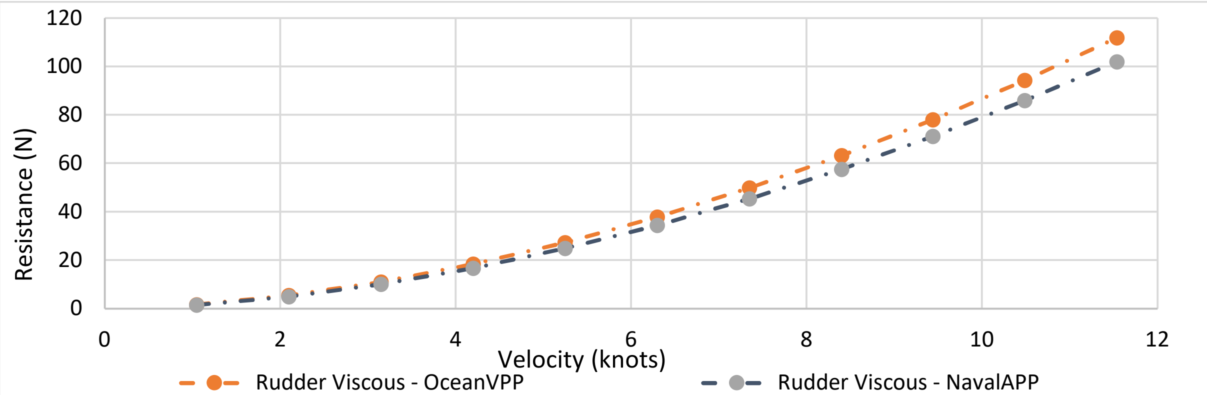

Figure VII-2: Rudder Upright Resistance

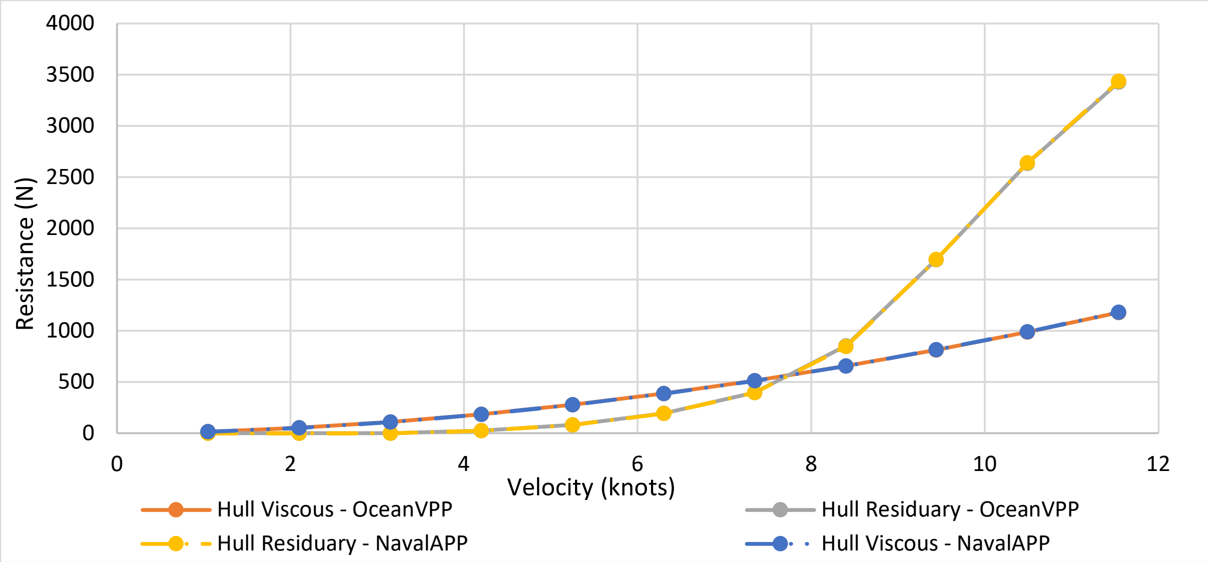

Figure VII-3: Hull Upright Resistance

Table VII-2: Total Upright Resistance Results

Boat Speed [knts]	**MaxSurf VPP** [N]	**OceanVPP** [N]		**Boat Speed** [knts]	**MaxSurf VPP** [N]	**OceanVPP** [N]
0.3	1.4	1.7		5.6	524	503.1
0.5	4.9	5.3		5.8	583	562.6
0.8	10.4	10.9		6.1	646	626.4
1.1	17.9	18.3		6.4	712	695.2
1.3	27.3	27.4		6.6	784	771.4
1.6	38.7	38		6.9	869	860.7
1.9	52.3	50.3		7.2	975	969
2.1	68.1	64.2		7.4	1 109	1102.2
2.4	86.1	80.2		7.7	1 277	1263
2.7	107	96.9		8	1 474	1449.7
2.9	129	114.8		8.2	1 690	1660.2
3.2	155	135.3		8.5	1 917	1892.4
3.5	183	160.5		8.8	2 143	2146.5
3.7	214	188.9		9	2 364	2426.1
4	247	221.4		9.3	2 585	2734.6
4.3	284	258.3		9.6	2 818	3075.5
4.5	324	299.7		9.8	3 070	3442.3
4.8	367	345.3		10.1	3 353	3817.9
5.1	415	394.7		10.4	3 671	4184.3
5.3	467	447.3		10.6	4 019	4524.3

Table VII-3: Keel Residuary Deltas

Velocity (knots)	Keel (φ =5º)	Keel (φ =10º)	Keel (φ =15º)	Keel (φ =20º)	Keel (φ =25º)	Keel (φ =30º)
1.0	0.68	1.36	2.05	2.73	3.41	4.09
2.1	2.73	5.46	8.18	10.91	13.64	16.37
3.1	6.14	12.28	18.41	24.55	30.69	36.83
4.2	10.91	21.82	32.74	43.65	54.56	65.47
5.2	17.05	34.10	51.15	68.20	85.25	102.30
6.3	24.55	49.10	73.66	98.21	122.76	147.31
7.3	33.42	66.84	100.25	133.67	167.09	200.51
8.4	43.65	87.30	130.94	174.59	218.24	261.89
9.4	55.13	110.25	165.38	220.50	275.63	330.75
10.5	68.07	136.14	204.21	272.28	340.35	408.42
11.5	82.38	164.76	247.14	329.52	411.90	494.27

Table VII-4: Canoe Body Residuary Deltas

Velocity (knots)	Residuary (φ=5º)	Residuary (φ =10º)	Residuary (φ =15º)	Residuary (φ =20º)	Residuary (φ =25º)	Residuary (φ =30º)
1.0	0.0	0.1	0.2	0.3	0.4	0.56
2.1	0.1	0.2	0.3	0.6	0.8	1.13
3.1	0.1	0.3	0.5	0.8	1.2	1.69
4.2	0.1	0.3	0.7	1.1	1.7	2.25
5.2	0.1	0.4	0.9	1.4	2.1	2.82
6.3	0.6	2.0	4.0	6.5	9.5	13.01
7.3	3.2	10.3	20.6	33.5	49.0	66.81
8.4	13.8	45.0	89.6	146.2	213.6	291.26
9.4	23.0	74.8	149.0	242.9	355.0	483.96
10.5	34.6	112.5	224.2	365.6	534.2	728.29
11.5	46.4	150.8	300.3	489.8	715.8	975.82

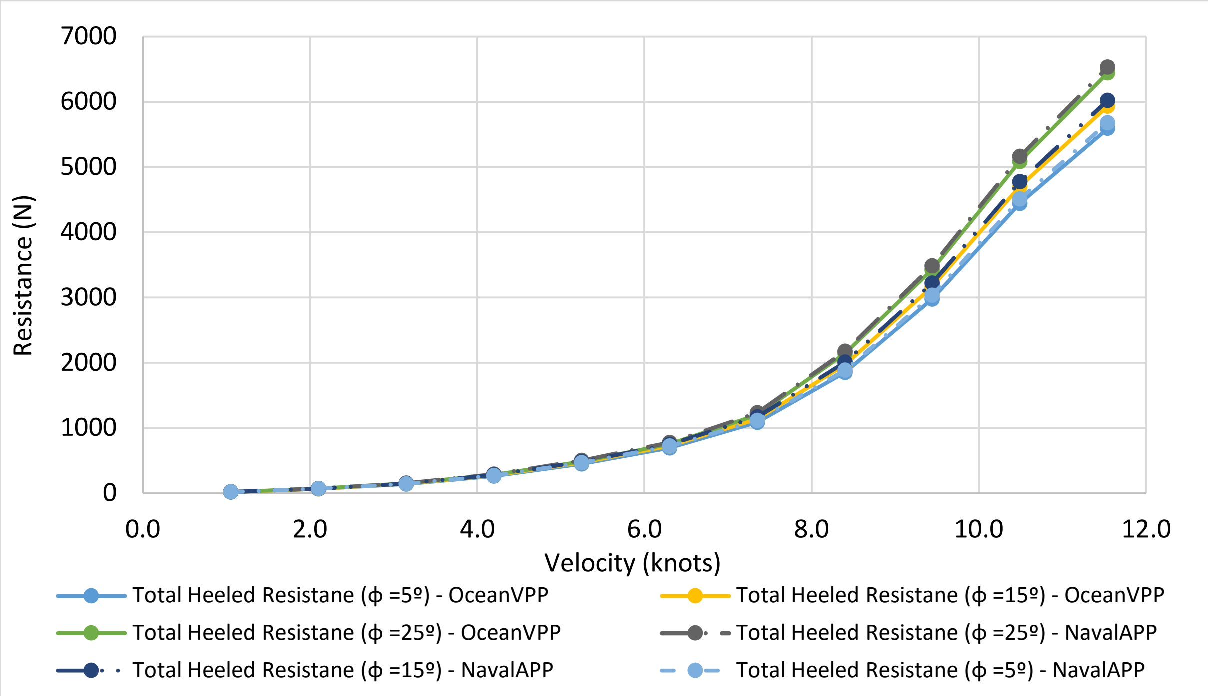

Figure VII-4: Total Heeled Resistance (Upright + Deltas) per heel angle (5º, 10º, 25º)

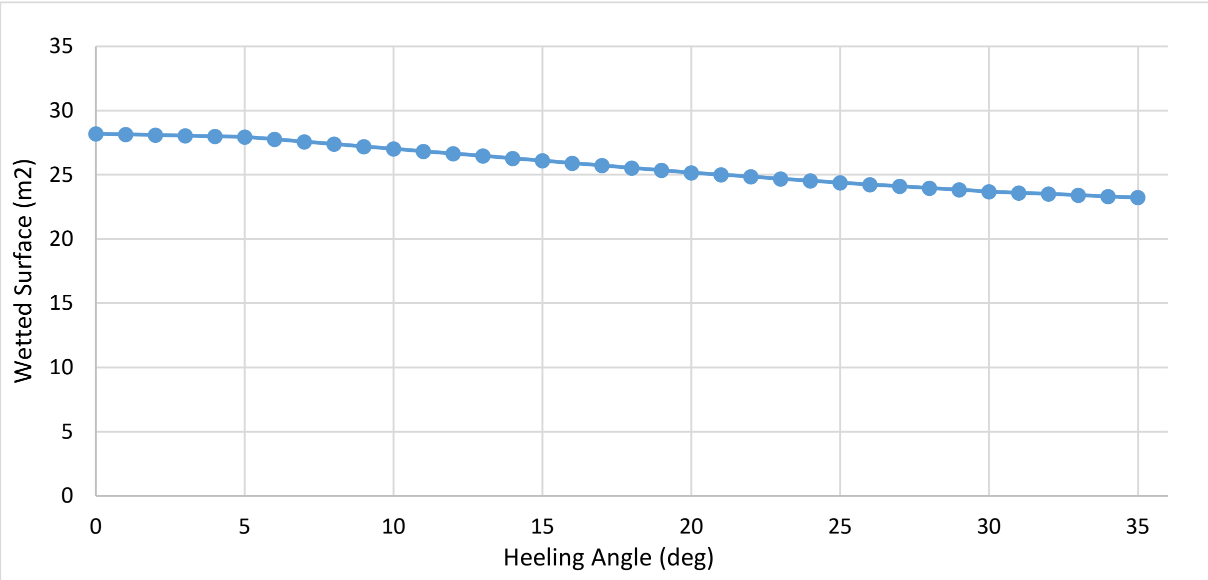

Figure VII-5: Hull's Wetted Surface Variation with the heeling Angle

Appendix VIII. Aerodynamical Model Results

Table VIII-1: Aerodynamical Model Results Upwind

AWA (deg)	Drive Force – Hazen (N)	Side Force – Hazen (N)	Lift Force – Hazen (N)	Drag Force – Hazen (N)
5	-172	361	345	203
10	-55	1104	1077	246
15	123	1655	1631	309
20	323	1949	1942	363
25	507	1989	2017	381
30	667	1950	2022	398
35	815	1915	2036	431
40	953	1875	2049	475
45	1077	1816	2046	523
50	1161	1749	2014	593
55	1234	1629	1945	627
60	1278	1497	1856	658
65	1306	1373	1764	692
70	1322	1260	1673	732
75	1328	1161	1583	778
80	1326	1078	1493	831
85	1319	1012	1402	893
90	1312	964	1312	964
95	1307	934	1221	1044
100	1310	918	1130	1131
105	1322	910	1041	1221
110	1345	906	954	1311
115	1376	900	867	1397
120	1414	889	781	1477
125	1456	869	695	1547
130	1500	840	609	1608
135	1544	802	524	1659
140	1586	756	441	1701
145	1626	701	358	1734
150	1662	639	278	1759
155	1693	570	199	1775
160	1718	494	123	1783
165	1736	413	50	1784
170	1747	329	-20	1777
175	1749	241	-87	1763
180	1741	150	-150	1741

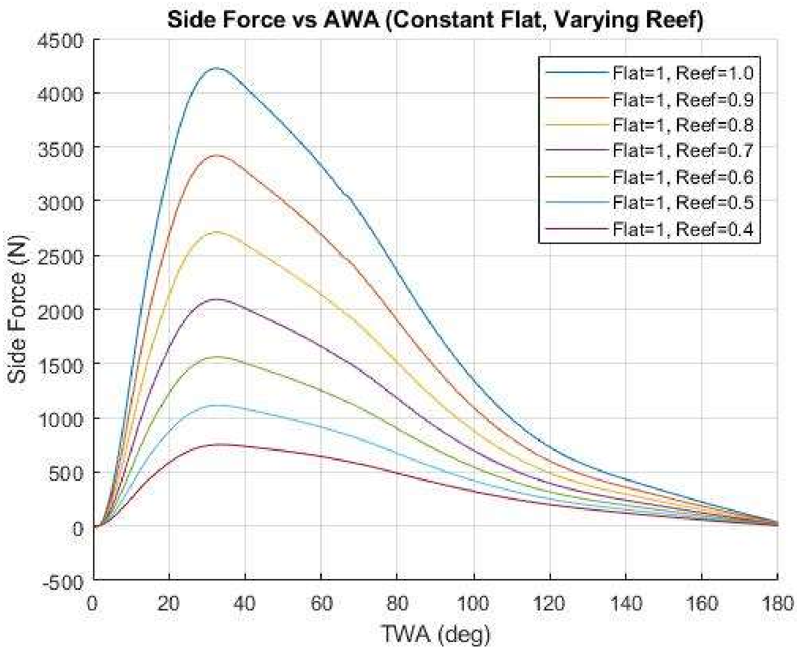

Figure VIII-1: Reefing Impact on the Heeling Force (for TWS = 5; V = 2.57 (m/s); Heel = 0º)

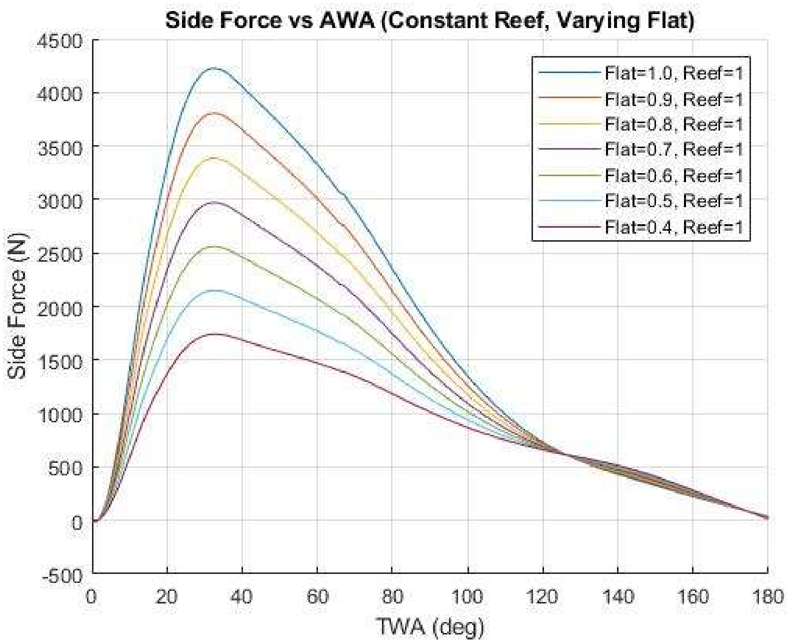

Figure VIII-2: Flattening Impact on the Driving Force (for TWS = 5; V = 2.57 (m/s); Heel = 0º)

Appendix IX. Stability Results

Table IX-1: GZ Results

YD-41 (Larsson et. al 2022)			Maxsurf Stability	
phi (deg)	GZ (m)		phi (deg)	GZ (m)
0	0		3	0.143
2	0.0866		6	0.284
5	0.2135		9	0.42
8	0.3332		12	0.55
11	0.4457		15	0.673
14	0.551		18	0.786
17	0.6491		21	0.89
20	0.74		24	0.982
23	0.8237		27	1.064
26	0.9002		30	1.136
29	0.9695		33	1.199
32	1.0316		36	1.255
35	1.0865		39	1.305
38	1.1342		42	1.348

Appendix X. Main particulars of the YD–41

Table X-1: Main particulars of the YD–41 (Larsson et. al, 2022)

	Half-loaded displacement	Light displacement	Units		Half-loaded displacement	Light displacement	Units
Loa	12.5	12.5	[m]	**Cku**	1	1	[m]
Lwl	11.9	11.62	[m]	**Ckl**	0.78	0,78	[m]
Bmax	4.2	4.2	[m]	**Tk**	1.9	1.9	[m]
Bwl	3.18	3.12	[m]	**Cru**	0.48	0.48	[m]
Tc	0.4	0.38	[m]	**Crl**	0.22	0.22	[m]
T	2.3	2.28	[m]	**Tr**	1.15	1.15	[m]
VC	6.05	5.46	[m2]	**V**	5.5	5.5	[deg]
mc	6200	5600	[kg]	**V**	10	10.06	[deg]
Sw	28.20	26.92	[m2]	**LCB**	-4.20	-4.50	[%]
Swc	34.97	33.64	[m2]	**LCF**	-7.30	-7.80	[%]
Aw	26.75	25.64	[m2]	**Cp**	0.56	0.56	[-]
mc	6500	5900	[m]	**Cmc**	0.715	0.715	[-]
Ballast	2300	2300	[kg]	**SA/Sw**	2.52	2.62	[-]
I	16.2	16.2	[m]	**SA/V1/3**	25.7	27.4	[-]
J	5.1	5.1	[m]	**Loa/B**	2.98	2.98	[-]
P	16.7	16.7	[m]	**Lwl/T**	5.17	5.1	[-]
E	5.6	5.6	[m]	**Lwl/Tc**	2975	30.58	[-]
ASL	18	18	[m]	**Lwl/V1/3**	6.43	6.48	[-]
SMW	10.7	10.7	[m]	**Loa/Lwl**	1.15	1.07	[-]
SAF	41.3	41.3	[m]	**Ff/Lwl**	0.121	0.123	[-]
SAM	46.8	46.8	[m]	**Ff/Fa**	1.23	1.23	[-]
SA	88.1 i	88.1	[m]	**Ballast Rto**	0.35	0.89	[-]

Table X-2: Initial design variables comparison with Maxsurf outputs

	Design Variables	Maxsurf	%	
L_{oa}	12.50	12.64	1.1%	[m]
L_{WL}	11.90	11.86	-0.4%	[m]
B_{WL}	3.18	3.16	-0.6%	[m]
B_{MAX}	4.20	4.23	0.7%	[m]
T_C	0.40	0.40	0.0%	[m]
T	2.30	2.30	0.0%	[m]
D	1.70	1.70	0.0%	[m]
A_W	26.8	26.4	-1.2%	[m2]
∇_{cb}	6.05	6.02	-0.5%	[m3]
$\triangle_{cb}$	6.20	6.17	-0.5%	[ton]
L_{CB}	5.46	5.62	2.9%	[m]
L_{CF}	5.08	5.23	2.9%	[m]
C_b	0.40	0.40	0.4%	[-]
C_p	0.56	0.57	1.4%	[-]
C_m	0.72	0.74	3.5%	[m]

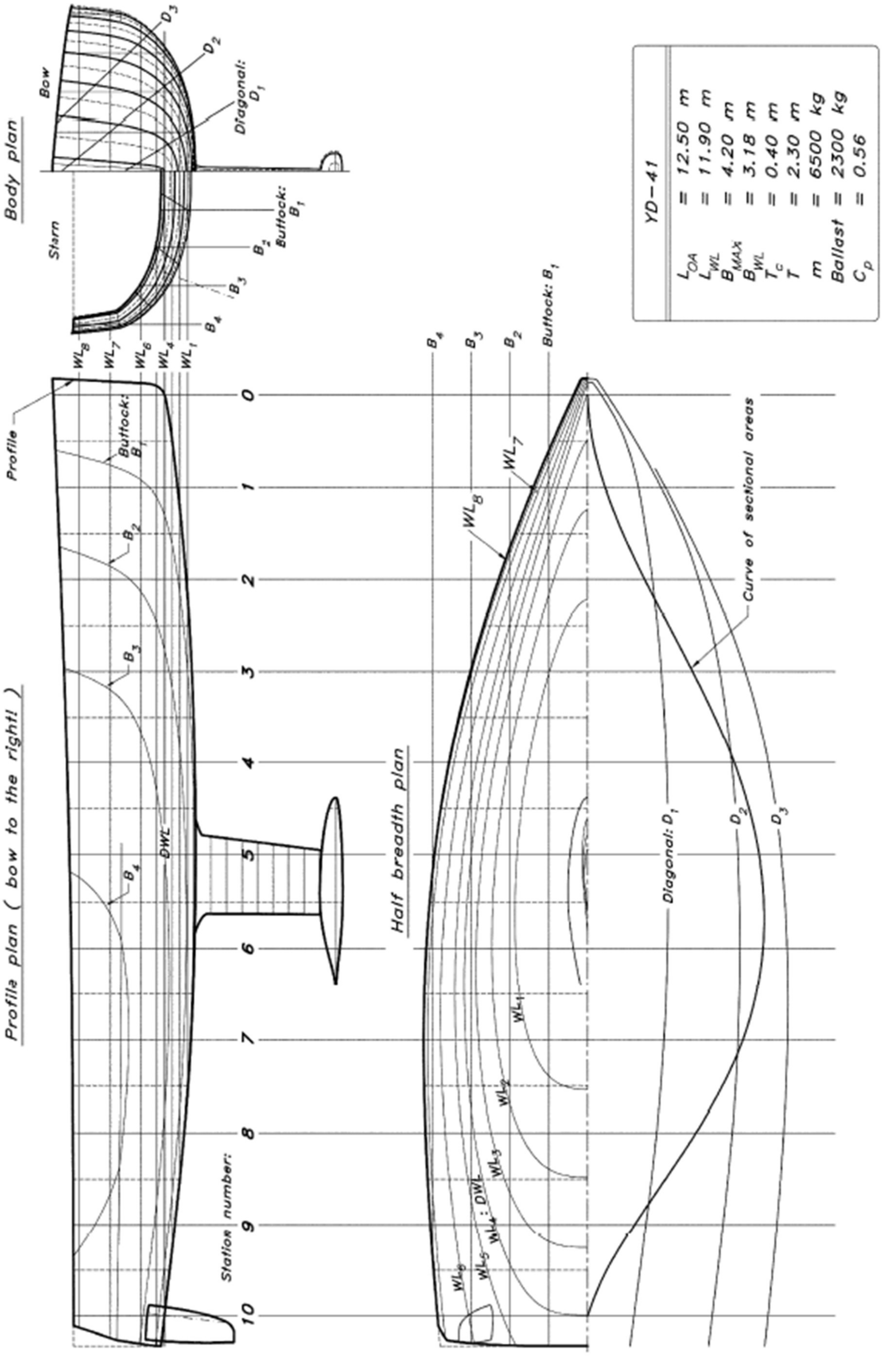

Figure X-1: Lines Plan for Forsatio YD-41 (Larsson et. al, 2022)

Appendix XI. OceanVPP Upwind Results

Table XI-1: Upwind Results

TWS	**TWA**	**AWA**	**AWS**	**V**	**VMG**	**Heel**	**Fdrive**	**Fside**	**Reef**	**Flat**	**Mheel**	**Hydro Heel**	**Hull RM**	**McrewRM**
[knt]	[deg]	[deg]	[knt]	**[knt]**	[knt]	[deg]	[N]	[N]	[0-1]	[-]	[Nm]	[Nm]	[Nm]	[Nm]
5	35	20.4	8.2	**3.6**	2.95	3.28	249	1 466	1.00	1.00	14 070	1 450	9 485	6 048
5	40	21.9	8.6	**4.14**	3.17	3.58	319	1 627	1.00	1.00	15 611	1 609	10 363	6 874
5	45	23.5	8.8	**4.57**	3.23	3.78	389	1 730	1.00	1.00	16 598	1 711	10 937	7 392
5	50	25.2	9.0	**4.92**	3.16	3.89	454	1 784	1.00	1.00	17 111	1 764	11 240	7 657
5	55	26.9	9.1	**5.21**	2.99	3.92	511	1 796	1.00	1.00	17 232	1 777	11 313	7 720
5	60	28.6	9.0	**5.43**	2.72	3.88	559	1 776	1.00	1.00	17 041	1 757	11 200	7 622
5	65	30.4	9.0	**5.61**	2.37	3.78	597	1 728	1.00	1.00	16 576	1 709	10 926	7 383
5	70	32.2	8.8	**5.73**	1.96	3.64	623	1 653	1.00	1.00	15 863	1 635	10 512	7 010
5	75	34.2	8.6	**5.8**	1.5	3.45	638	1 556	1.00	1.00	14 933	1 539	9 979	6 516
5	80	36.3	8.3	**5.83**	1.01	3.23	640	1 440	1.00	1.00	13 820	1 424	9 348	5 917
5	85	38.5	8.0	**5.81**	0.51	2.98	631	1 308	1.00	1.00	12 559	1 294	8 639	5 234
5	90	41.0	7.6	**5.74**	0	2.71	610	1 165	1.00	1.00	11 186	1 152	7 861	4 495
5	95	43.8	7.2	**5.63**	-0.49	2.43	577	1 014	1.00	1.00	9 733	1 002	7 030	3 722
5	100	47.2	6.7	**5.42**	-0.94	2.12	523	855	1.00	1.00	8 214	846	6 139	2 934
5	105	50.9	6.2	**5.22**	-1.35	1.8	472	698	1.00	1.00	6 708	691	5 223	2 186
5	110	55.4	5.7	**4.95**	-1.69	1.47	412	543	1.00	1.00	5 221	537	4 269	1 498
10	35	21.9	15.0	**5.77**	4.73	12.28	900	4 562	0.96	1.00	39 888	4 512	34 137	10 345
10	40	23.5	15.6	**6.62**	5.07	15	1 154	5 119	0.98	1.00	45 965	5 062	40 917	10 226
10	45	25.3	15.8	**7.21**	5.1	16.98	1 403	5 446	0.99	1.00	50 057	5 386	45 461	10 125
10	50	27.5	15.8	**7.6**	4.88	17.33	1 623	5 472	1.00	1.00	50 782	5 412	46 241	10 107
10	55	30.0	15.7	**7.88**	4.52	16.75	1 807	5 337	1.00	1.00	49 636	5 278	44 930	10 138
10	60	32.5	15.5	**8.09**	4.05	15.91	1 959	5 138	1.00	1.00	47 941	5 081	42 991	10 182
10	65	35.1	15.3	**8.25**	3.49	14.84	2 076	4 887	1.00	1.00	45 773	4 833	40 514	10 234
10	70	37.8	14.9	**8.37**	2.86	13.64	2 154	4 589	1.00	1.00	43 155	4 538	37 538	10 288
10	75	40.6	14.5	**8.44**	2.18	12.28	2 194	4 251	1.00	1.00	40 146	4 205	34 127	10 345
10	80	43.5	14.1	**8.46**	1.47	10.81	2 192	3 878	1.00	1.00	36 765	3 835	30 308	10 399
10	85	46.7	13.5	**8.39**	0.73	9.3	2 107	3 493	1.00	1.00	33 231	3 454	26 329	10 448
10	90	50.0	12.9	**8.32**	0	7.68	2 024	3 068	1.00	1.00	29 281	3 034	21 898	10 492
10	95	53.5	12.3	**8.2**	-0.71	5.99	1 899	2 625	1.00	1.00	25 122	2 596	17 246	10 529
10	100	57.3	11.7	**8.03**	-1.39	4.75	1 735	2 188	1.00	1.00	20 969	2 164	13 709	9 469
10	105	61.5	11.0	**7.82**	-2.02	3.89	1 549	1 783	1.00	1.00	17 107	1 764	11 245	7 661
10	110	66.1	10.3	**7.57**	-2.59	3.2	1 356	1 426	1.00	1.00	13 690	1 411	9 279	5 850
15	35	23.4	20.9	**6.9**	5.65	15.34	1 482	6 669	0.83	1.00	45 195	6 596	41 705	10 210
15	40	25.7	21.2	**7.61**	5.83	17.46	1 887	7 107	0.85	1.00	49 463	7 028	46 546	10 099
15	45	28.3	21.2	**8.07**	5.71	18.46	2 261	7 242	0.86	1.00	51 466	7 163	48 760	10 042
15	50	30.9	21.1	**8.45**	5.43	19.64	2 625	7 345	0.88	1.00	53 750	7 264	51 235	9 971
15	55	33.6	20.9	**8.76**	5.03	20	2 941	7 285	0.89	1.00	54 541	7 205	52 002	9 949
15	60	36.3	20.5	**9.03**	4.52	20.96	3 258	7 271	0.91	1.00	56 510	7 191	54 036	9 886
15	65	39.1	20.1	**9.26**	3.91	21.1	3 515	7 102	0.93	1.00	56 922	7 024	54 296	9 877
15	70	41.9	19.6	**9.46**	3.23	21.86	3 766	6 968	0.95	1.00	58 403	6 892	55 710	9 826
15	75	44.8	19.0	**9.62**	2.49	22.47	3 982	6 777	0.98	1.00	59 676	6 702	56 846	9 783
15	80	48.2	18.5	**9.69**	1.68	21.43	4 019	6 392	1.00	1.00	58 206	6 321	54 915	9 855
15	85	52.0	18.0	**9.75**	0.85	18.45	3 992	5 729	1.00	1.00	52 912	5 666	48 745	10 043
15	90	56.1	17.4	**9.72**	0	15.34	3 856	5 003	1.00	1.00	46 779	4 948	41 691	10 210
15	95	60.4	16.8	**9.59**	-0.84	12.35	3 624	4 267	1.00	1.00	40 284	4 220	34 300	10 342
15	100	65.0	16.1	**9.4**	-1.63	9.64	3 330	3 577	1.00	1.00	34 010	3 538	27 216	10 438
15	105	69.8	15.3	**9.16**	-2.37	7.27	2 999	2 960	1.00	1.00	28 274	2 928	20 778	10 502
15	110	75.0	14.5	**8.89**	-3.04	5.37	2 654	2 427	1.00	1.00	23 249	2 401	15 453	10 252
20	35	24.9	26.2	**7.35**	6.02	16.49	1 973	8 317	0.74	1.00	46 118	8 226	44 334	10 151
20	40	27.6	26.4	**8.04**	6.16	18	2 498	8 651	0.75	1.00	49 132	8 555	47 787	10 069
20	45	30.5	26.3	**8.55**	6.05	19.39	3 010	8 853	0.77	1.00	51 745	8 755	50 706	9 987
20	50	33.4	26.2	**8.97**	5.77	20	3 468	8 858	0.78	1.00	52 981	8 760	52 002	9 949
20	55	36.3	25.8	**9.33**	5.35	21	3 927	8 876	0.80	1.00	54 987	8 778	54 109	9 884
20	60	39.4	25.4	**9.62**	4.81	21.53	4 328	8 751	0.82	1.00	56 057	8 654	55 104	9 848
20	65	42.4	24.8	**9.88**	4.18	22.41	4 715	8 624	0.84	1.00	57 733	8 529	56 732	9 788
20	70	45.7	24.2	**10.06**	3.44	22.78	4 959	8 392	0.86	1.00	58 615	8 300	57 420	9 762
20	75	48.9	23.5	**10.28**	2.66	23.47	5 258	8 142	0.89	1.00	60 098	8 053	58 720	9 711
20	80	52.2	22.8	**10.47**	1.82	24	5 500	7 818	0.93	1.00	61 350	7 732	59 703	9 672
20	85	55.8	22.0	**10.64**	0.93	24	5 663	7 390	0.96	1.00	61 769	7 308	59 703	9 672
20	90	59.4	21.2	**10.78**	0	24.07	5 773	6 943	1.00	1.00	62 324	6 866	59 826	9 666
20	95	64.2	20.8	**10.79**	-0.94	20.02	5 574	6 077	1.00	1.00	55 727	6 010	52 042	9 947
20	100	69.3	20.2	**10.62**	-1.84	16.25	5 235	5 214	1.00	1.00	48 586	5 156	43 780	10 164
20	105	74.6	19.5	**10.35**	-2.68	12.95	4 802	4 414	1.00	1.00	41 604	4 366	35 808	10 318
20	110	80.2	18.8	**10.05**	-3.44	10.22	4 327	3 726	1.00	1.00	35 373	3 685	28 759	10 419
25	35	26.2	31.1	**7.47**	6.12	16.74	2 346	9 679	0.67	1.00	45 312	9 572	44 892	10 139
25	40	29.1	31.4	**8.25**	6.32	18.29	2 992	10 058	0.68	1.00	48 324	9 947	48 395	10 052
25	45	32.1	31.3	**8.83**	6.25	19.89	3 640	10 330	0.70	1.00	51 307	10 217	51 773	9 955
25	50	35.2	31.1	**9.31**	5.98	20.67	4 221	10 357	0.71	1.00	52 848	10 243	53 409	9 906
25	55	38.5	30.7	**9.69**	5.56	21.23	4 760	10 271	0.73	1.00	54 005	10 158	54 534	9 869
25	60	41.6	30.2	**10.04**	5.02	22.33	5 303	10 208	0.75	1.00	56 026	10 096	56 589	9 793
25	65	44.8	29.5	**10.37**	4.38	23.29	5 799	10 060	0.77	1.00	57 873	9 949	58 379	9 724
25	70	48.3	28.8	**10.64**	3.64	23.79	6 138	9 796	0.79	1.00	59 022	9 688	59 318	9 687
25	75	51.7	28.1	**10.96**	2.84	24	6 480	9 421	0.82	1.00	59 751	9 317	59 703	9 672
25	80	55.2	27.3	**11.26**	1.96	24.36	6 767	9 007	0.85	1.00	60 711	8 908	60 294	9 645
25	85	58.7	26.4	**11.53**	1.01	24.93	7 003	8 574	0.89	1.00	62 032	8 480	61 245	9 601
25	90	62.5	25.5	**11.76**	0	25.29	7 165	8 091	0.93	1.00	63 073	8 002	61 849	9 572
25	95	66.5	24.5	**11.93**	-1.04	25.66	7 265	7 593	0.97	1.00	64 138	7 509	62 461	9 543
25	100	71.1	23.7	**12.02**	-2.09	24.13	7 188	6 949	1.00	1.00	62 365	6 873	59 913	9 662

25	105	76.6	23.3	**11.86**	-3.07	20.05	6 790	6 082	1.00	1.00	55 762	6 015	52 108	9 945
25	110	82.6	22.7	**11.47**	-3.92	16.47	6 255	5 264	1.00	1.00	49 017	5 206	44 292	10 152

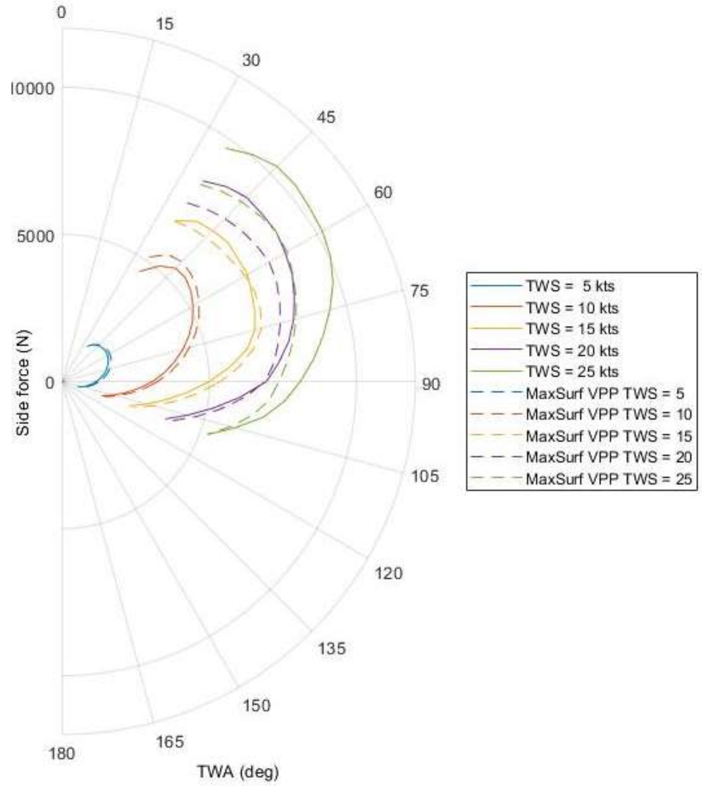

Figure XI-11: Upwind polar plot, OceanVPP and Maxsurf (Side Force)

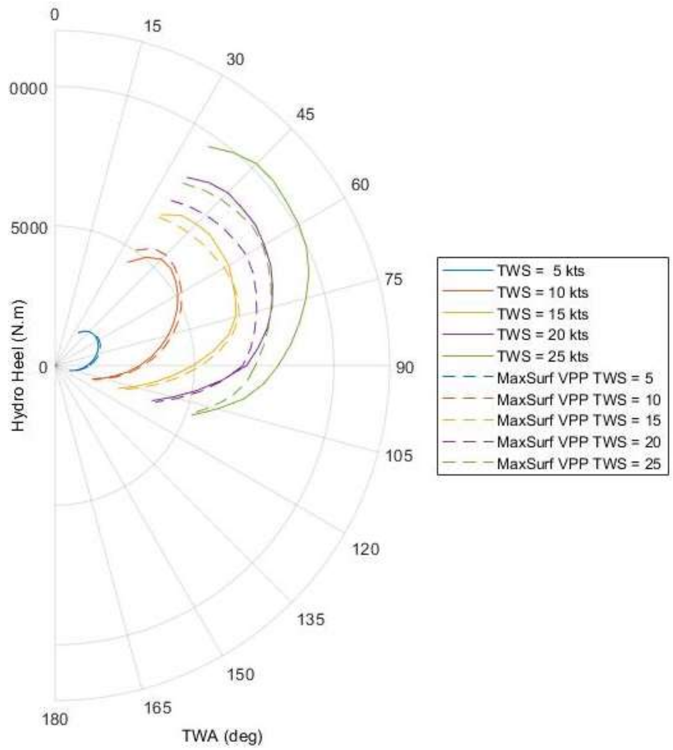

Figure XI-2: Upwind polar plot, OceanVPP and Maxsurf (HydroHeel)

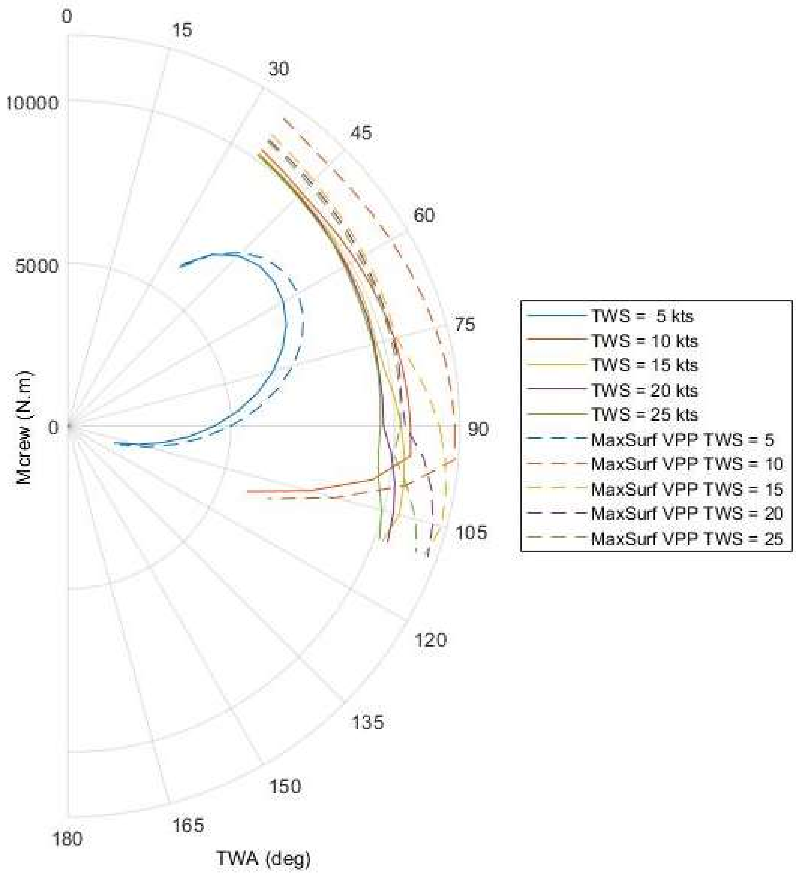

Figure XI-3: Upwind polar plot, OceanVPP and Maxsurf (Crew Righting Moment)

Table XI-2: Upwind Results (ORC format)

	6kt	8kt	10kt	12kt	14kt	16kt	20kt	24kt
52º	5.79	7.04	7.72	8.12	8.44	8.71	9.12	9.41
60º	6.24	7.43	8.09	8.54	8.88	9.17	9.62	9.96
75º	6.63	7.72	8.44	9.02	9.45	9.71	10.28	10.82
90º	6.56	7.60	8.32	8.94	9.48	9.94	10.78	11.56
110º	5.62	6.81	7.57	8.13	8.64	9.13	10.05	11.14
120º	4.85	5.94	6.90	7.56	8.07	8.55	9.44	10.32
135º	3.75	4.73	5.64	6.52	7.24	7.80	8.75	9.65
150º	3.26	4.23	5.13	5.99	6.82	7.48	8.55	9.51

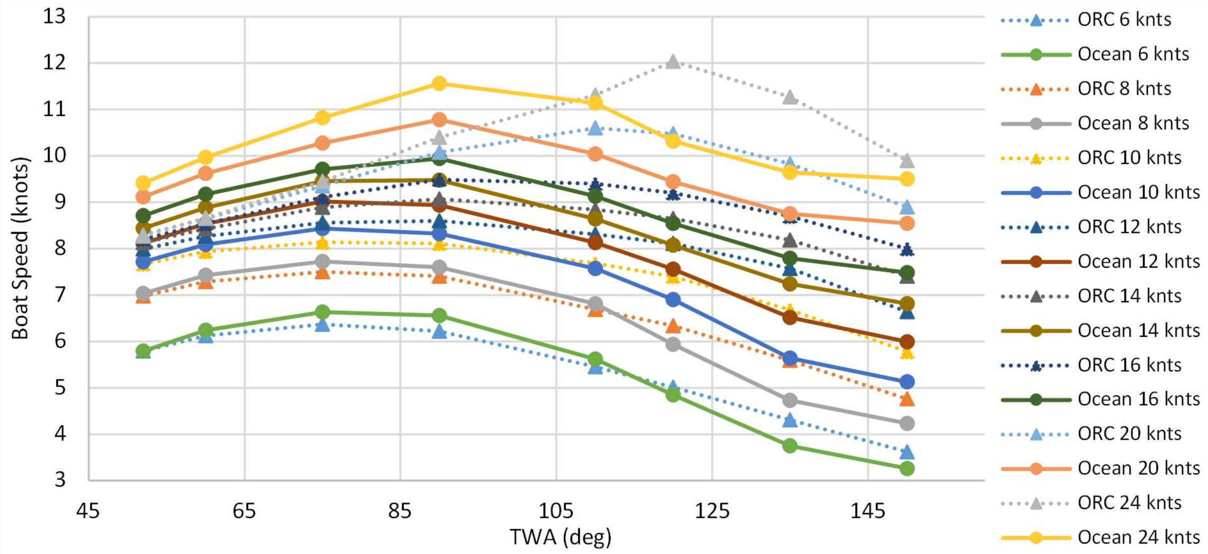

Figure XI-4: ORC and OceanVPP comparison (non-spinnaker)

Appendix XII. OceanVPP Downwind Results

Table XII-1: Downwind Results

TWS	TWA	AWA	AWS	V	VMG	Heel	Fdrive	Fside	Reef	Flat	Mheel	Hydro Heel	Hull RM	McrewRM
[knt]	[deg]	[deg]	[knt]	[knt]	[knt]	[deg]	[N]	[N]	[0-1]	[-]	[N]	[Nm]	[Nm]	[Nm]
5	80	36	8	5.94	1.03	4.56	680	1 787	1	1	20460	1767	13141	9117
5	85	37	8	6.15	0.54	4.71	741	1 842	1	1	21095	1822	13566	9384
5	90	38	8	6.32	0	4.75	788	1 860	1	1	21289	1839	13700	9463
5	95	40	8	6.42	-0.56	4.69	819	1 835	1	1	21009	1815	13509	9350
5	100	41	7	6.47	-1.12	4.5	831	1 766	1	1	20226	1747	12991	9016
5	105	43	7	6.45	-1.67	4.22	823	1 652	1	1	18925	1634	12171	8420
5	110	46	7	6.3	-2.15	3.86	770	1 504	1	1	17238	1488	11164	7591
5	115	48	6	6.15	-2.6	3.42	723	1 309	1	1	15006	1295	9891	6434
5	120	52	6	5.93	-2.97	2.93	657	1 087	1	1	12470	1075	8482	5084
5	125	56	5	5.64	-3.23	2.41	575	854	1	1	9791	844	6977	3674
5	130	62	4	5.28	-3.4	1.91	486	637	1	1	7312	630	5528	2426
5	135	69	4	4.93	-3.48	1.49	406	467	1	1	5357	462	4306	1522
5	140	77	3	4.58	-3.51	1.12	336	331	1	1	3804	328	3251	887
5	145	87	3	4.24	-3.47	0.79	275	219	1	1	2517	217	2291	447
5	150	100	3	3.89	-3.37	0.51	222	134	1	1	1534	132	1481	188
5	155	115	2	3.56	-3.23	0.32	181	80	1	1	917	79	923	74
5	160	129	2	3.31	-3.11	0.21	154	51	1	1	583	50	603	31
5	165	142	2	3.16	-3.05	0.14	138	33	1	1	376	32	395	13
5	170	155	2	3.05	-3.01	0.08	129	19	1	1	222	19	236	5
5	175	168	2	2.99	-2.98	0.04	124	9	1	1	107	9	115	1
10	80	41	14	8.79	1.53	19.18	2 705	5 547	0.94	1	54581	5486	50264	10000
10	85	44	14	8.95	0.78	19.78	2 893	5 563	0.95	1	55795	5501	51541	9962
10	90	46	13	9.015	-0.005	19.89	2 953	5 443	0.965	1	56135	5383	51771	9955
10	95	49	12	9.08	-0.79	20	3 013	5 323	0.98	1	56474	5264	52002	9949
10	100	52	12	9.13	-1.58	19.23	3 038	5 031	1	1	55192	4976	50376	9996
10	105	55	11	9.12	-2.36	16.6	2 963	4 513	1	1	50087	4463	44580	10146
10	110	58	11	9.03	-3.09	13.82	2 814	3 942	1	1	44208	3898	37971	10281
10	115	62	10	8.88	-3.75	11.16	2 614	3 374	1	1	38151	3337	31217	10387
10	120	67	9	8.69	-4.34	8.72	2 387	2 841	1	1	32319	2810	24752	10465
10	125	71	9	8.47	-4.86	6.49	2 147	2 342	1	1	26752	2316	18613	10519
10	130	77	8	8.22	-5.28	4.78	1 898	1 871	1	1	21416	1850	13794	9518
10	135	83	7	7.95	-5.62	3.7	1 645	1 431	1	1	16407	1416	10687	7169
10	140	90	6	7.64	-5.85	2.82	1 397	1 041	1	1	11934	1029	8186	4803
10	145	99	6	7.28	-5.96	2.09	1 161	714	1	1	8191	706	6054	2861
10	150	110	5	6.86	-5.94	1.49	957	468	1	1	5372	463	4317	1530
10	155	122	5	6.44	-5.84	1.06	804	308	1	1	3536	305	3060	789
10	160	134	5	6.12	-5.75	0.76	704	209	1	1	2395	206	2195	411
10	165	145	5	5.9	-5.7	0.52	642	138	1	1	1580	136	1521	199
10	170	157	4	5.75	-5.66	0.33	601	82	1	1	945	81	951	78
10	175	169	4	5.66	-5.64	0.17	577	41	1	1	466	40	487	20
15	80	48	19	9.94	1.73	21	4 585	7 636	0.8	1	56198	7552	54109	9884
15	85	51	18	10.11	0.88	21	4 814	7 427	0.82	1	56402	7345	54110	9884
15	90	54	17	10.24	0	21.56	4 998	7 217	0.84	1	57610	7138	55159	9846
15	95	57	17	10.34	-0.9	22.07	5 117	6 952	0.87	1	58765	6876	56095	9812
15	100	60	16	10.41	-1.81	22.44	5 178	6 647	0.9	1	59730	6574	56791	9785
15	105	64	15	10.46	-2.71	22.69	5 198	6 325	0.94	1	60497	6255	57261	9768
15	110	68	14	10.48	-3.59	22.89	5 191	5 993	0.97	1	61188	5927	57641	9753
15	115	72	13	10.49	-4.43	22.14	5 138	5 577	1	1	60260	5515	56240	9806
15	120	77	13	10.44	-5.22	18.51	4 940	4 891	1	1	53832	4837	48854	10040
15	125	82	12	10.28	-5.9	14.72	4 653	4 132	1	1	46201	4087	40225	10239
15	130	88	11	10.04	-6.45	11.01	4 274	3 341	1	1	37794	3304	30836	10392
15	135	95	11	9.73	-6.88	7.55	3 821	2 579	1	1	29405	2551	21546	10495
15	140	102	10	9.38	-7.19	4.88	3 329	1 906	1	1	21814	1885	14078	9674
15	145	111	9	9.03	-7.4	3.55	2 851	1 368	1	1	15676	1353	10274	6792
15	150	120	9	8.7	-7.54	2.68	2 442	974	1	1	11176	964	7763	4403
15	155	129	8	8.42	-7.63	2.05	2 125	697	1	1	8003	690	5944	2769
15	160	139	8	8.2	-7.71	1.55	1 898	493	1	1	5655	487	4501	1656
15	165	149	8	8.03	-7.76	1.12	1 740	331	1	1	3800	327	3251	887
15	170	159	7	7.91	-7.79	0.73	1 632	201	1	1	2308	199	2128	386
15	175	170	7	7.82	-7.79	0.4	1 564	102	1	1	1172	101	1161	116
20	80	52	23	10.95	1.9	21.97	6 386	9 360	0.71	1	56203	9258	55922	9818
20	85	55	23	11.23	0.98	22.62	6 699	9 146	0.74	1	57568	9046	57138	9772
20	90	58	22	11.47	0	23.15	6 928	8 859	0.76	1	58777	8762	58114	9735
20	95	62	21	11.67	-1.02	23.5	7 085	8 524	0.79	1	59729	8430	58769	9709
20	100	65	20	11.83	-2.05	23.72	7 194	8 164	0.81	1	60479	8074	59187	9692
20	105	69	19	11.96	-3.1	23.89	7 272	7 786	0.84	1	61143	7700	59496	9680
20	110	73	18	12.09	-4.13	24	7 329	7 383	0.87	1	61735	7302	59703	9672
20	115	77	17	12.2	-5.16	24	7 368	6 941	0.91	1	62168	6865	59703	9672
20	120	82	16	12.3	-6.15	24	7 394	6 467	0.95	1	62635	6396	59703	9672
20	125	86	15	12.39	-7.11	24.14	7 410	5 973	1	1	63346	5907	59941	9661
20	130	92	14	12.32	-7.92	19.56	7 118	5 089	1	1	55735	5033	51073	9976
20	135	99	14	11.93	-8.44	14.44	6 632	4 069	1	1	45542	4025	39515	10253
20	140	108	13	11.31	-8.66	9.85	6 021	3 086	1	1	35014	3052	27764	10431
20	145	116	13	10.71	-8.78	6.29	5 380	2 296	1	1	26237	2271	18063	10523
20	150	125	12	10.28	-8.9	4.37	4 793	1 711	1	1	19601	1692	12602	8743
20	155	134	12	9.97	-9.04	3.34	4 322	1 272	1	1	14586	1258	9664	6219
20	160	143	11	9.75	-9.16	2.56	3 971	921	1	1	10569	911	7424	4085
20	165	152	11	9.58	-9.26	1.89	3 714	631	1	1	7236	624	5487	2394

20	170	161	11	9.46	-9.31	1.29	3 531	391	1	1	4487	387	3731	1157
20	175	171	11	9.37	-9.33	0.75	3 412	206	1	1	2366	204	2175	403
25	80	54	28	12.01	2.09	23.06	8 039	11 065	0.65	1	56428	10943	57953	9741
25	85	57	27	12.41	1.08	23.7	8 420	10 799	0.67	1	57819	10680	59148	9694
25	90	61	26	12.77	0	24	8 697	10 442	0.69	1	58691	10327	59702	9672
25	95	64	25	13.09	-1.14	24	8 896	10 033	0.71	1	59087	9923	59703	9672
25	100	68	24	13.38	-2.32	24	9 057	9 611	0.73	1	59495	9506	59703	9672
25	105	72	23	13.64	-3.54	24	9 185	9 150	0.76	1	59945	9049	59704	9672
25	110	76	22	13.89	-4.75	24	9 313	8 688	0.78	1	60396	8593	59705	9672
25	115	80	21	14.13	-5.97	24.19	9 427	8 183	0.82	1	61179	8093	60012	9658
25	120	85	20	14.34	-7.16	24.55	9 514	7 632	0.86	1	62284	7548	60612	9630
25	125	89	19	14.54	-8.34	24.91	9 601	7 080	0.91	1	63389	7002	61211	9602
25	130	95	17	14.71	-9.45	25.29	9 645	6 480	0.97	1	64575	6409	61845	9572
25	135	100	17	14.78	-10.45	22.78	9 444	5 682	1	1	61173	5619	57423	9761
25	140	107	16	14.45	-11.07	16.96	8 823	4 577	1	1	50724	4527	45410	10126
25	145	116	16	13.64	-11.17	11.72	8 106	3 493	1	1	39430	3454	32705	10366
25	150	126	15	12.72	-11.01	7.84	7 485	2 641	1	1	30093	2612	22333	10488
25	155	135	15	12.05	-10.92	5.16	6 988	1 998	1	1	22863	1976	14868	10043
25	160	144	15	11.62	-10.92	3.78	6 596	1 467	1	1	16813	1451	10930	7386
25	165	153	14	11.31	-10.93	2.77	6 300	1 017	1	1	11663	1006	8040	4664
25	170	162	14	11.1	-10.93	1.92	6 085	640	1	1	7340	633	5552	2446
25	175	171	14	10.95	-10.91	1.16	5 941	345	1	1	3962	341	3368	950

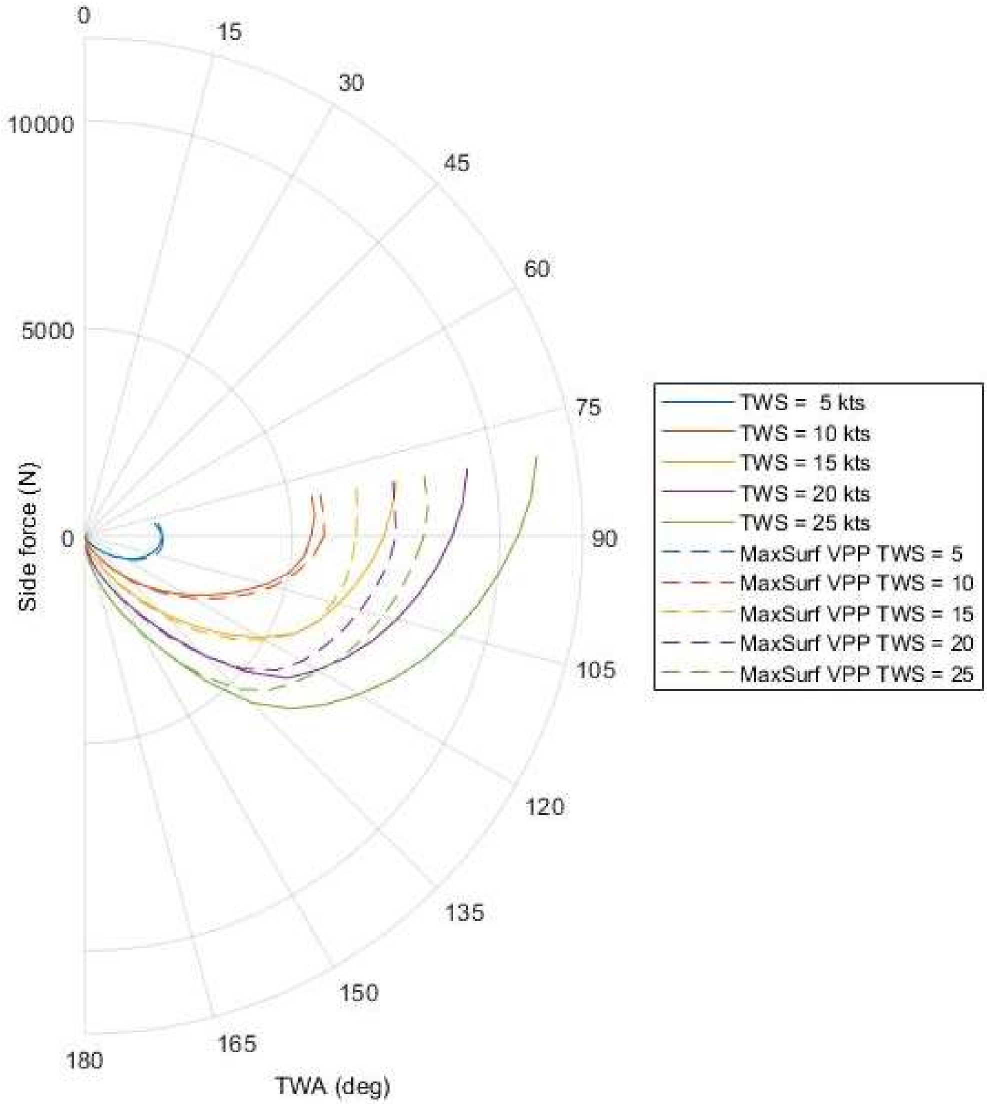

Figure XII-1: Downwind polar plot, OceanVPP and Maxsurf (Side Force)

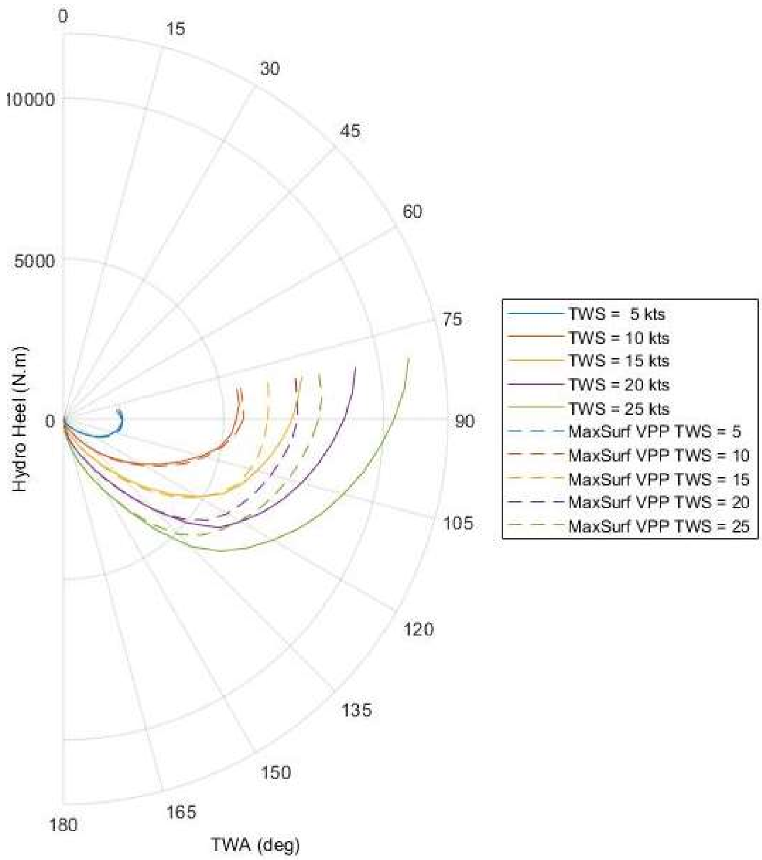

Figure XII-2: Downwind polar plot, OceanVPP and Maxsurf (Hydro Heel)

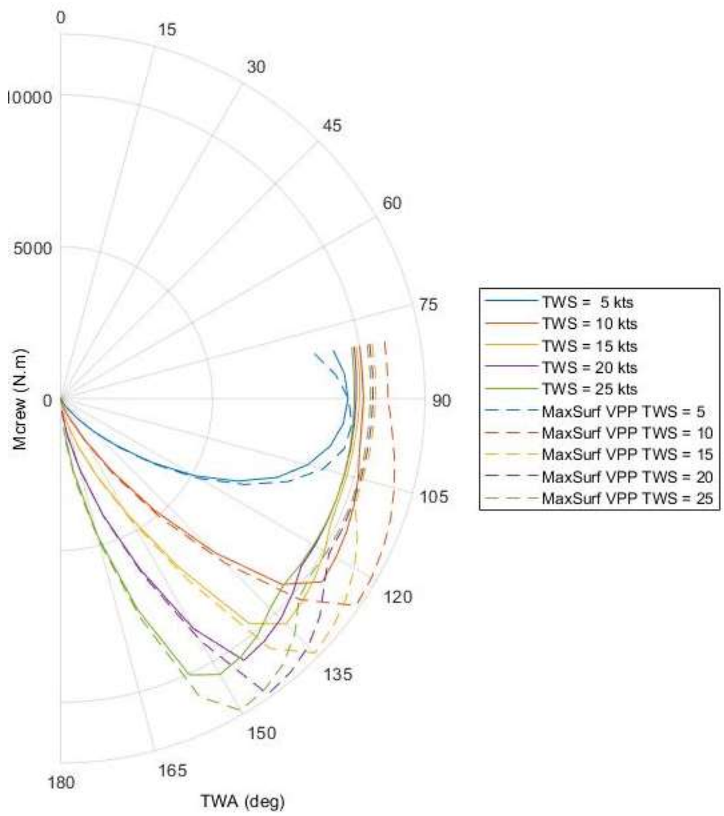

Figure XII-3: Downwind polar plot, OceanVPP and Maxsurf (Crew Righting Moment)

Table XII-2: Downwind Results (ORC format)

Wind Velocity	6kt	8kt	10kt	12kt	14kt	16kt	20kt	24 kt
52º	5.79	7.04	7.72	8.12	8.44	8.71	9.12	9.41
60º	6.24	7.43	8.09	8.54	8.88	9.17	9.62	10.04
75º	6.63	7.87	8.58	9.14	9.60	9.92	10.63	11.37
90º	7.24	8.35	8.99	9.55	10.02	10.47	11.47	12.51
110º	7.16	8.23	9.03	9.68	10.22	10.77	12.09	13.55
120º	6.79	7.87	8.69	9.43	10.10	10.79	12.30	13.96
135º	5.68	7.04	7.95	8.69	9.39	10.08	11.93	14.27
150º	4.53	5.73	6.86	7.70	8.38	9.02	10.28	12.12

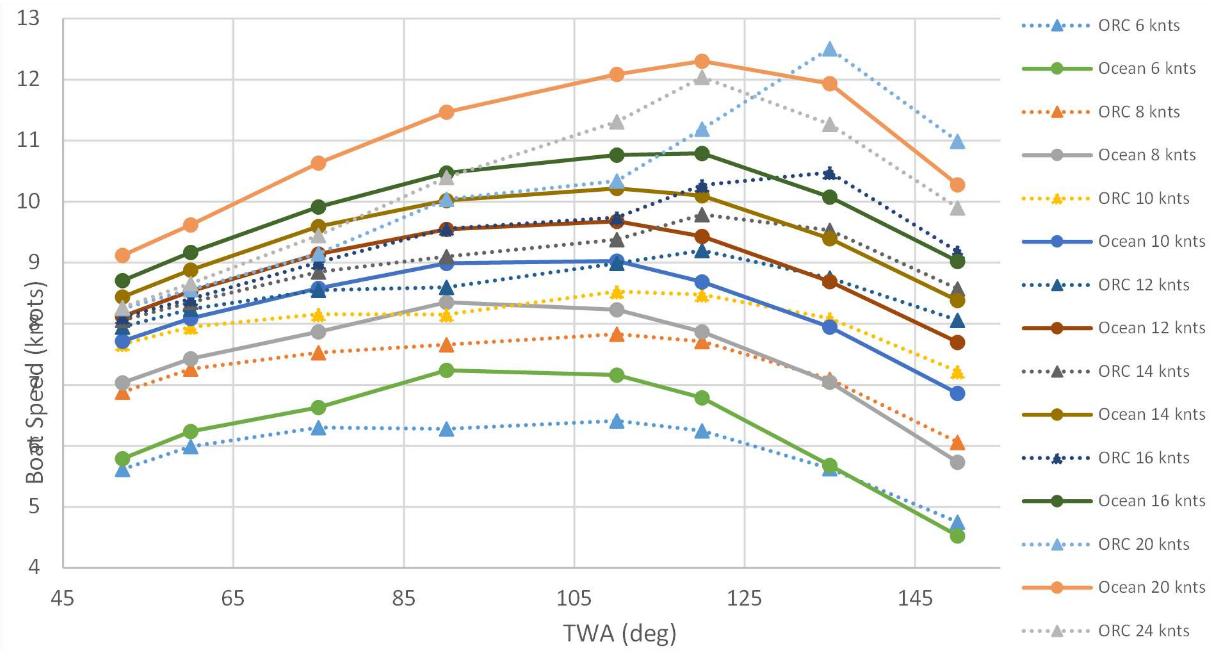

Figure XII-4: ORC and OceanVPP comparison (Main + Jib + Spinnaker)

Appendix XIII. ORC Certificates

Table XIII-1: ORC Certificate for MIRIAM POL 000YED *(non-spinnaker).*

Wind Velocity	6 kt	8 kt	10 kt	12 kt	14 kt	16 kt	20 kt	24 kt
52º	5.79	6.98	7.67	7.99	8.13	8.21	8.3	8.27
60º	6.12	7.29	7.94	8.27	8.43	8.54	8.65	8.66
75º	6.37	7.5	8.14	8.56	8.89	9.11	9.35	9.45
90º	6.22	7.41	8.11	8.6	9.07	9.49	10.08	10.4
110º	5.45	6.69	7.68	8.31	8.84	9.4	10.6	11.31
120º	5.01	6.34	7.4	8.11	8.65	9.2	10.48	12.04
135º	4.31	5.59	6.68	7.57	8.19	8.7	9.83	11.27
150º	3.62	4.76	5.78	6.64	7.41	8	8.9	9.9

Table XIII-2: OceanVPP results for MIRIAM POL 000YED

Wind Velocity	6kt	8kt	10kt	12kt	14kt	16kt	20kt	24kt
52º	5.62	6.88	7.67	7.95	8.06	8.11	8.25	5.62
60º	5.99	7.26	7.95	8.24	8.35	8.41	8.56	5.99
75º	6.3	7.53	8.16	8.55	8.85	9.01	9.15	6.3
90º	6.28	7.66	8.15	8.6	9.1	9.56	10.04	6.28
110º	6.41	7.83	8.53	8.99	9.38	9.74	10.34	6.41
120º	6.25	7.71	8.48	9.2	9.79	10.27	11.19	6.25
135º	5.63	7.09	8.09	8.75	9.53	10.48	12.51	5.63
150º	4.75	6.06	7.22	8.06	8.57	9.18	10.99	4.75

Table XIII-3: ORC Certificate for Forsatio POL 20941 (Double Handed Certificate).

Wind Velocity	6kt	8kt	10kt	12kt	14kt	16kt	20kt
52º	5.62	6.88	7.67	7.95	8.06	8.11	8.25
60º	5.99	7.26	7.95	8.24	8.35	8.41	8.56
75º	6.3	7.53	8.16	8.55	8.85	9.01	9.15
90º	6.28	7.66	8.15	8.6	9.1	9.56	10.04
110º	6.41	7.83	8.53	8.99	9.38	9.74	10.34
120º	6.25	7.71	8.48	9.2	9.79	10.27	11.19
135º	5.63	7.09	8.09	8.75	9.53	10.48	12.51
150º	4.75	6.06	7.22	8.06	8.57	9.18	10.99

Table XIII-4: OceanVPP results for Forsatio POL 20941

Wind Velocity	6kt	8kt	10kt	12kt	14kt	16kt	20kt
52º	5.79	7.04	7.72	8.12	8.44	8.71	9.12
60º	6.24	7.43	8.09	8.54	8.88	9.17	9.62
75º	6.63	7.87	8.58	9.14	9.60	9.92	10.63
90º	7.24	8.35	8.99	9.55	10.02	10.47	11.47
110º	7.16	8.23	9.03	9.68	10.22	10.77	12.09
120º	6.79	7.87	8.69	9.43	10.10	10.79	12.30
135º	5.68	7.04	7.95	8.69	9.39	10.08	11.93
150º	4.53	5.73	6.86	7.70	8.38	9.02	10.28